Selective Laser Melting of Advanced Metal Alloys for Aerospace Applications

2007-2011

Submitted by Peter George Eveleigh Jerrard to the University of Exeter
as a thesis for the degree of
Doctor of Philosophy in Engineering
In August 2011

I certify that all material in this thesis which is not my own work has been identified and that no material has previously been submitted and approved for the award of a degree by this or any other University.

Signature: ……

ABSTRACT

Research focused on the selective laser melting (SLM) of stainless steels and aluminium alloys. For steels, the possibility of creating a magnetically graded material was demonstrated as well as the ability to improve consolidation with austenitic and martensitic stainless steel powder mixtures. Stainless Steel/CoCr hybrid samples were also manufactured and tested to investigate the advantages of functionally graded materials (FGMs).

Al alloy research began with examining the requirements for successful Al alloy consolidation in SLM and through experimentation it was found that Al alloys with good welding properties were the best choice: pure Al was found to be completely unsuitable. 6061 Al alloy was then used as a base material to manufacture Al-Cu alloy samples. Single layer SLM samples were produced first, which resulted in recognised Al-Cu microstructures forming. Multilayer Al alloy SLM research resulted in the discovery of the theorised ability to manufacture Al-Cu alloy parts with a nanocrystalline Al matrix with dispersed Al_2Cu quasicrystals, resulting in a material comparable to a metal matrix composite that showed excellent corrosion resistance and compressive strength.

Finally, a demonstration part was made to test the capability of the SLM process producing an aerospace type geometry using a customised Al alloy. Observations during manufacture and post process analysis showed that Al alloys were susceptible to changes in mechanical properties due to the geometry of the manufactured part.

ACKNOWLEDEMENTS

For my grandparents and parents.

"*As for me, all I know is that I know nothing*"

- Socrates, recorded by his student Plato.

At the start of the PhD, I was essentially given free reign to choose a research area in Additive Manufacturing (AM) that I believed to be important: I must thank my supervisors Dr Liang Hao and Dean Ken Evans for this freedom. The better part of six months was spent reading about the various areas of AM. Fields such as functionally graded structures, process improvement and the management of AM were amongst the potential research fields but I decided that a combination of material and design research would really show the abilities of AM. The Selective Laser Melting (SLM) of Al alloys however was far harder than anticipated and thus more time was spent attempting to devise methods to successfully consolidate them.

The PhD has been exciting. From what I have learned of other PhD projects, most do their work having a well established technology level. In my case, dramatic developments occurred during the course of my research. When I first proposed researching Al alloys for SLM, I can only remember one paper on the subject, which wasn't actually focusing on the manufacturing process itself: instead it was focusing on producing novel heat sinks. By the end of my PhD several manufacturers were offering Al alloys to use in their machines and several new papers had been published on the SLM of Al alloys. Still, such is the nature of working on the bleeding edge of technology.

I would now like to thank various people who supported me during the PhD. In no particular order:

- Liang and Ken for supervising me and allowing me to have flexibility in my research. I appreciate your faith in me.
- Dr Neil Sewell for developing the custom software for the Realizer, for being a beacon of good advice and moral values and being a good friend.

- Mike Felstead for actually getting the Realizer in the first place as well as being a friend; I'll miss teaching SolidWorks together.
- Dave Baker, for teaching me to use the Realizer, for helping and for the interesting conversations.
- Dr Wayne Miller for being the unofficial office manager and always being available to talk to; I hope your baby does well.
- Ian Moon for being friendly and approachable and always willing to give me advice on machining.
- Pete Gerry for, well, just being Pete!
- Sasan Dadbakhsh for being a wonderful housemate and colleague. Without you I would have never understood Al alloy microstructures!
- Everyone in room 020.2 for making life interesting.
- Paul Brookbank for allowing me to be the godfather to Lilly.
- Dr Martin Jenkins and Dr Bill Hooper; you two old coots have been an absolute pleasure to talk to and I consider myself lucky to have been taught by you.
- And of course, my parents, who have fed and watered me over the years!

PUBLICATIONS

- Jerrard, P., Hao, L., Sewell, N.T., Evans, K.E. and Felstead, M., Consolidation of Austenitic and Martensitic powder mixtures via selective laser melting, 9th National Conference on Rapid Design, Prototyping & Manufacturing, Lancaster, United Kingdom, 13th June 2008, pp.145-152.
- Jerrard, P., Hao, L. and Evans, K.E., Selective Laser Melting of Pure Aluminium Powder - A preliminary Study, 10th National Conference on Rapid Design, Prototyping & Manufacturing, Buckinghamshire, United Kingdom, 12th June 2009, pp.53-61.
- Jerrard, P.G.E., Hao, L. and Evans, K.E., Experimental Investigation into Selective Laser Melting of Austenitic and Martensitic Stainless Steel Powder Mixtures, Proceedings of the Institution of Mechanical Engineers, Part B: Journal of Engineering Manufacture November 1, 2009 vol. 223 no. 11 1409-1416.
- Jerrard, P.G.E., Hao, L. and Evans, K.E., Consolidation behaviour and microstructure characteristics of pure aluminium and alloy powders following Selective Laser Melting processing, proceedings of the 36th International MATADOR Conference, 14th - 16th July 2010, pp. 487-490.
- Dadbakhsh, S., Hao, L., Sewell, N. and Jerrard, P., Direct fabrication of an in-situ Al composite using selective laser melting process, Innovative Developments in Design and Manufacturing - Advanced Research in Virtual and Rapid Prototyping, 2010, pp. 319-325.
- Jerrard, P.G.E., Hao, L., Dadbakhsh, S., Evans, K.E. Consolidation behaviour and microstructural characteristics of Al and mixture of Al-Cu alloy powders following Selective Laser Melting processing, Lasers in Engineering (in press).

CONTENTS

PART II: EXPERIMENTAL STUDIES AND APPLICATION

PART III: DEMONSTRATION

PART IV: POSTLUDE

FIGURES AND TABLES

Figures

Tables

INTRODUCTION

The aerospace industry is a very large entity, dealing with large amounts of wealth and advanced technologies. The UK aerospace industry (UKAI) believes in investing in research and development to keep a competitive edge, often using universities to benefit from academic feedback. Materials development takes a high priority as improved materials enable new technologies to be used. Manufacturing wise, a recurring theme is a lack of complete geometric freedom. The phrase 'design for manufacture' holds true. Material usage in aircraft is diverse but two material groups stand out in particular due to their current dominance: aluminium alloys and composites. Aluminium alloys remain a staple material in aircraft and due to their competitive prices will likely remain so for many years.

Additive manufacturing (AM) is an area which is still growing to maturity and shows great promise for manufacturing future components with sophisticated geometries. AM clearly can be of use to the aerospace industry due to the ability to manufacture parts with truly complex geometry and/or the ability to make small volumes of parts without the need for tooling. Airbus Filton currently own several SLS/SLM machines [1, 2], which reinforces the argument that AM will grow in use for aerospace applications. Given that AM is on the rise, it is an area in which more expertise will soon be needed.

Looking over the information for AM, it becomes apparent that material capability is lacking for all processes for higher level aerospace use. Not only are there limitations in mechanical properties which are inferior to conventionally produced materials, qualification of materials for aerospace use is also a huge issue that is currently an in-house procedure, though steps are being taken to standardise material qualification in the form of the ASTM Committee F42. Research into AM material improvement is a popular field. Hence, material research is a logical path to follow and it makes sense to choose a process that has the ability to adapt to a wide range of materials.

Of the AM methods available, selective laser sintering (SLS) and selective laser melting (SLM) are considered the most likely technologies to benefit the aerospace industry. The two aforementioned processes are of considerable interest either due to considerable design freedom (SLS) or the ability to manufacture strong parts with a

respectable design freedom (SLM). SLS appears to be entering a new stage of feasibility with the advent of PEEK becoming available but still offers little improvement in terms of material strength when compared to the effect alloying can have. For example, if it is assumed that adding MWCNTs to PEEK has the same effect as it did for PA12 [3], PEEK tensile strength would increase to approximately 104 MPa: taking the density of PEEK as 1.3 g cm^{-3} [4], this gives a specific strength of 80 MPa g^{-1} cm^3. Compare this to the Al-Sc alloy processed by Schmidtke *et al* [5] with a tensile strength of 530 MPa and density of 2.7 g cm^{-3}, resulting in a specific strength of 196 MPa g^{-1} cm^3 - over twice that of a theoretically reinforced PEEK composite. SLM has the most flexibility in materials choice, which would be desirable for researching new materials. The capability of SLM to fully melt and consolidate metals means that parts can be produced with specific strengths far in excess of polymer parts produced by SLS also adds weight to the decision to pursue SLM research. The difficulty of introducing continuous fibre reinforcement into SLS (discontinuous reinforcement having been shown to have a comparatively small advantage compared to alloying) means that investing time in researching alloy and/or composite materials in SLM may be the more cost effective path to currently follow, with development time being shorter due to the ease of material mixing. Hence, material research for the PhD has been undertaken using the SLM process.

Only very recently has research on the SLM of Al components been published, using commercially available low and medium strength Al alloy powders. Little research has investigated the microstructure characteristics of the Al alloy processed by SLM and the development of new Al alloys for SLM. Thus, it was decided that research into this area would be a chance to discover new high performance Al alloy materials for SLM that are more appropriate to utilise the benefits of AM to produce advanced and lightweight aerospace components. Very recently the work reported by Wong *et al* [6] was primarily concerned with the manufacture of heat sinks rather than full mechanical and metallurgical analysis of the resulting consolidated material. In addition, high performance Al alloys were not commercially available for SLM processing. Given the fact that Al alloys are still subject to considerable usage within aerospace applications, they are a logical choice to research for SLM use. SLM can be thought of as a large scale welding process: indeed, the phenomena that govern it are shared with conventional welding. With this in mind, it is logical to assume that materials with a good weldability should perform well in SLM processing.

The key parameters and resulting phenomena of SLM arediscussed, showing that careful experimental observation and consideration of material properties, especially welding behaviour, will be critical for success. It is likely that a compromise will have to be reached for materials with undesirable characteristics for SLM. Successful SLM consolidation is heavily influenced by the phenomena that occur during processing and appears to be an optimisation problem since there is a compromise between competing phenomena. For example, in the SLM processing of steels, the maximum scan speed is limited by Rayleigh instability formation. For aluminium, increasing the temperature of the weld pool may result in better wetting of previous layers, but also may melt too much of the existing layer thereby exacerbating balling. The Marangoni convection phenomena may be of benefit when attempting SLM of mixed powders. The stirring effect could help even distribution of molten elements or allow filler particles with a higher melting point and high diffusivity in a lower melting point matrix material to evenly disperse.

Steels are the most prominent material currently used in SLM and are therefore a sensible starting point for the development of customised alloys due to the relative abundance of literature both inside and outside of SLM research areas. Al alloys should be more difficult to process in SLM compared to steels. Al alloys have a low Prandtl number, which in addition to its poor wetting will exacerbate balling phenomena. The one advantage that Al alloys may have is their high thermal diffusivity, which could prevent issues with Rayleigh instabilities; the high diffusivity will however require higher laser powers to overcome the 'heat sink' effect that aluminium is known for [7].

The SLM of Al alloys is predicted to be difficult as the inherent nature of the materials mean that most of the key phenomena observed in SLM are likely to be exacerbated in an unfavourable way. It is essential to utilise experimental approaches to provide an insight into overcoming these challenges. The capabilities and specifications of the SLM machine available for research have been presented and evaluated, allowing comparison to work published by others.

PART I: LITERATURE REVIEW

1. An overview of the aerospace industry and the materials it uses

1.1 The aerospace industry

If one were to ask an engineer what words form in their head when the word 'aerospace' was mentioned, one would expect to hear things such as 'advanced', 'high value', 'accurate' and 'futuristic'. As such, the aerospace industry represents the cutting edge of human engineering, leading the way in developments that provide new products and great benefit to our society.

In the UK, the aerospace industry is one of the most successful sectors of manufacturing and is considered, in terms of value, to be the second largest aerospace industry in the world. Major UK based aerospace companies include BAE Systems, Airbus SAS, Rolls-Royce plc, Bombardier Aerospace and the Smiths Group. In 2003, the UK aerospace industry (UKAI) had a turnover of over £17 billion, of which 93 % was represented by aircraft production, and received 10% of the world market for aerospace products; in the same year the UKAI also generated a trade surplus of over £2.6 billion. The UKAI also invest heavily in research and development, having spent over £2 billion in 2003 alone, which the Society of British Aerospace Companies (SBAC) believes "stimulates innovation and knowledge creation, supports research in universities, and has considerable spin-off benefits into non-aerospace activities" [8].

The aerospace sector can be considered to produce some of the most complex parts in existence today, both in terms of geometry and materials, using both conventional and advanced manufacturing methods.

Whilst there are many scientific fields within the aerospace industry that are vital to its continuation, it can be argued that materials development is the main driving factor behind advances made [9]. The industry strives to develop lighter, stronger materials with higher thermal operating envelopes. Of particular interest are what are termed 'enabling materials'. Enabling materials usher in new technology that was previously unfeasible for varying reasons. An example of an enabling material is a

superalloy (discussed in Section 1.3); these materials allow the deployment of high performance turbine engines - other materials are simply not up to the task.

1.2 Manufacturing processes [9-11]

Aerospace manufacturing utilises some of the most advanced manufacturing techniques available but that does not mean that more conventional processes are ignored. Although Additive Manufacturing (AM) is the focus of this thesis, it is important to analyse existing manufacturing methods in order to allow comparison. Examples of some processes are discussed in this section.

1.2.1 Machining

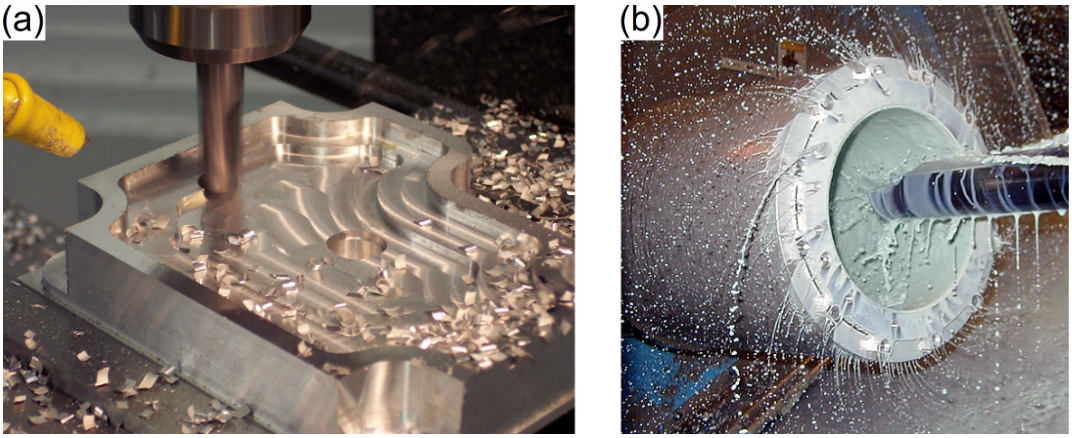

Fig. 1.1: Machining examples: (a) milling [12]; (b) turning [13].

Machining refers to processes that rely on removing material from an initial volume to form the geometry desired for the part in question. This involves operations such as drilling, turning, milling and grinding, as well as various corrosive chemical methods.

The type of material processed has an affect upon machining. Hard, strong materials require slower material removal rates compared to softer, weaker materials: materials also have their own machining 'character', referred to as *machinability*. For

example, titanium alloys are considered difficult to machine (poor machinability) and have somewhat strict guidelines for successful processing; on the other hand, most aluminium alloys demonstrate excellent machinability, allowing High Speed Machining (HSM) to take place. HSM can be considered an advanced machining technique which allows comparatively fast removal rates and (perhaps counter-intuitively) more advanced geometries to be processed.

Downsides of machining include limited geometric freedom in design (the tool must be able to physically get to the material) and typically large waste material generation.

1.2.2 Forging

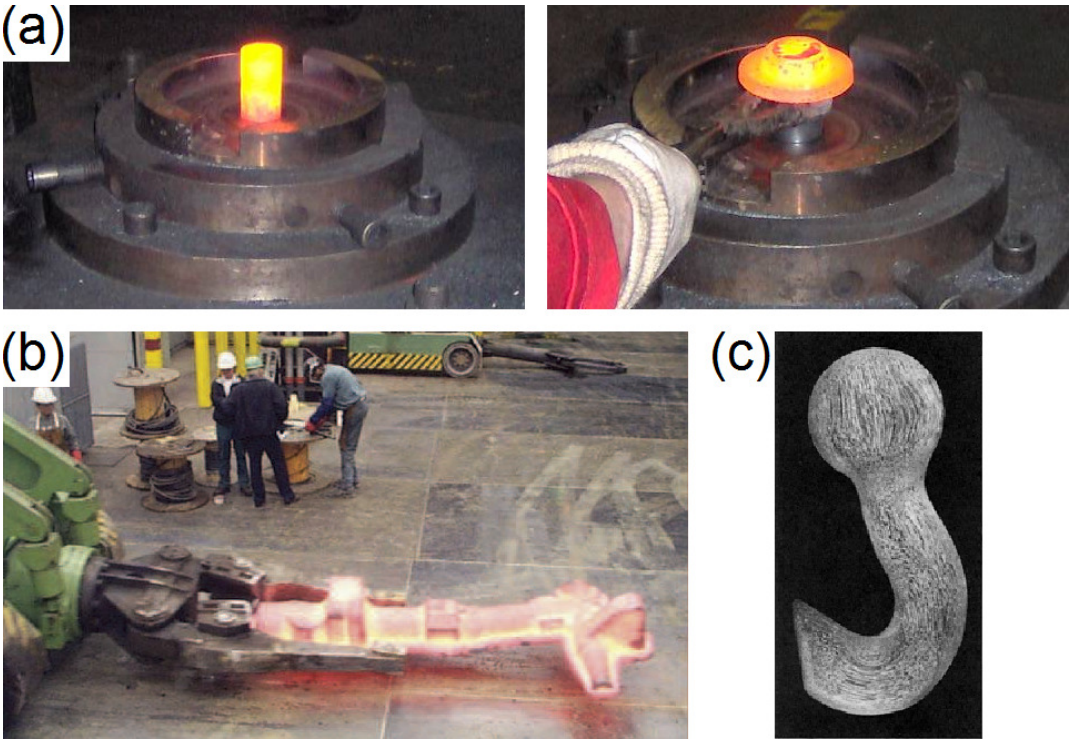

Fig. 1.2: Forging examples: (a) forging process in action [14]; (b) landing gear forging [9]; (c) forged microstructure [15].

Forging is the process of forming metal parts using compressive forces to achieve a near net shape part from a billet of material. Forging encourages favourable grain orientation over the entirety of the part volume, improving fatigue life, strength and fracture

toughness. The scale of forging can vary from small, e.g. beating a part with a hammer, to large, involving hydraulic presses and dies able to exert thousands of tonnes: in addition, forging can also take place at a variety of temperatures, which are related to the recrystallization temperature of the metal in question. Examples of aircraft components that are forged are bulkheads and landing gears.

Disadvantages of forming include a severe limit in geometric freedom and a typical need to set up a dedicated foundry due to the large scale of forging presses; this means that forging is typically only viable with large production runs. Additionally, machining is typically necessary to remove excess material, which can result in warping due to internal stresses inevitably introduced by forging.

1.2.3 Casting

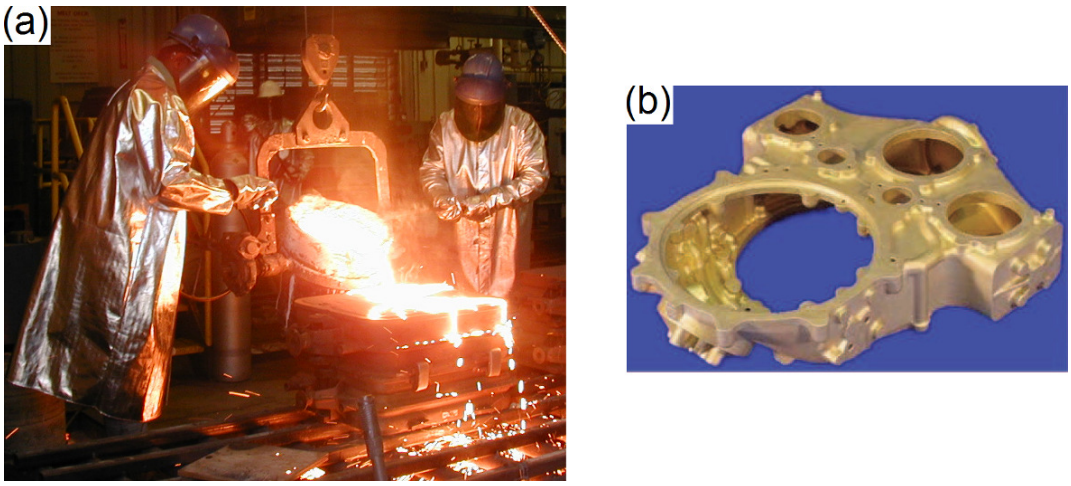

Fig. 1.3: Casting examples: (a) molten metal being poured into a mould [16]; (b) cast magnesium gearbox housing [9].

Casting involves pouring a molten metal into a cavity that has the desired shape of the part: the metal cools and solidifies, taking the shape of the mould. There are several casting methods e.g. Sand casting, die casting, investment casting and continuous casting. Continuous casting can be considered the 'odd one out' in that it does not have a closed mould or die; rather, material is continually extruded through a cooled, open ended die that has the cross section wanted.

Disadvantages depend upon the exact type of casting employed, though there are common drawbacks. All casting methods are susceptible to shrinkage which must be taken into account, and small batches of parts are economically undesirable; parts also typically have a rough surface finish. Additionally, cast parts can be susceptible to porosity if the manufacturing conditions are unsuitable.

A notable derivative of casting is investment casting (also called the 'lost wax' process). It is used to manufacture single crystal turbine blades that show superior fatigue properties and corrosion resistance

1.2.4 Injection Moulding

Injection moulding is fundamentally similar to casting but is the polymer equivalent. The polymer material is heated beyond its melting point, then injected at pressure into a mould. The mould is then cooled (solidifying the polymer), opened and the formed part is ejected.

Disadvantages are as for casting, though part production must be greater to become economically favourable. Geometry is more limited as well since draft angles must be added if the part is to be successfully ejected from the mould; parts also have limits in thicknesses since thick geometry is susceptible to shrinkage which can warp the part.

1.2.5 Powder metallurgy

Powder metallurgy (PM) utilises metal and/or ceramic powders which are compacted and heated to initiate sintering, a diffusion process (described in Chapter 3). Since the technique relies on the sintering phenomenon, it is usually referred to as 'sintering'. Powder metallurgy is especially suitable for materials with exceptionally high melting points (the process typically takes place at less than half the melting point of the material) and/or low ductility. Despite the nature of the process, parts can effectively reach a fully dense constitution.

Disadvantages of PM are the need to take into account shrinkage from the closing of pores, as well as limits in geometric freedom.

1.2.6 Assembly

Assembly is an inevitable part of aerospace manufacturing since produced parts have to link together to form a mechanism. As much as 50 % of the total cost of an aerospace product can be attributed to assembly, hence there is a drive to reduce the amount of parts.

1.3 Materials used within aerospace manufacturing [9]

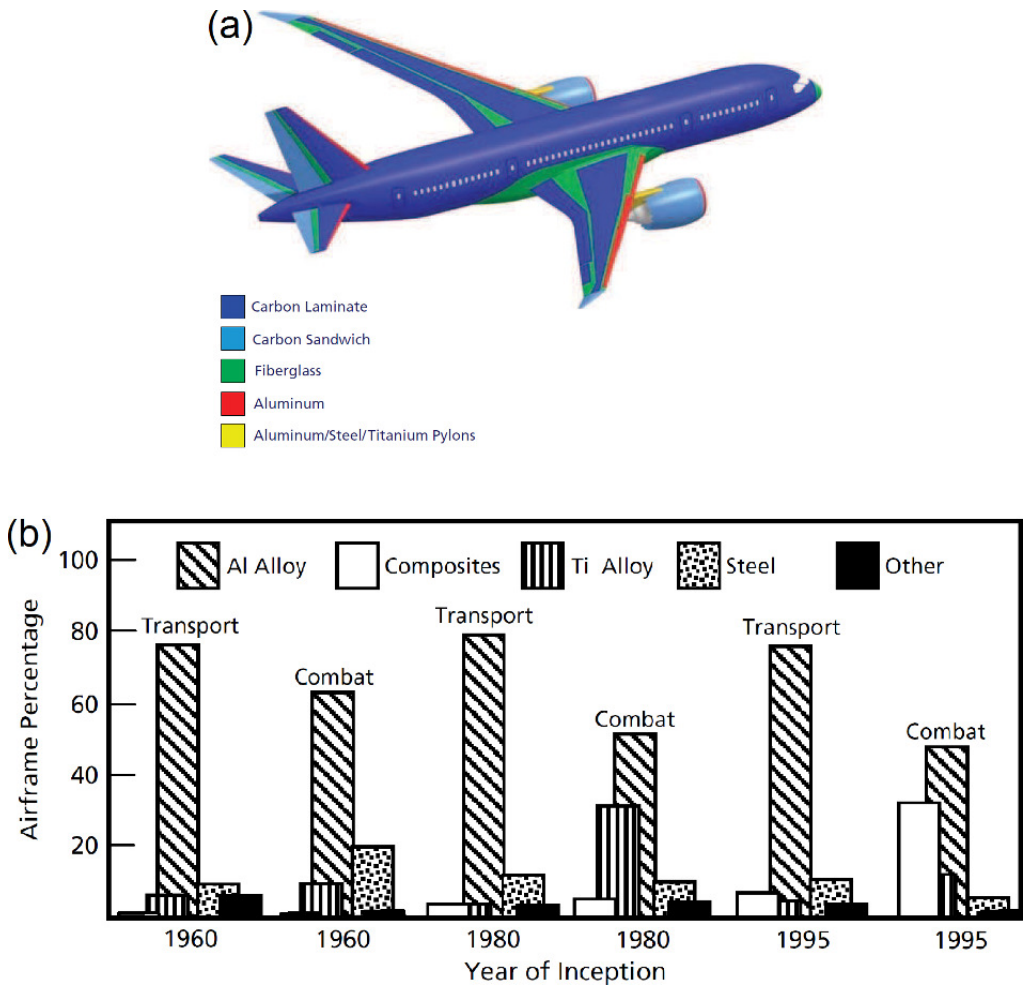

Fig. 1.4: Example of material use in aircraft: (a) Material distribution in the Boeing 787 [9]; (b) Comparison of material use in aircraft over the years [17]

Aerospace engineers have a wide selection of materials available, which all have advantages and disadvantages. Hence, when designing parts for an aircraft, material consideration is extremely important; typical aircraft material usage is shown in Fig. 1.4. A brief introduction to each material follows.

1.3.1 Aluminium alloys

Aluminium alloys have, to date, always been indispensible materials in the aerospace industry and remain highly dominant in usage. This is due to specific strengths comparable to titanium alloys and steel at a lower cost. Good cryogenic, thermal and electrical properties and fabricability are also a feature. Aluminium alloys also display excellent corrosion resistance for the most part due to a naturally occurring oxide layer that forms almost instantaneously when exposed to oxygen. The primary use of aluminium alloys in aerospace is structural applications. Manufacturing wise, aluminium alloys are generally well suited for any process applicable to metals.

Naturally, aluminium alloys have disadvantages: their elastic modulus is comparatively low, as is working temperature. In addition, some of the higher strength alloys can be susceptible to corrosion.

1.3.2 Magnesium alloys

Magnesium alloys are able to compete on specific strength with aluminium alloys. Use of magnesium alloys is limited in aerospace and is typically used for secondary structural components that see high vibration in use (such as gearboxes) due to good damping properties. Downsides of magnesium alloy usage is typically poor corrosion resistance, a result of its high reactivity and anodic position. Additionally, casting and machining of magnesium can be exceptionally dangerous.

1.3.3 Beryllium

Beryllium is a very attractive material choice due to its very low density (around two thirds that of aluminium), high specific strength, good electrical conductivity and low

thermal expansion coefficient. Main uses of the material include high value electronic and optical parts.

There are a number of disadvantages of beryllium, chiefly its limited choices in suitable manufacturing processes. Production methods are almost always limited to powder metallurgy as casting leaves porosity and the material doesn't take well to forming or machining [18]. Beryllium in the form of dust or fine powder is also toxic which therefore requires adequate facilities and equipment to protect those who work with the material [19]. As such, it is more commonly used as an alloying agent, especially when added to copper.

1.3.4 Titanium alloys

Titanium alloys can be considered synonymous with aerospace applications; they enjoy an 'elite' reputation due to high specific strength, corrosion resistance, fatigue strength and operating temperature [20]. Currently, the titanium alloy Ti6Al4V is the most commonly used. Titanium alloys are used in many applications for aerospace including (but not limited to) structural components and low pressure/temperature sections in turbine engines.

The disadvantages of titanium alloys includes high material cost (due to difficulty in extraction and purification) and difficulty to machine.

1.3.5 High strength steels

High strength steels (a steel is considered high strength if its yield strength is above ~1380MPa) are often used for critical applications such as landing gear, where the high volumetric strength, stiffness and fatigue strength are advantageous. Even so, steels typically only account for approximately 5-15% of an aircraft's weight [9]. Steels also have an advantage in that they have a longer history of use so are more understood as a material.

Disadvantages of high strength steels are high densities and susceptibility to brittle fracture.

1.3.6 Superalloys

Superalloys are nickel based alloys. The term 'superalloy' is perhaps somewhat misleading as it would imply a material that has extraordinary mechanical strength; rather, the name refers to the alloys' high performance at high temperatures. Some superalloys are able to operate under load bearing conditions in excess of 80-85% of their melting temperatures [9]. The characteristics of a superalloy are high strength, fatigue, creep and corrosion resistance whilst operating at high temperatures for extended periods [21]. A disadvantage of superalloys is their relatively high density and difficulty to machine but this is compensated for by their other properties.

In aerospace applications, superalloys are generally used to produce turbine blades for the high pressure/temperature sections of turbine engines as well as parts for rocket engines [22]. Mentioned in Section 1.2.3, superalloys are perhaps best known for their use in the production of single crystal turbine blades.

1.3.7 Composites

'Composites' refers to materials which are made from a combination of two or more sub-materials which retain their properties (rather than forming a compound or alloy). The term 'composite' refers to Polymer Matrix Composite (PMC), Metal Matrix Composite (MMC) and Ceramic Matrix Composite (CMC). Different composites offer different advantages but they all share a common disadvantage: high cost.

PMCs are by far the most common of the composite materials. PMCs offer very high specific strengths and moduli at very low densities, especially in the case of carbon fibre reinforced materials. Corrosion and fatigue resistance is also excellent [23]. PMCs are typically used for the aircraft skin. On the downside, PMCs can be susceptible to water absorption.

MMCs have higher specific strengths, moduli and temperature resistance as well as lower thermal expansion coefficients when compared to the base metal. However, this is countered by reduced toughness [24]. MMC use is currently highly specialised and scarce but could be used as a structural material [25].

CMCs combine the desirable properties of ceramics; high moduli, compressive strength, temperature capability, corrosion resistance and low thermal conductivity; and combine the higher toughness of the reinforcing material. One use of a CMC is the

leading edges of the Space Shuttle, which are subject to incredible temperatures during re-entry. CMCs are currently incredibly expensive, possibly the most expensive material available today [26].

2. Additive manufacturing

Additive manufacturing (AM) is the name given to a group of processes that directly manufacture computer aided design (CAD) models by adding material to a part, typically in a layer by layer approach [27]. The official definition of AM is:

"Additive manufacturing is the process of creating a physical object through the selective fusion, sintering or polymerisation of a material." [28]

AM is also referred to as additive layer manufacturing (ALM), rapid prototyping (RP), rapid manufacturing (RM), additive fabrication (AF), as well as a host of other names: suffice to say there are several monikers currently available since the ASTM Committee F42 (discussed later) is fairly new at the time of writing. Additionally, AM includes several manufacturing processes that can produce parts out of polymers, resins, metals and composites which have their own names and abbreviations, some of which are discussed later in this chapter.

AM is seen as a technology that is still in development though it has existed since 1988 with stereolithography (SL) being the first commercial AM process [29]. In truth, it is possible to argue that AM is both a mature and immature process. An example of AM's successful use is in the manufacture of dental implants [30]; conversely an example of its immaturity is the currently limited selection of materials, though more are being added to the repertoire with continuing research [31].

2.1 Overview of additive manufacturing

AM offers new possibilities compared to conventional manufacturing but also has limitations, be it in geometry, materials or otherwise, which are discussed in this section.

2.1.1 Standard manufacturing technique

Regardless of the exact nature of an AM process (of which a few are covered later in this chapter), the overall manufacturing method is more or less equivalent.

First, a computer aided design (CAD) model must be generated. This can be done by any method, so long as the file can be read or translated by the machine used. Currently, the de facto file format for AM is the STL file which was the open file format developed for SL [32]. STL, originally an abbreviation of 'stereolithography', is now treated as a backronym standing for 'standard triangle layout' (or an equivalent nomenclature) which is logical since converting a CAD file into an STL translates it into an approximated surface model consisting of linked triangles.

Having produced the CAD model, the model is then processed by the software running the AM machine. This involves digitally 'slicing' the model into discrete layers that typically vary from 20 to 100 μm [33]: each layer is then translated into machine code.

The AM process then begins the actual manufacturing phase. In most cases, a layer of material is deposited and the cross section of the CAD model corresponding to the layer height position is consolidated using a scanning laser or other means. After the cross section of the layer in question has been consolidated the platform on which the model rests moves one layer thickness down and more material is deposited for the next layer. The cross section of the next layer is then consolidated into this newly deposited material, adhering to the previous layer. The cycle repeats until the part has been produced in its entirety.

Once the part in question has been finished, there are post process procedures to follow. Unconsolidated material must be removed, as well as any supporting structures (discussed later). Depending on requirements, the part may then have to undergo further treatments to improve surface roughness, UV resistance etc.

2.1.2 Design freedom

When using conventional manufacturing techniques, designers have to be mindful of process limitations. Consider injection moulding: when designing for injection moulding, features such as draft angles, non re-entrant geometry, split line location and wall thickness all have to be taken into account [31]. With the advent of AM, many

design challenges that designers have had to overcome in the past can be alleviated; however as with any process AM does have limitations which are dependent on the technology used. For example, each AM process has a limit on the minimum feature size it can build and new geometry limitations are imposed depending on the AM technique used.

2.1.3 Geometry limitations and supports

Although AM techniques have considerably more design freedom than conventional manufacturing techniques, there are new limitations introduced that must be taken into account for part design. All parts designed by AM should allow for unused material removal, either by designing the part as an open cell structure or allowing a post process machining operation to open up closed volumes, though the designer may opt to leave unused material within the model if necessary or desired.

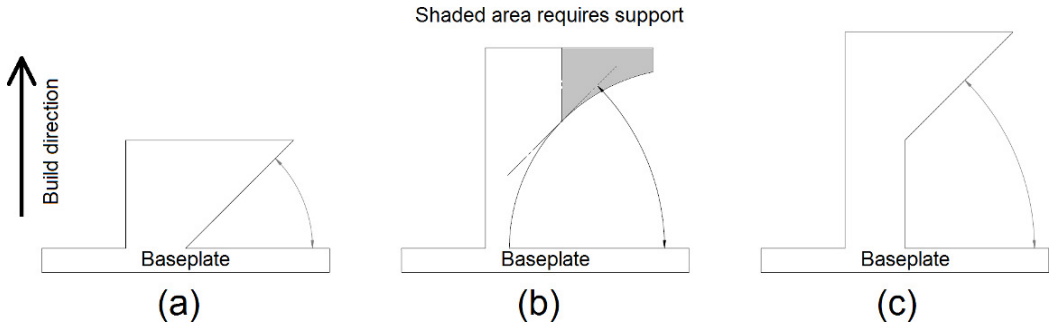

Fig. 2.1: Basic geometry limitations in most AM processes: (a) angles less than a certain value to the base plate require support to maintain integrity; (b) fillets are possible but still require support when the tangent angle decreases to less than a certain value; (c) overhangs can start from any point on the model provided they are at a suitable angle or greater to the base plate or have support.

Additional limitations take form in the required support of processed material. Due to the nature of many AM techniques (for example SL), overhanging features typically have to be supported during manufacture (see Fig. 2.1).

Support structures are required in most AM processes for geometries that have significant overhangs (though the exact reason for supports will depend upon the process used), and also act as a method of attaching a part to a base plate if required. An example of support structures is shown in Fig. 2.2.

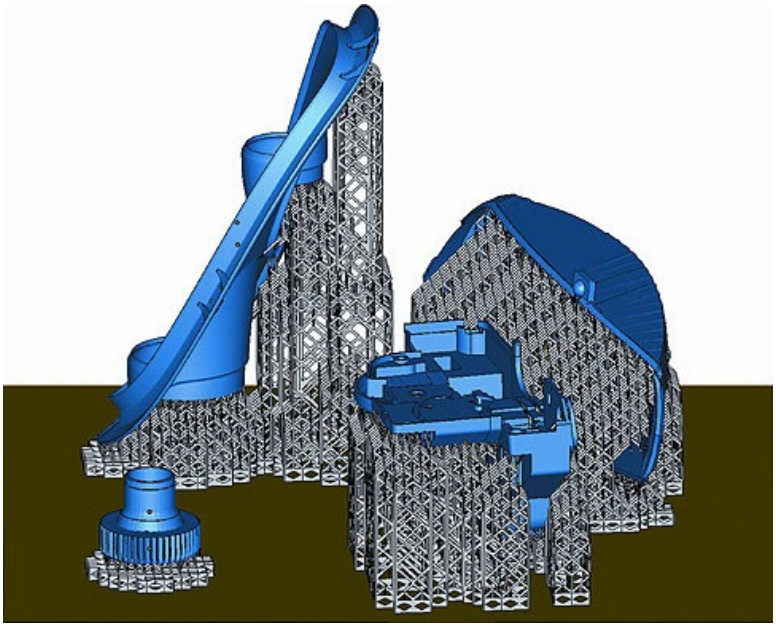

Fig. 2.2: Example of supports generated for parts for AM processing [34].

Part orientation is also important within AM to optimise support requirement and pertinent properties. Most, if not all, AM techniques have anisotropic properties, particularly in the build direction [35-37]. Surface roughness is also affected by part orientation due to the 'step' effect which is a result of the layer by layer building routine; optimisation of surface roughness through part orientation is able to be computationally modelled [38].

2.1.4 Materials

Currently, AM has a limited range of material choices available but it does at least offer some choices in polymers, metals and composites. Metal AM parts can be produced from CoCr alloys, steels, Ni alloys and Ti alloys [33]: recently, Al and Cu alloys have

been commercially released for AM use [39, 40]. Polymer AM parts are primarily produced in DuraForm PA (a nylon-like material) [41] and acrylonitrile butadiene styrene (ABS) [42]; additionally polymers are typically reinforced with a filler material, an example being DuraForm GF which is Duraform PA blended with glass particles [43]. Recently, polyetheretherketone (PEEK) has been released for commercial AM use [44]; a significant advance since PEEK is considered a high strength engineering polymer. Resin parts (mentioned due to resin's similarity to polymers) can be produced by the SL process, which are able to have translucent properties. As with any manufacturing process, research in materials is an ongoing process for AM [42]: potential composite material use is also keenly investigated [45].

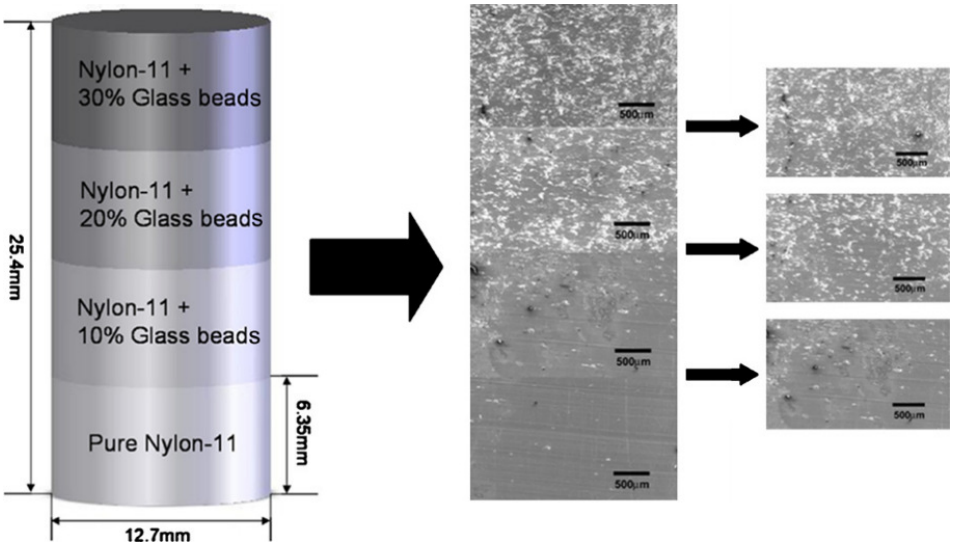

Fig. 2.3: Example of a functionally graded material. In this case the overall material is a polymer matrix composite with varying glass filler levels, manufactured using SLS [46].

Functionally graded materials (FGMs) are a favourable research topic in AM. Simply put, FGM refers to a composite-like material that has different mechanical properties in different regions typically due to varying the mixing ratio of two or more materials (see Fig. 2.3). The term 'FGM' is perhaps a bit misleading as an FGM requires a change in material properties over a distance, hence the term 'functionally graded part' may be more apt, though FGM will be used from hereon regardless. Algorithms for

FGM implementation in AM have already been researched [47] but actually producing an AM machine that will allow FGM production is difficult. FGMs also raise material recycling issues since most AM processes rely on depositing a bed of powder, which makes extracting different materials difficult. Note that FGMs should not be confused with functionally graded structures, being a part designed with an internal structure that varies from unit cell to cell in geometry and/or in scale [48].

2.1.5 Additive manufacturing standards

Until recently, AM parts were either assessed in-house or by the end user using proprietary testing methods. However in 2009 an ASTM committee, 'ASTM Committee F42 on Additive Manufacturing Technologies', was formed to start laying down industrial standards for AM [28]. The aims of the committee are to:

"*allow manufacturers to better compare and contrast the performance of different additive processes; improve the purchaser/supplier relationship by enabling part requirements to be more accurately specified; help new adopters to more appropriately use and implement these technologies; and enable researchers and process developers to provide repeatable results that can be independently verified.*"

There are five technical subcommittees:

- F42.01: Test Methods
- F42.02: Processes
- F42.03: Materials
- F42.04: Design
- F42.91: Terminology

Standards have yet to be implemented since there is still much discussion to be had, however the introduction of F42 indicates that AM is now becoming a mature process that will soon be considered a true manufacturing method rather than a niche technique.

2.2 Leading additive layer manufacturing processes

There are several technologies available today that fall under the AM umbrella: of these technologies, a few arguably come to the forefront in terms of production capability and are discussed below. It must be pointed out that the choice of 'suitable' technologies is essentially a personal choice and may always be debated, but in the interests of keeping discussion to a suitable size, many AM technologies and derivatives have been omitted. As such, the following AM technologies are discussed: SL, Selective Laser Sintering (SLS), Selective Laser Melting (SLM) and Fused Metal Deposition (FMD).

2.2.1 Stereolithography

Stereolithography (SL) was the first commercial AM process to be released [29]. As such, the process currently has the most machines available worldwide and is therefore considered worthy of discussion.

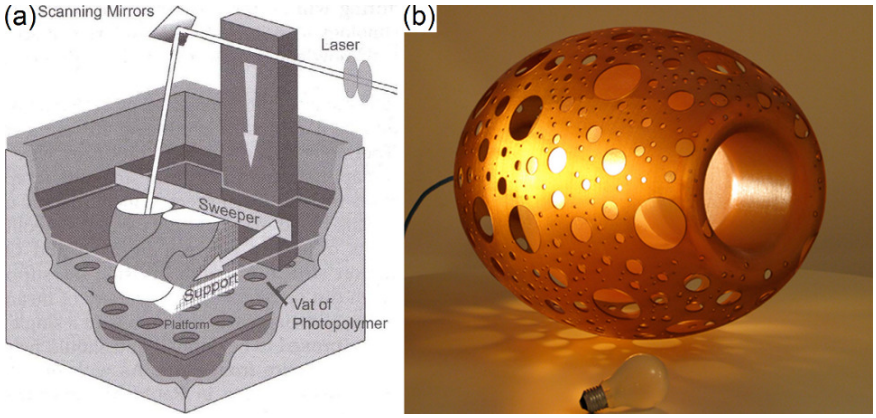

Fig. 2.4: (a) Schematic of the stereolithography process [33]; (b) example of a stereolithography art piece ('Handshake Big' by Arik Levy [54]).

The SL process uses an ultraviolet laser to consolidate a photo-curable resin and is therefore considered a liquid-based process. SL works just like any typical AM process (see Fig. 2.4a). As each layer is consolidated, the part is then submerged one layer deep in the resin and the next cross section consolidated. Consolidated

components typically have a translucent, amber coloured appearance which is visually pleasing; it is common to find artistic pieces manufactured by SL due to the aesthetic qualities of the consolidated resin (see Fig. 2.4b).

Until recently SL parts were (and for the most part still are) made out of unreinforced materials but research in this area is ongoing. Currently, new composite materials have been developed that dramatically improve the mechanical properties of SL parts, such as Accura Xtreme Plastic [49] (a ceramic filled composite) and Accura Bluestone Material [50] (a nanocomposite) but these materials are still nowhere near as strong as a continuous composite: in fact, the strength is more akin to conventional injection moulded parts. Glass fibre additions have been investigated and initially showed great promise for reinforcing SL parts but ran into difficulties upon attempting to manufacture thicker parts due to uncured material at the matrix/fibre interface [51]. Later, the possibility of carbon fibre reinforcement has been demonstrated but requires a post process heating regime to fully consolidate the resulting material [52]. Finally, FGM manufacture via SL has been successfully demonstrated by Choi *et al* [53], which can be considered a huge leap forward for SL technology.

Advantages of SL are superior accuracy and surface finish compared to other AM processes, as well as the distinction of currently being the only AM process that can manufacture translucent parts (this extends to any resin based AM technique): SL can also build the smallest scale parts out of any AM process, being able to process sub micron geometry [55]. Disadvantages are typically low mechanical properties (though this has recently been remedied with the addition of composite materials) and brittleness [51], caused by susceptibility to ageing due to the UV sensitive nature of the consolidated material [56]. SL parts also require supports for overhanging geometry since the liquid resin is incapable of supporting material, which in itself limits geometry and can reduce the surface finish quality of parts [42]. No literature has been found on the recycling of SL materials, though it is logical to assume that recycling cannot be maintained indefinitely since liquid next to the processed geometry will still be subtly altered and this 'semi-processed' material will increase in volume with each build.

2.2.2 Selective laser sintering

Selective laser sintering (SLS) was the second AM process released commercially, following on the heels of SL [29]. It is referred to as a 'powder bed' process. The process

functions similarly to SL but uses powder in place of the liquid resin (see Fig. 2.5): laser types vary for the material being processed. SLS can process many materials but is predominantly associated with producing polymer and polymer composite parts [57]; an example of a model produced by SLS is shown in Fig. 2.6. In 2009 EOS released the first commercial SLS machine, the EOSINT P 800, to successfully process PEEK [44]. PEEK parts produced by SLS are reported by EOS to be able to attain a tensile strength of up to 95 MPa, which is 95 % of what is believed to be the conventionally produced grade [4].

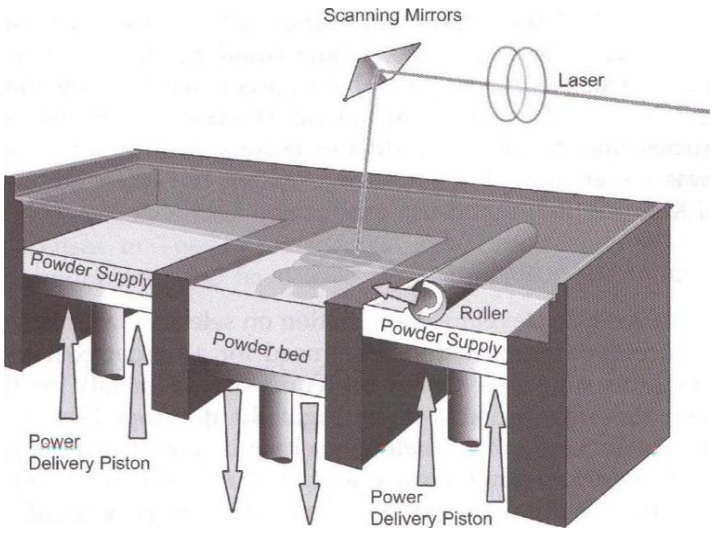

Fig. 2.5: Schematic of the selective laser sintering process [33].

Since SLS is commercially used to produce polymer parts, there is interest in manufacturing *in situ* polymer composites. Due to the layer based nature of the SLS process it is currently difficult to produce a continuous fibre based composite [45], but the process lends itself well to investigating discontinuous reinforcement since any filler particles can simply be blended with a polymer powder. Indeed DuraForm GF, a powder blend consisting of DuraForm PA and glass, is currently available [43] as a material choice: it offers an approximate 160 % increase in stiffness of unfilled Duraform PA [59] but at a cost of a 40 % reduction in tensile strength and a density increase of 49 %. The enabling of PEEK processing in SLS also opens up new avenues in the manufacture of carbon fibre composites since PEEK demonstrates ideal qualities

as a matrix material [60], however as mentioned the difficulty of deploying continuous fibres within SLS still has to be overcome. Nanocomposites are also being considered: work by Salmoria *et al* has looked at the influence of MultiWalled Carbon NanoTubes (MWCNTs) [3], which found that a 0.5 wt% MWCNT/PA12 composite showed a 9.3 and 31.5 % increase in tensile strength and flexural modulus respectively. Fatigue load capacity was also found to increase by approximately 12 % as did elastic modulus (18 %).

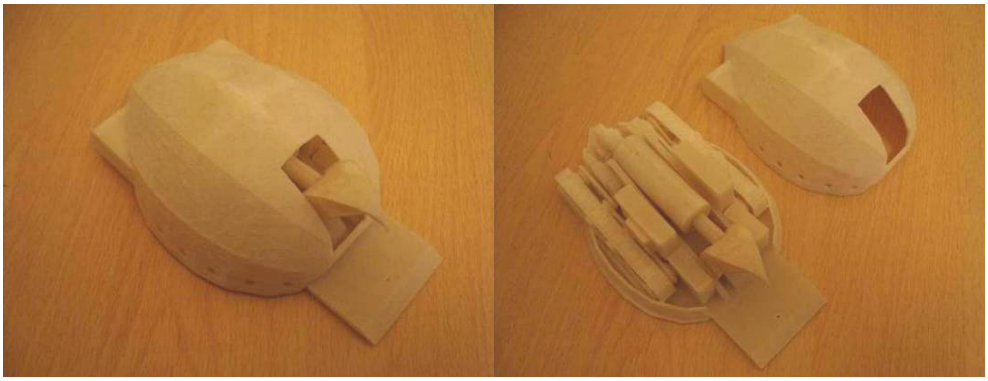

Fig. 2.6: Photographs of a demonstration model designed and produced by SLS by the author for an undergraduate project. The model also has moving parts.

The SLS process has a significant advantage compared to other AM procedures: no support structures are required. The deposited powder bed itself acts as a support and geometry does not have to be attached to a previously consolidated layer, also meaning that a base plate is not needed. As such, SLS is the AM technique with the most design freedom. Disadvantages are comparatively poor consolidation of non-polymer materials compared to SLM and an initial lower quality surface finish (though this is subjective in nature). Materials also cannot be recycled ad nauseam: Duraform PA can only be recycled six times [61] and EOS PEEK cannot currently be recycled at all [1].

2.2.3 Selective laser melting

Selective laser melting (SLM) is a derivative of SLS, effectively swapping polymer for metal (examples of SLM parts are shown in Fig. 2.7). As such, perhaps the main

difference between the two processes is the use of a considerably more powerful laser which is necessary to counter the increased melting points, reflectivity and thermal conductivity of metals [40].

Fig. 2.7: Photographs of examples of 316L stainless steel parts manufactured by the author (not designed) using SLM: (a) an enlargement of a synthetic bone structure; (b) a light capturing part for the Met Office. As far as is known, the part in (b) is actually in service on an aircraft as part of some test equipment, though considerable post processing was required to bring the part up to spec.

SLM is actually a trademark of the MTT Technologies Group [62]. Similar technologies exist such direct metal laser sintering (DMLS) by EOS [63], LaserCusing by Concept Laser [39] and electron beam melting (EBM) by Arcam [64][1]: EBM differs from SLM in that in place of a laser, an electron beam is used to consolidate material.

Material research is very active in SLM and involves ceramics [65], composites [66] and alloys [5]. The amount of material research in SLM appears to be greater than other AM processes, likely due to the ease of creating a new composite/alloy simply by mixing different powders together. As such, it is difficult to single out particular examples since all show benefits, ranging from improved strength to increased wear resistance.

Advantages of SLM are the ability to directly manufacture full metal parts and the ease of material investigation. Unused materials are also believed to be recycled

[1] The author has found that company representatives can get quite upset when it is implied that their technologies are effectively identical but has yet to see proof of any fundamental differences.

indefinitely, after having been sieved to remove large agglomerates that have formed during processing (though from experience effectively all unused material can be recovered). Disadvantages are the need for supports for overhanging parts due to reasons discussed later in Chapter 3, relatively poor surface finish prior to post-processing and a need for post process annealing [67].

2.2.4 Fused metal deposition

Fused Metal Deposition (FMD), also known as Laser Consolidation (LC) or Direct Metal Deposition (DMD) has a significant difference compared to the AM techniques already discussed. Whereas the AM techniques covered up to this point rely upon layers of material (powder or liquid) being deposited prior to consolidation of a cross section of the part, FMD deposits material as the laser scans (see Fig. 2.8). Hence, FDM and its derivatives are referred to as 'blown powder' processes. In these processes, the material is suspended in a gas and blown at the point at which the laser is scanning, resulting in material consolidating at this point. The author, during his tenure, was able to observe LC in action since the Damascus project [68] was active in the same work area.

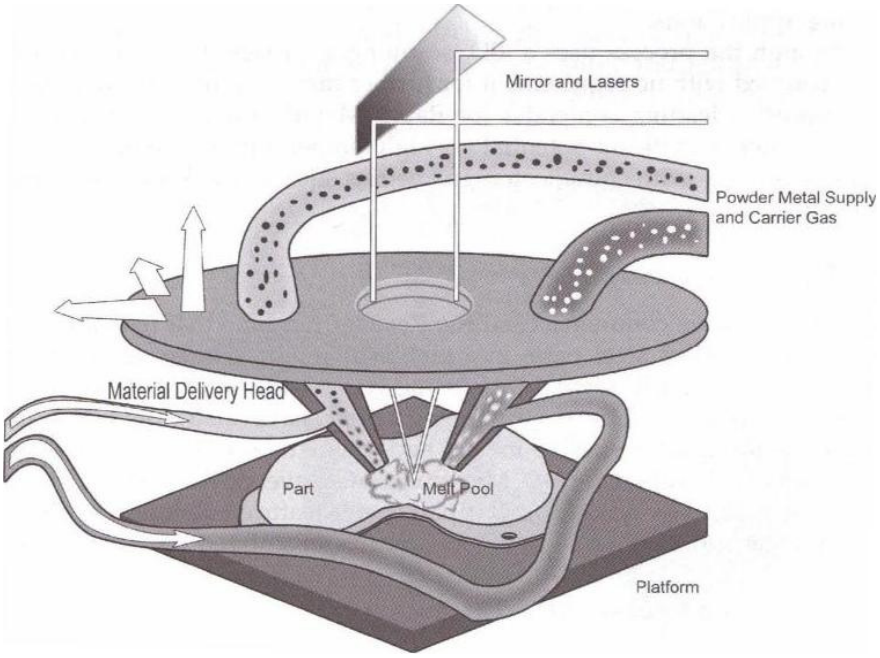

Fig. 2.8: Schematic of a typical fused metal deposition process [33].

Geometry potential is limited in FMD. As with SL and SLM, parts must be built on a base plate and have limits to the overhang angle that can be built: however, FMD cannot generate support structures. In the case of LC, the parts were limited to 'shell' structures i.e. parts with wall thicknesses but the base plate was mounted on a five axis mechanism, meaning the part being built could be moved to allow a wider range of geometries to be built.

Materials research for FMD is dominated by metals research which is believed to be due to the fact that polymer particles need to be 'still' to successfully bond, as do ceramics particles to allow sintering: either way, no literature could be found for FMD processing of polymers or ceramics. MMCs are capable of being produced by FDM, an example being the development of a steel/TiC MMC by Novichenko *et al* [69]: hardness of resultant materials could be boosted by up to 96 %, which could have implications for strength and wear properties.

As with SLM, unused material can be easily recycled, with negligible losses.

2.3 Aerospace use of additive layer manufacturing

The aerospace industry is secretive by nature and so aerospace deployment of AM parts still remains relatively unknown to the general public. Fortunately, access was granted to the AM engineers at Airbus Filton, for which the author is extremely grateful [1, 2].

The primary interest in using AM to manufacture parts for aerospace is to reduce weight through AM's ability to produce parts with complex, lightweight structures. Reduction in weight translates to a decrease in fuel usage, which saves money as well as reducing carbon emissions. Mentioned earlier, AM excels at producing geometries conventional manufacturing either has great difficulty with or simply cannot. In particular, advances in computational resources mean that advanced geometry refining methods such as topological optimisation [70] can be implemented. Another perk of using AM is the ability to merge multiple components into one. Assembly is perhaps the most time consuming process when looking at the overall manufacture of an aircraft, so the ability to reduce the number of parts required results in both time and money savings.

Currently AM parts are not used in aerospace structural/critical applications due to a lack of a proven track record (though AM use in defence/military applications may be more common) but this is something that AM aerospace engineers would like to

change. As such, use is limited to applications where a potential failure is not of immediate concern. A couple of case studies concerning AM use in aerospace applications have been published by Hopkinson *et al* [33] which are discussed below.

2.3.1 F/A-18E/F Super Hornet cooling duct

The US Navy wanted to reduce costs (both manufacturing and servicing) in the forward section of the F/A-18, as well as incorporating new systems. The additional systems required supplementary cooling ducts that would fit within the limited confines of the aircraft. Two criteria were particularly important: firstly, the ducts required a guaranteed minimum material strength even though they were not structural components; secondly, the parts must be accurate enough to integrate correctly into the aircraft.

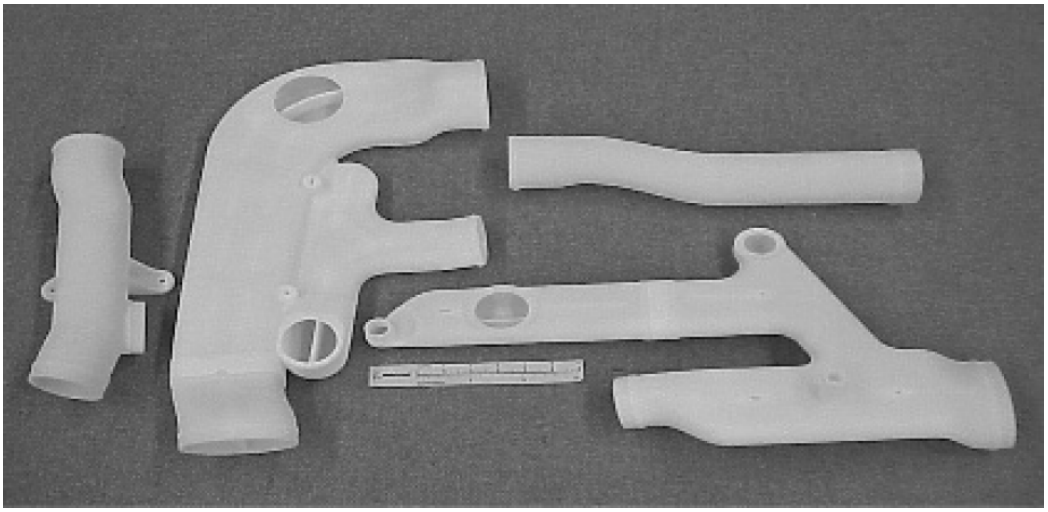

Fig. 2.9: Cooling ducts for the F/A-18E/F Super Hornet manufactured from Duraform PA, produced using SLS [33].

The SLS process showed its advantages for the manufacture of the ducts in several ways. Firstly, assemblies that would have to be produced as two or more parts by conventional means could be merged into one part: parts such as flow straighteners and mounting brackets. Secondly, advanced geometries could be simply integrated, allowing the designers to fit the cooling ducts around existing obstructions. Thirdly,

designs could be easily modified and updated since the lack of fixed tooling allowed revision freedom. Example duct components are shown in Fig. 2.9. It is also estimated that the SLS parts effected a 20 % weight saving compared to conventional manufacturing techniques.

The ducts were successfully implemented and as a result other ducts were later replaced and updated with SLS parts.

2.3.2 International Space Station capacitor box

Originally, the part shown in Fig. 2.10 was to be manufactured by conventional injection moulding. The engineers involved in the project were keen to minimise manufacturing time where possible and the injection moulding tooling would require two months to make for what would be a limited production run.

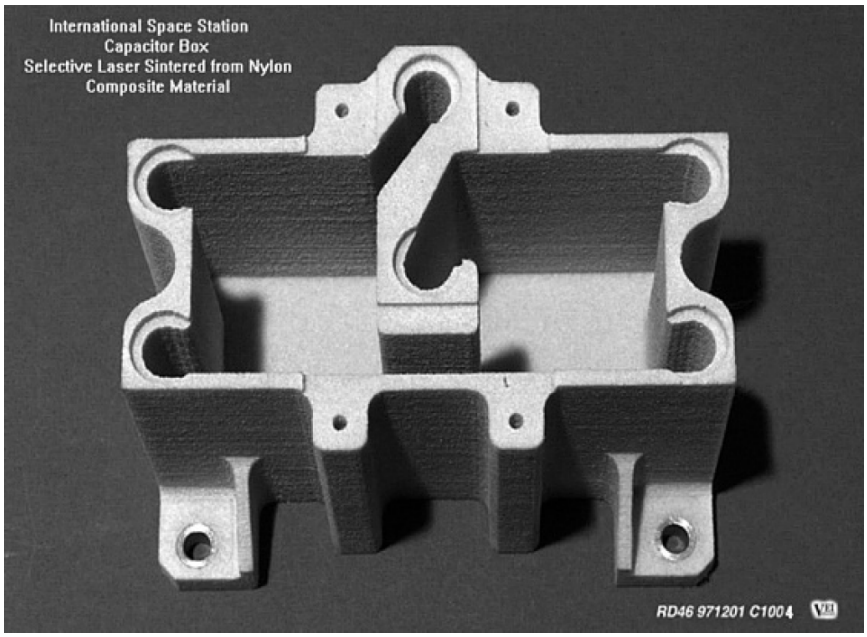

Fig. 2.10: Capacitor box for the International Space Station, manufactured from Duraform GF using SLS [33].

At the time, little was known about the material used and so a verification process was undertaken. As well as basic mechanical tests, toxicity and resistance to

fungal growth was also a concern since the part would be contained within a confined human atmosphere. Quality assurance was considered paramount and so was implemented at every stage; the most significant perhaps being the inclusion of tensile test samples with each build to check material conformity between batches.

The mounting holes for the part were required to be stable, and so undersize holes were put in the model. Post process, these undersize holes were reamed to size and allowed stainless steel inserts to be pressed and bonded into the part. Additionally, extra material was added to the base of the box so that a post process surfacing operation could bring the overall height of the box to within tolerances.

The project was successful and led to the manufacturing of other parts by SLS.

3. Selective laser melting

Selective laser melting (SLM) is a powder bed AM process that is currently used to process a range of metals as it is briefly discussed in Chapter 2. Of the AM processes available, SLM is deemed the most suitable for aerospace use due to its capability to process the stronger materials available to AM while maintaining an acceptable level of geometric freedom. Like any other manufacturing process, SLM has many areas that can be discussed and researched, from optimisation of production parameters to implementation in a manufacturing line.

In keeping with discussion up to this point, the main area of interest is material development while secondary interest lies with the production of advanced geometries. Both of these interests depend upon the capability of the SLM process, so it is necessary to examine the parameters in SLM, as well as phenomena that occur during and even after processing.

This chapter looks at the important parameters within the SLM process, as well as the phenomena encountered during and after processing. Current material use is analysed, as well as key material research areas: geometric considerations are investigated in more detail. Finally, an evaluation of the SLM machine used for experimentation is undertaken.

It should be noted that many parameters and resulting phenomena can display linked behaviours and so it can be difficult to talk about one without referring to the other. As such, it is recommended that relevant sections of this chapter are read more than once to allow a deeper understanding of the relationships that occur in the SLM process.

3.1 Key parameters in selective laser melting

As with any engineering process, SLM has its own set of parameters. The effect of the parameters on consolidation of parts is discussed later in Section 3.2: for now, a brief description of the parameters is provided.

3.1.1 Laser type

Different types of laser are used in AM processes type of laser used has an influence on the material being processed. Typical lasers used in SLM are CO_2, Nd:YAG and IR fibre. Aside from reflectivity issues at different wavelengths, there is also the matter of using either a pulsed or continuous laser: influence of laser type is discussed later in Section 3.2.

3.1.2 Laser power

Laser power can be considered to be the most important parameter to consider in SLM when combined with laser spot size. After all, if a laser does not supply enough power, a thermal equilibrium will be reached where the material being processed can conduct thermal energy away at the rate at which it is supplied: conversely, too high a laser power will result in scission of the material. Laser power and *laser scan speed* have a critical relationship, discussed later.

3.1.3 Laser scan speed

Laser scan speed is simply that: the speed at which the laser spot moves over the surface of the material. The most obvious influence scan speed has on SLM is the length of time it takes to complete processing a part - doubling the scan speed will approximately halve the build time, although this ignores other factors such as additional time incurred due to powder deposition etc. Scan speed also influences some of the more prominent phenomena that occur in SLM when considered along with *laser power.*

3.1.4 Laser spot size

Laser spot size, combined with laser power, defines the *energy/heat flux* the laser can exert. The spot size also defines the minimum thickness possible during manufacture since the spot size, in conjunction with *laser power*, defines the weld pool size (Section 3.2).

3.1.5 Layer thickness

Like laser scan speed, layer thickness directly affects build time and surface finish, as well as overall consolidation. Layer thickness is limited by the size of the powder used and the time allowed to produce a part.

3.1.6 Hatching spacing

Since the SLM process relies on consolidating cross sections of the part, these cross sections must be filled in by multiple laser passes using a raster technique or variant thereof. Hence, the distance between each raster is called the 'hatching spacing' (or 'scan spacing'). This can have significant effects upon consolidation and is subject to optimisation, as demonstrated by Xie *et al* [71].

3.1.7 Energy density and heat flux

There are two types of energy phenomena that can be calculated in SLM, which are all related to heating material:

- The heat flux of the laser spot ($\vec{\phi}_q$), measured in W m^{-2}.
- The energy delivered per unit volume, energy density ($E_{Density}$), measured in J m^{-3}.

The values of these definitions can be calculated from a combination of the parameters previously described and are described in the following equations:

$$\vec{\phi}_q = \frac{P_{Laser}}{\pi R_{Laser}{}^2} \tag{3.1}$$

$$E_{Density} = \frac{P_{Laser}}{v_{Scan} \times d_{Hatching} \times d_{Layer}} \tag{3.2}$$

where P_{Laser} is the laser power, R_{Laser} is the laser spot radius, v_{Scan} is the laser scan speed, $d_{Hatching}$ is the hatching spacing and d_{Layer} is the layer thickness.

It is important to note that the energy density is independent of the heat flux. Additionally, the effect of multiple scans per layer on energy density can be taken into account simply by multiplying by the number of scans per layer. If a heating system is used (such as for reducing residual stresses, see Section 3.3.7), this can also be added by calculating the heat energy supplied over the course of the build and dividing by the part volume: one must bear in mind though that this does not represent the actual sum of energy at a point in the model since all deposited material is being heated as well.

3.2 Laser parameters [72]

The laser (light amplification by stimulated emission of radiation [73]) is a key component in many ALM processes. Lasers are a research area unto themselves and so only the essential information that affects SLM is discussed.

Lasers supply energy in the form of a beam of electromagnetic radiation. Apart from perhaps the most obvious characteristic of power, lasers also have the following characteristics which affect materials processing: wavelength, mode, spot diameter, Q-switching and polarisation. There are also other variables that rely on the previously mentioned parameters: reflectivity, laser/material interaction

3.2.1 Wavelength

The wavelength of a laser also gives its frequency since the beam travels with a speed of *c*; wavelength is limited by the lasing medium (the material used to generate the laser beam). For materials processing, the wavelength can significantly alter reflection of the beam from a surface (discussed later).

3.2.2 Mode

The laser, simply put, is typically a cylinder containing the lasing medium with a mirror at one end and some sort of combination of mirror and aperture at the other. Due to this arrangement, there are light waves generated in the medium that do not run parallel to the cylinder's central axis. Suffice to say, this results in a laser spot that has an uneven intensity distribution. These distributions can be calculated and are assigned 'modes'. Of these modes, the most common is 'TEM00 and TEM01', shown in Fig. 3.1.

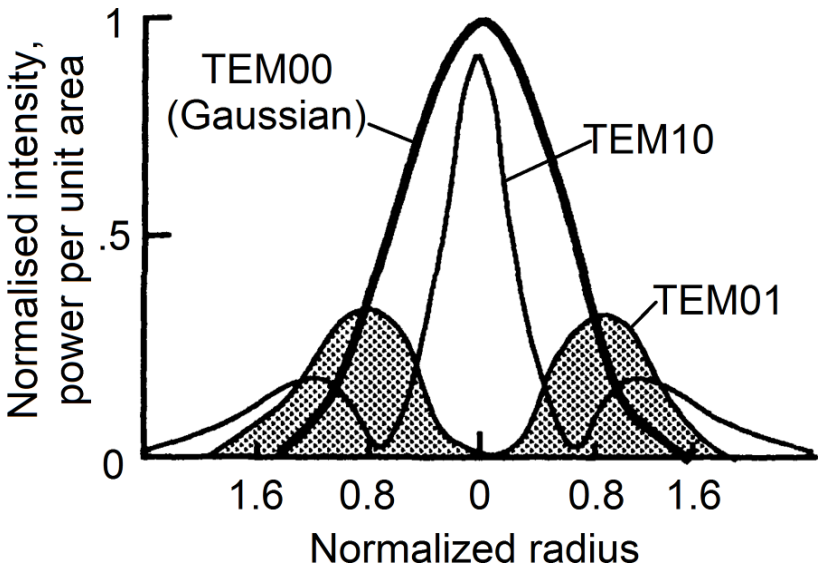

Fig. 3.1: Graph of the intensity distribution of a laser beam spot for TEM00, TEM01 and TEM10 laser modes [72].

From henceforth, this thesis will only concern itself with TEM00 mode, a Gaussian distribution.

3.2.3 Laser spot

Whilst detailing the diameter of a laser beam may seem to be unnecessary, due to the Gaussian distribution of the beam intensity it is important to define where the 'edge' of the laser spot is. Sharp [74] recommends that the beam diameter should defined by

when the energy drops to $1/e^2$ of the highest laser energy – meaning that ~86% of the laser energy is taken into account. Needless to say the beam diameter can also be affected by various methods, the most obvious being optical lenses. The size of the laser spot is limited by two factors: diffraction limits and spherical aberration. Diffraction limits come about for the same reason that lasers can operate in different modes. Spherical aberration refers to the inability to produce a perfectly shaped lens - the smaller the desired laser spot size, the more meticulous (and therefore expensive) lens crafting is required. For the aforementioned reasons, a laser may never focus to a singular point.

3.2.4 Polarisation

Polarisation can be thought of as in what way light is orientated – that is to say what plane a light wave is parallel to. The polarisation phenomenon can be effected on any light source and is relevant as it affects reflection, discussed later.

3.2.5 Q-switching

Q-switching is essentially using a shutter system (mechanical or otherwise) to build up high energy density pulses in a laser. This method allows, for example, a 20W laser to effectively function as a 100kW laser for brief instances. Potential advantages of using a pulsed laser are discussed later.

3.2.6 Laser/material interaction

Upon striking a surface, laser radiation is subject to a combination of reflection, absorption and transmission. Due to the opaque nature of the materials being processed in SLM (metals), it is only necessary to consider reflection and absorption. Narrowing this down to two variables means the two are directly linked; what is not reflected is absorbed by the material in question. This absorption can subsequently be considered as energy taking the form of heat.

3.2.7 Reflectivity

In general, absorbance in metals increases with a decrease in wavelength. Aluminium is a notable exception, having a relatively poor absorption at most wavelengths; only the 1μm range (Nd-YAG) shows a small improvement in absorption. Temperature of the material being lased also affects reflectivity (see Fig. 3.2).

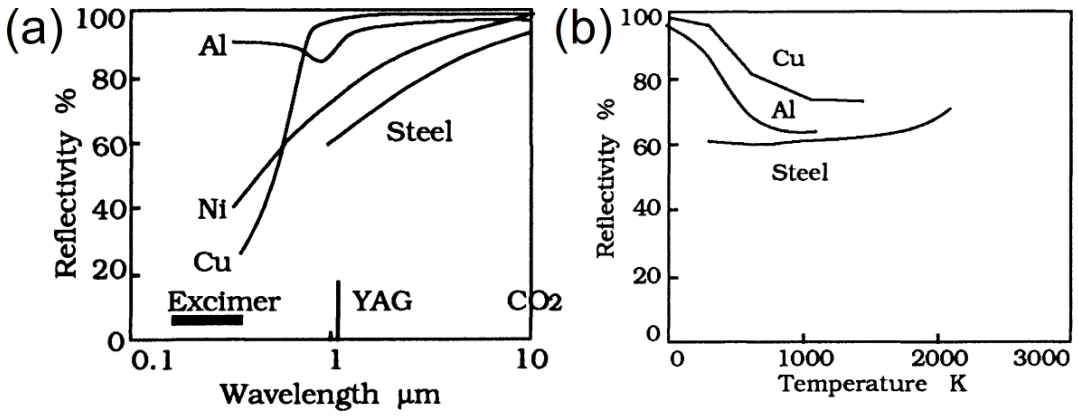

Fig. 3.2: Graphs of the effect of (a) wavelength and (b) temperature on reflectivity of a selection of materials. [75]. Note that (b) is for a wavelength of 1.064μm.

The angle of incidence at which a beam strikes a surface also influences reflectivity, as does the orientation of the plane of polarisation [76]. Reflectivity is given by:

$$R_p = \frac{[n - (1/\cos\phi)]^2 + \kappa^2}{[n + (1/\cos\phi)]^2 + \kappa^2} \tag{3.3}$$

$$R_s = \frac{(n - \cos\phi)^2 + \kappa^2}{(n + \cos\phi))^2 + \kappa^2} \tag{3.4}$$

where: R_p is reflection when the plane of polarisation is in the plane of incidence, R_s is reflection when the plane of polarisation is parallel to the plane of incidence, κ is the complex reflective index, n is the reflection coefficient and $\emptyset$ is angle of incidence.

Equations 3.3 and 3.4 results in a lower and upper bound for laser reflection. Since a laser is typically unpolarised until passed through a filter, the reflectivity can be plotted as an average of R_p and R_s as is demonstrated in Fig. 3.3.

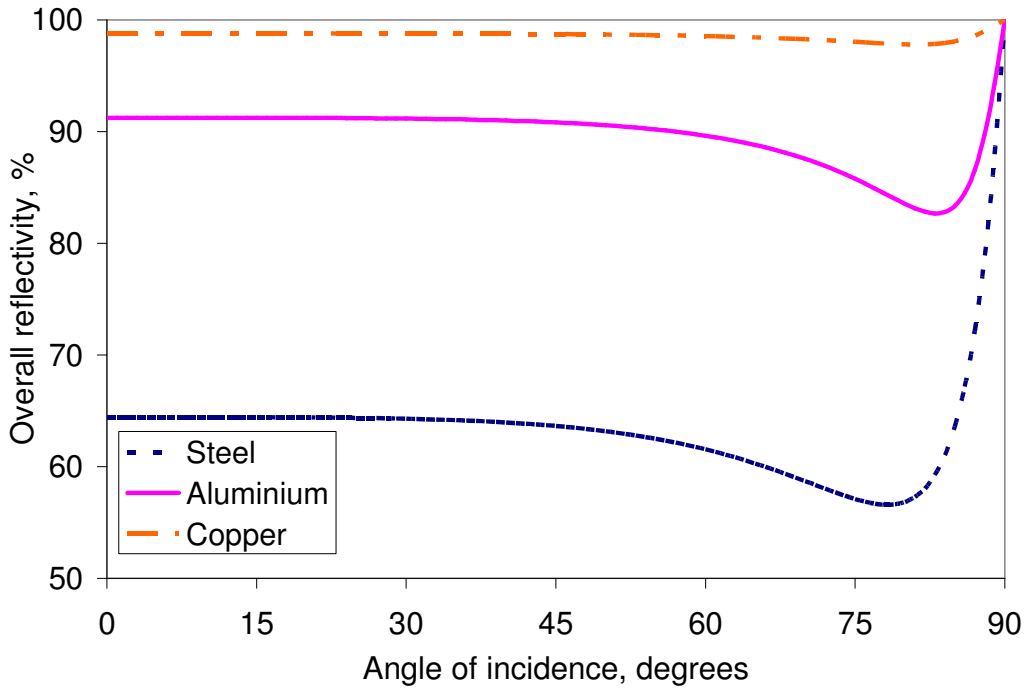

Fig. 3.3: Graph of angle of incidence *versus* overall reflectivity for a selection of materials using equations 3.3 and 3.4.

Table 3.1: Typical reflectivity values of materials to 10.6 µm laser radiation [72]

Surface type	**Reflectivity, %**
Sandpaper-roughened (1 µm)	92.7
Sandblasted (19 µm)	31.8
Sandblasted (50 µm)	21.8
Oxidised	10.5

Since the angle of incidence of light affects reflectivity, it is natural to assume that roughness will have an effect on overall reflectivity of a surface. Some experimental results are shown in Table 3.1.

Provided the surface roughness is below the wavelength of the laser beam, the beam will perceive the surface as 'flat' and reflect according to equations 3.3 and 3.4. If the surface roughness is greater, the beam will undergo diffuse reflection. This is especially important for SLM as the laser is acting on a powder bed, since the particles will encourage diffuse reflection resulting in internal reflections [77].

3.2.8 Laser spot eclipsing

When a laser beam is projected with perfect perpendicularity onto a flat surface, the resulting spot is assumed to be more or less circular (though laser mode may alter this); increasing the angle of incidence of the laser beam results in the spot geometry changing from circular to elliptical (shown in Fig. 3.4). This results in a larger spot area which leads to a reduction in energy flux of which examples are shown in Fig. 3.5.

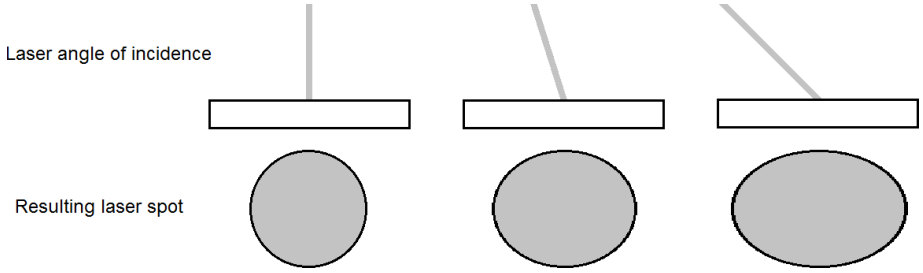

Fig. 3.4: Schematic representation of the change in laser spot geometry with a change in angle of incidence.

As such, the only effective method of reducing spot eclipsing is to minimise the angle of incidence.

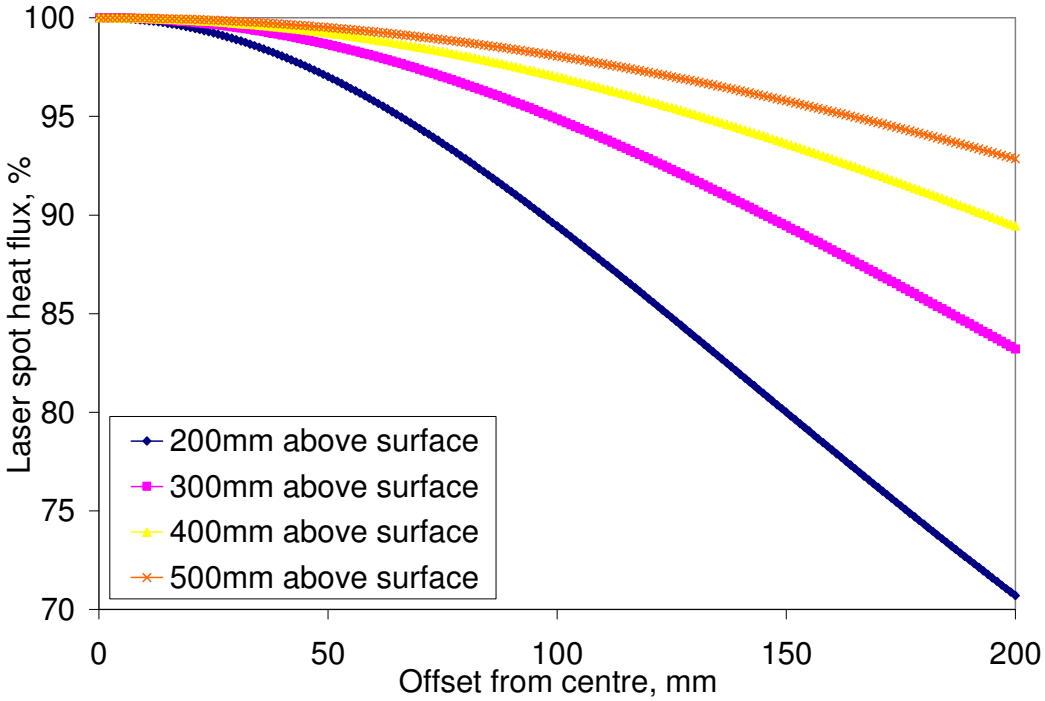

Fig. 3.5: Graph of the offset of a laser spot from a perfect perpendicular position *versus* the equivalent laser spot heat flux for various distances above a surface.

3.3 Phenomena in selective laser melting

During SLM processing, there are several phenomena in play that affect consolidation of material. A description of the most influential phenomena follows.

3.3.1 Sintering [78]

Traditionally sintering is the process of forming parts from compacted powder that is heated to approximately half the melting point of the material in question; atomic diffusion occurs and allows a solid structure to form. Due to the thermal nature of SLM, sintering is an observed phenomena in the process [58]. There are three types of sintering: Solid State Sintering (SSS), Liquid Phase Sintering (LPS) and full melting.

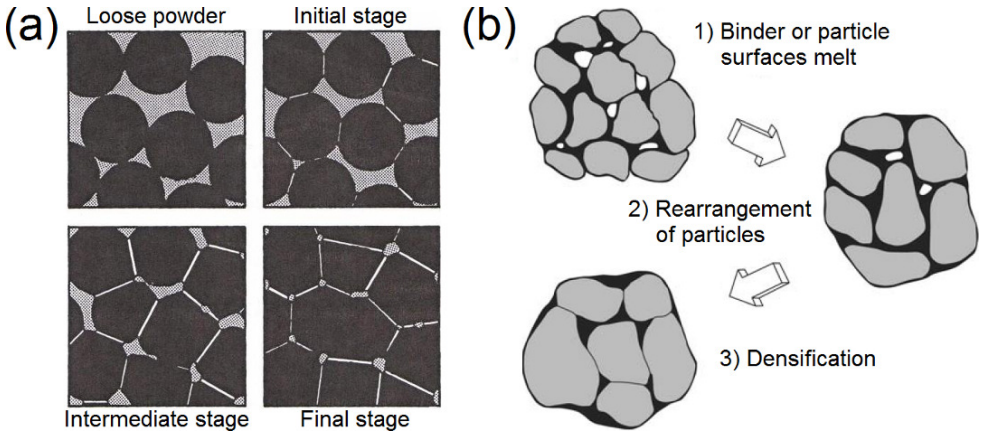

Fig. 3.6: Schematic of (a) solid state and (b) liquid phase sintering [78, 79].

SSS occurs between particles when temperatures are in the range of $0.5T_m$ to $<T_m$ (T_m = melting temperature) for a material, which can be achieved by a combination of heating and compaction. The bond created is due to solid state diffusion bonding (volume, grain boundary and surface diffusion). Particles that are touching form 'necks' due to the diffusion mechanism [80]. Compared to LPS and full melting, SSS is a more time consuming process, due to its reliance on diffusion, which makes it more suitable for the consolidation of ceramic materials [81].

LPS (also referred to as 'partial melting' in certain circumstances) involves actual phase change from solid to liquid, though a percentage of the material (typically the centre of the powder particles) remains solid. Strong capillary forces (see *Capillary action*) allow rapid material transfer making the process faster than SSS. LPS is the consolidation mechanism behind composites where a filler material with a higher melting point than the matrix material is used as reinforcement, without the filler material melting. If a single phase material is used (or a mixture of materials without a distinct binder), partial melting is said to have occurred.

Full melting is just that: all the material involved completely changes to the liquid phase prior to cooling to form the final part. This can ensure a homogenous material but comes at the cost of a large volumetric change, resulting in large residual stresses [82] (discussed later). Other phenomena can also occur during full melting (Balling, Rayleigh instabilities). Owing to the nature of SLM, the primary consolidation mechanism is full melting.

Sintering behaviour in a metal powder bed has been demonstrated by Tolochko *et al* [83] (see Fig. 3.7).

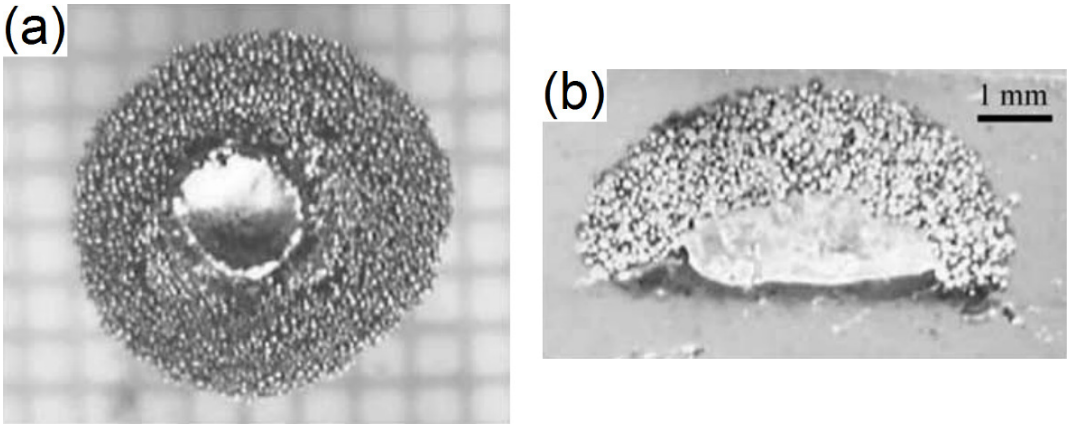

Fig. 3.7: Examples of a sintering formation for a titanium powder bed when exposed to a static laser spot (Nd:YAG, 1.06 µm wavelength, 5.1 mm diameter) for 10 s. (a) top view (60 W) and (b) cross-section (80 W) [83].

3.3.2 Marangoni convection

Marangoni convection (also called Marangoni effect or motion) describes the flow behaviour in molten material subjected to a heat source [84]. Temperature gradients in a weld pool will encourage convective motion in order to reduce the aforementioned temperature gradients, resulting in movement at the surface of the liquid (see Fig. 3.8), which is on the order of 1 m s^{-1} [85]. There are two key considerations in Marangoni convection: the surface tension temperature coefficient and the Prandtl number.

The surface tension temperature coefficient is comparatively easy to understand in that its sign denotes the direction of flow. A positive value results in the liquid being drawn to the centre of the top surface and then sinking (increasing temperature increases surface tension), resulting in a narrower, deep weld pool; a negative value reverses the flow, with the liquid rising from beneath the top surface and then flowing outwards (increasing temperature decreases surface tension), resulting in a wider, more shallow weld pool. Pure metals and most alloys have a negative value, which through adding certain elements can be made positive (e.g. adding sulfur to steel) [86]. This can aid deeper penetration of a weld, therefore ensuring a deeper bond in the case of SLM.

The Prandtl number, Pr, is a ratio of the kinematic viscosity, v, to thermal diffusivity, α [86]. Calculation of the Prandtl number is shown in equation 3.5:

$$\mathrm{Pr} = \frac{\nu}{\alpha} = \frac{\mu/\rho}{k/(\rho C_p)} = \frac{C_p \mu}{k} \tag{3.5}$$

where μ is dynamic viscosity, ρ is density, k is thermal conductivity and C_p is specific heat capacity. Equation 3.5 shows that *Pr* is dependent on specific heat capacity, dynamic viscosity and thermal conductivity. For materials with comparatively low *Pr* values, such as aluminium with a *Pr* of 0.02, the weld pool geometry is spherical in nature and heat flow is conduction dominated. For materials with high *Pr* values such as steel (*Pr* of 0.1), convection is the primary form of heat flow (see Fig. 3.8).

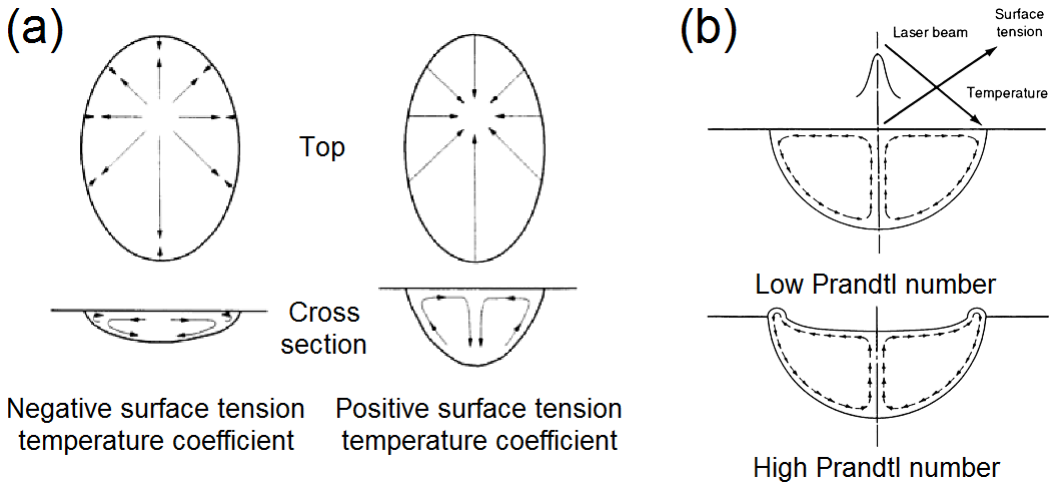

Fig. 3.8: Schematic representation of Marangoni convection for a weld bead subject to laser heat input: (a) flow orientation according to surface tension temperature coefficient; (b) effect of Prandtl number on a negative surface tension temperature coefficient liquid. Images adapted from ASM Metal Handbook Vol. 6 [86].

3.3.3 Rayleigh instability

Rayleigh instability (or to be more correct, Plateau-Rayleigh instability) describes the behaviour of a liquid cylinder and the conditions under which this cylinder breaks into droplets; this was first characterised by Plateau [87] and then explained analytically by Rayleigh [88]. The instability comes about due to sinusoidal components within a liquid caused by small perturbations that are inherent to any system, which are

exacerbated by a liquid's natural tendency to reach a balance between surface energy and internal energy. In essence, a liquid cylinder will break into smaller droplets when a sinusoidal component has a wavelength greater than the cylinder's circumference: that is to say, a liquid cylinder with a length to diameter ratio larger than π will deteriorate into two or more liquid bodies.

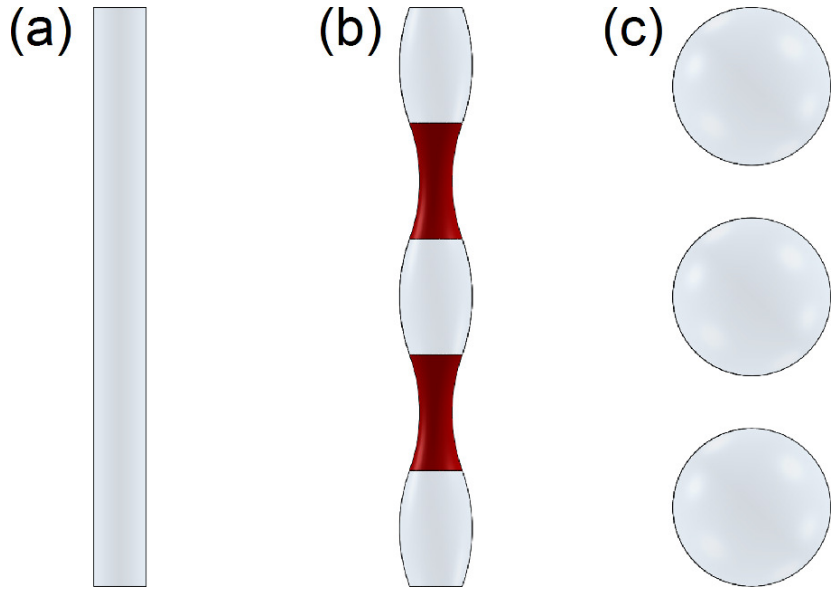

Fig. 3.9: Schematic representation of Rayleigh instabilities: (a) t=0, a liquid cylinder in an unperturbed state; (b) t, inherent instabilities deform the surface of the cylinder, leading to regions of high and low pressure (highlighted pinched regions have a higher pressure); t=∞, the cylinder breaks into droplets upon rupture of the pinched regions.

The perturbations mentioned previously distort the curvature of the liquid surface, resulting in a pressure difference which is described by the Young-Laplace equation:

$$\Delta p = \gamma\left(\frac{1}{R_x}+\frac{1}{R_y}\right) \tag{3.6}$$

where γ is surface tension and R is the radius of curvature for the particular axis (see Fig. 3.10). Given the relationship described by equation 3.6, one can see that pressure difference increases exponentially with a decrease in radius.

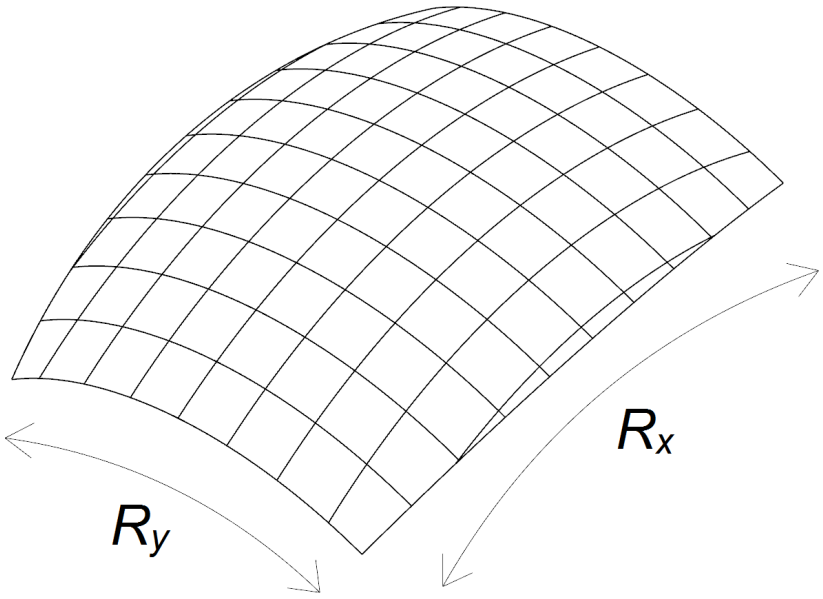

Fig. 3.10: Schematic of curvature of a liquid surface.

Rayleigh instabilities are often encountered in SLM due to the formation of molten material using a scanning laser; an example of this behavior is shown in Fig. 3.11. Single track formations are significantly affected by the phenomena, though the raster scanning inherent to the SLM process may alleviate issues by allowing the formation of weld beads with larger widths. Ultimately, the geometry of the part being manufactured will control the onset of Rayleigh instabilities [58].

Yadroitsev *et al* [89] further developed the Rayleigh instability model for a liquid cylinder in contact with a solid substrate (see Fig. 3.12). It is calculated that the critical length for instability onset is reduced to $\pi\sqrt{2/3}$ owing to a loss of axial symmetry caused by attachment to the substrate. Experimental results showed that a larger area of interface between liquid and substrate resulted in a more stable weld bead: the larger interface area was linked to an increase in penetration of the substrate. Hence, in order to effectively counter Rayleigh instabilities, a weld bead must have satisfactory penetration of the material below.

Since SLM uses a laser to melt material, temperatures gradients are comparatively high and results in Marangoni convection. As a result, Rayleigh instabilities within SLM are further influenced by the internal and surface motion of the liquid [90]. Furthermore, Rayleigh instabilities dictate that a liquid cylinder over the

critical length to diameter ratio will break into spheres therefore the balling phenomenon is typically affiliated (see Balling).

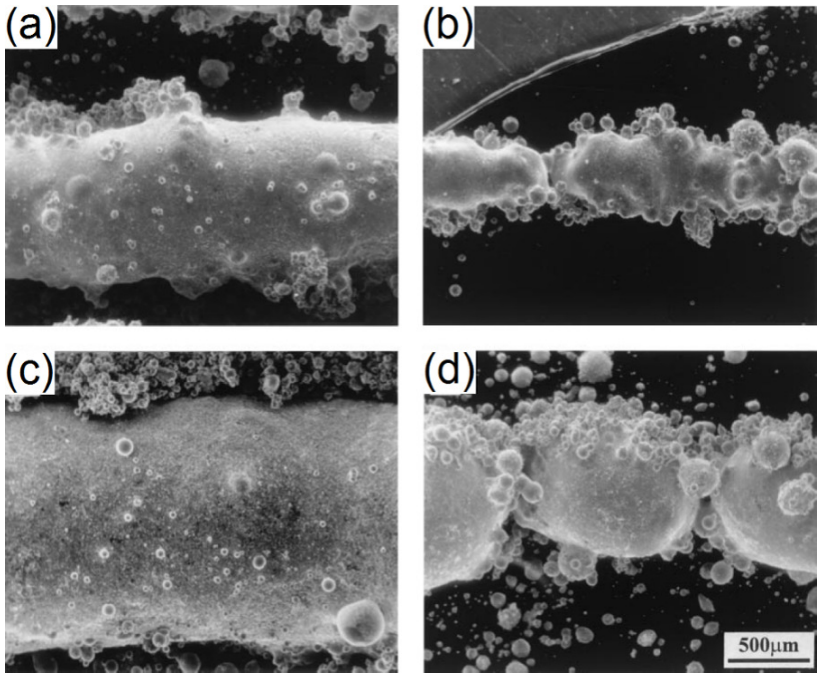

Fig. 3.11: Example of Rayleigh instabilities affecting a single line laser scan of M2-117 HSS steel powder (scanning electron micrographs): (a) 50 W, 5 mm s^{-1}; (b) 50 W, 20 mm s^{-1}; (c) 150 W, 5 mm s^{-1}; (d) 150 W, 20 mm s^{-1} [90].

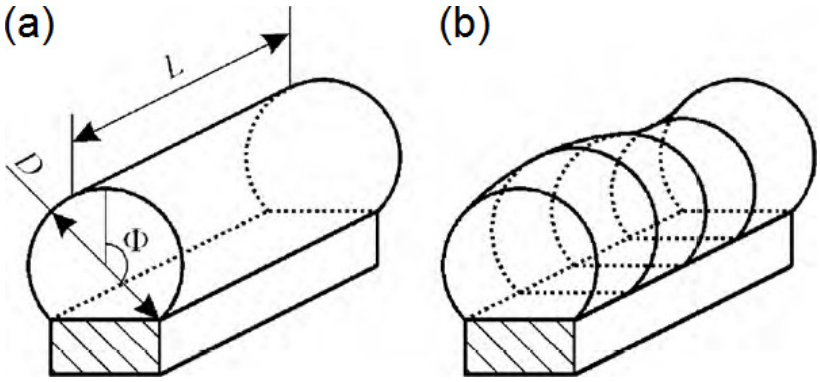

Fig. 3.12: Schematic of a liquid cylinder on a substrate: (a) undisturbed; (b) disturbed [89].

3.3.4 Wetting [91]

Wetting refers to a liquid's interaction with a surface, resulting from intermolecular interactions that are a balance between adhesive (liquid attraction to a surface) and cohesive (liquid's internal attraction) forces. Since SLM relies upon melting material in consecutive layers that must bond to allow successful consolidation, wetting is perhaps the most important phenomena to account for and is studied intently in SLM (see Fig. 3.13).

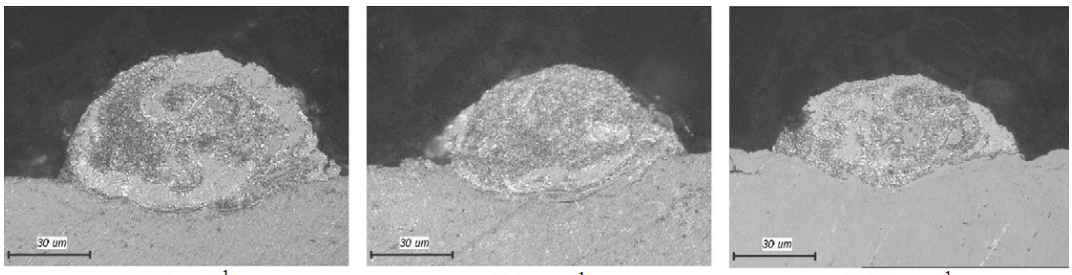

Fig. 3.13: Cross-sections of single laser scan tracks (CuNi10 powder on stainless steel 304L substrate). 50 μm powder layer, Nd:YAG laser operating at 1075 nm, 50 W and 70 μm spot size [89].

The degree of wetting is determined by the contact angle of the liquid and the surface it is contacting. A high angle (see Fig. 3.14) represents low wettability, resulting in a proud standing droplet, whereas a low angle represents high wettability, resulting in a thin film.

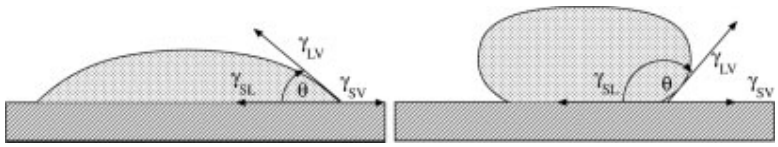

Fig. 3.14: Schematic of isothermal surface wetting: the left side represents high wettability whereas the right side represents low wettability [91].

In a typical wetting scenario there are three surface tension energies: solid and liquid, γ_{SL}; liquid and gas, γ_{LV}; and solid and gas, γ_{SV}. using these values, a wetting angle can be calculated using Young's equation (equation 3.7):

$$\gamma_{SV} = \gamma_{SL} + \gamma_{LV} \cos\theta_{eq} \tag{3.7}$$

where θ_{eq} is the equilibrium wetting angle. Owing to the short interaction time of SLM processing, equation 3.7 holds true [92].

In the case of molten metals, oxide formation on the solid substrate can affect wetting for the worse, which leads to poor interlayer bonding. Hence, the use of an inert gas or vacuum to enforce a low oxygen content atmosphere is standard practice in SLM type processes, as well as supplying sufficient laser energy to remelt part of the previous layer in order to break up any potential oxide layer formation [92].

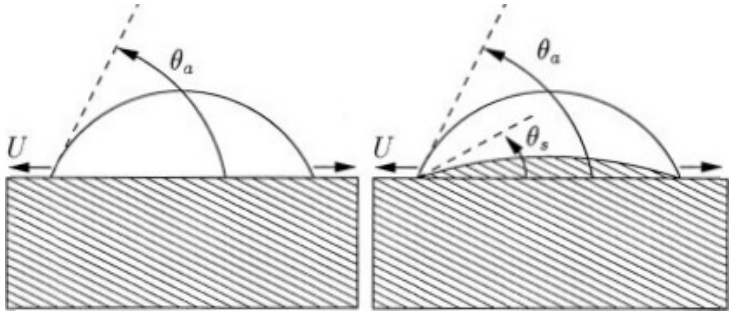

Fig. 3.15: Example of homologous surface wetting: the left side represents isothermal wetting whereas the right side represents homologous wetting [91].

Homologous wetting (see Fig. 3.15) refers to the wetting of a solid substrate by molten liquid of the same material: as such all wetting in SLM should be homologous for ideal processing conditions. The value θ_s (the angle of solid formation compared to the base plane) is calculated as the arcsine of the Stefan number, *S*, which is calculated as:

$$S = \frac{c\left(T_f - T_t\right)}{L} \tag{3.8}$$

where c is the material's specific heat capacity, T_f is the temperature of fusion (melting), T_t is the target temperature and L is the latent heat of fusion. Please note that T_t refers to the temperature of the substrate.

Using equation 3.8, the behaviour of θ_s can be plotted for various materials: this has been done in Fig. 3.16. As expected, the behaviour of the graph shows that for a layer to penetrate a layer below, the surrounding material must be heated to above the melting point of the material.

A final note on homologous wetting: it is assumed that the wetting of a substrate by a like material is still referred to as homologous wetting (e.g. molten 316L stainless steel on a 304L substrate) since alloying must occur to allow successful bonding to a base plate.

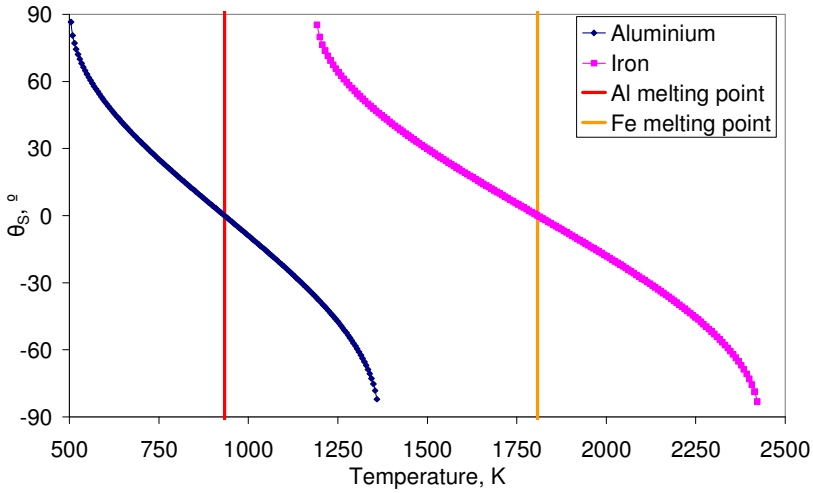

Fig. 3.16: Graph of the solid angle *versus* target temperature for homologous wetting, derived from equation 3.8.

3.3.5 Capillary action/forces [58, 93]

Capillary action refers to a liquid's interaction with a solid surface: this is caused by a combination of surface tension and adhesion. Owing to the fact that LPS occurs during the SLM process, capillary action plays a role. The capillary action can take two forms, either that of a liquid bridge between particles, or liquid travelling through pores of a sintered solid. Capillary force is given as:

$$F_{capillary} = 2T\pi r \tag{3.9}$$

where T is surface tension and r is the radius of the pore the liquid is travelling through.

It should be pointed out that owing to the small scale of the capillary actions occurring, the effect of gravity can be ignored.

3.3.6 Balling [91]

The 'balling' phenomenon is a result of a molten material attempting to reach an optimum value between surface area and volume due to surface tension and wetting. If the surface tension of a liquid on a substrate is great enough, the liquid will form a sphere (see Fig. 3.17). Balling is associated with Rayleigh instabilities as a result of liquid material attempting to find a new optimum geometry upon break up of a liquid cylinder, as well as poor wetting of the solid substrate beneath. As such, balling can be considered the culmination of phenomena occurring in SLM.

Pulsed laser modes have been shown to reduce balling effects in SLM processing, which leads to better consolidation [92]. This is due to the sudden vaporisation of material on the top surface, which acts effectively as a small explosion and generates recoil pressure, flattening any liquid formations. This also results in a better surface finish for the part.

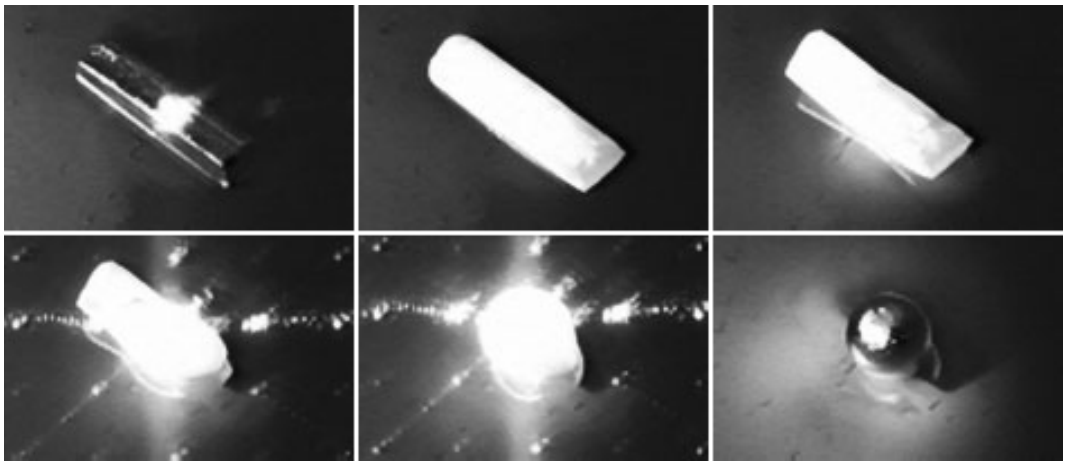

Fig. 3.17: Observation of the balling phenomenon. A 304L stainless steel strip 4mm long is heated and melted by a laser on top of a polished plate of the same material [91].

3.3.7 Residual stresses [67]

Although many manufacturing processes are subject to residual stresses from some form of heat treatment, SLM is especially vulnerable to residual stresses from the constant re-melting occurring within the process, which is coupled with rapid heating and cooling rates (see Fig. 3.18). Residual stress can cause undesired deformation and cracks within a part, reducing the fatigue life. Three methods exist that can alleviate residual stresses: multiple laser scanning of each layer; heating of the base plate and powder bed; and post SLM heat treatment.

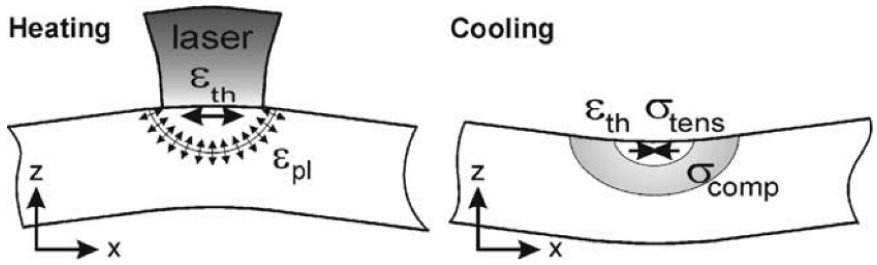

Fig 3.18: Simple schematic of the cause of residual stresses within SLM [92].

Multiple laser scanning of one layer is perhaps the easiest to implement since the laser scan can simply be repeated and has been shown to reduce residual stress by 55 % for certain steels. It has been found that increasing the laser power compared to the initial 'pass' further relieves stress.

Base plate and powder bed heating is believed to reduce cooling rates within the SLM process, which will decrease residual stresses. Experiments have shown that steel SLM parts can have residual stresses reduced by 40 % by heating the base plate and powder to 160 ºC, which is comparatively small given the high melting point of steels (approximately 1500 ºC).

Post SLM heat treatment is an approach that is also typical for conventionally produced parts. Heating a steel SLM part in the range of 600 to 700 ºC for an hour decreases residual stress by approximately 70 %

The aforementioned stress relief techniques can all be applied to the same part to significantly decrease residual stresses. An obvious downside however is the increase in energy required to apply all three techniques, increasing the environmental impact of a fabricated part.

3.3.8 Base plate attachment

Parts produced by SLM must always be produced by attaching to a base plate, either directly or by using supporting structures. There are two reasons for this. Firstly, the SLM process require the part to be 'anchored' otherwise the residual stresses resulting from processing will disrupt the geometry of the part [67]; this will happen during the process and cause the part to 'curl', causing the build to fail. Secondly, there must be material beneath the metal powder being lased to allow the newly molten material to wet the surface below; without this the molten material suffers balling as described earlier.

An SLM part can be joined to a base plate in one of two ways and is dictated by the part geometry. If the part has a large, flat surface that can act as the 'bottom', then the geometry can be extended and the part can be removed post process simply by sawing through the added material. However, if the part has a complex geometry, then support structures may be used.

3.3.9 Geometry limitations

In addition to requiring a base plate to act as an anchor, SLM parts are subject to geometric limitations. Chief amongst these limitations is the need for supporting overhanging materials.

The general rule of thumb for the angle at which an overhang must be supported is less than 45° to the base plate surface [94] but can vary according to the geometry of the part, material(s) used and machine specifications. Exceeding this angle can result in reduced part quality and even lead to failure of the build. A schematic representation is shown in Fig. 3.19.

Internal geometry must also have a 'starting point' to provide anchoring points: all parts must be anchored. This can be achieved by adding a support structure if necessary. Post process powder removal is also a concern and parts produced by SLM cannot have closed volumes or powder traps.

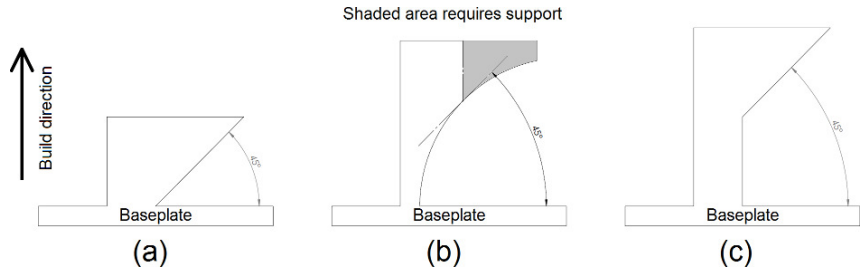

Fig. 3.19: Schematic of basic geometry limitations in SLM: (a) angles less than 45° to the base plate require support to maintain integrity [94]; (b) fillets are possible but still require support when the tangent angle decreases to less than 45°; (c) overhangs can start from any point on the model provided they are 45° or greater to the base plate or have support.

3.4 Material use in selective laser melting

Currently, the common SLM materials processed are metals. Stainless steels are at the forefront of usage, with titanium alloys (particularly Ti6Al4V) following suite [33]. CoCr is used primarily in dental applications [95]. Superalloys are also used [96] but it is thought that applications are limited since superalloy use in aersopace is focussed on turbine production which are 'grown' as single crystals [9], which SLM is currently unable to do.

After the start of the PhD, Al and Cu alloys have been commercially released for ALM use [39, 40]. As newly introduced materials for the SLM process, their usage has yet to catch up with the other materials mentioned.

3.4.1 Stainless steels

Stainless steels are currently the most dominant material in SLM use, perhaps owing to comparative low cost, ease of processing and relative safety of handling. The most common types of steel in use are 316L (an austenitic, paramagnetic steel), 17-4PH (a ferromagnetic, precipitation hardened maraged steel), and derivatives thereof. Both the aforementioned steels are used in aerospace applications [97].Owing to the dominant use of steel in SLM, most SLM research revolves around processing it. Issues such as residual stress reduction [67], effects of laser pulsing and scan strategy [92] all use steel

as the material of choice. Initial research revolved around using SLS machines to process samples of a few layers in thickness, but the samples produced were of poor density (which ironically allowed them to be produced with no support structures) [98]. Continuing research allowed the development of the SLM of steels, for example looking at new laser scanning strategies. Xie *et al* [71] experimented using H13 tooling steel powder and found that a knit strategy (where the next scan in a multilayer scan had the laser scanning in between previous scan lines) improved density further. Rombouts *et al* [100] have also looked into the effect of oxygen content in the inerting atmosphere and found that an increase in oxygen results in an increase in balling, which led to poorer surface roughness as well as an increase in porosity: this was attributed to the formation of CO and CO_2 through excess oxgen and carbon within the steel. Pulsed and continuous laser modes have been studied by Glardon et al [100], which found that pulsed laser modes allowed better consolidation owing to a lack of heat transfer and the influence of recoil pressure through the generation of plasma, which flattens the weld pool.

3.4.2 Aluminium alloys

Processing aluminium powder is potentially difficult due to several properties of the material. Perhaps the primary disadvantage of aluminium powders is the oxide layer that forms upon exposure to air. Current machines that are able to process aluminium alloys reduce this problem by keeping the powder in an inert atmosphere at all times, even from the point of manufacture of the actual powder itself. This oxide may however increase absorption, which leads onto another issue: the reflectivity of aluminium. Since aluminium is highly reflective, the laser power and/or energy density needed to process the powder may be increased compared to that of, for example, steel [7]. Aluminium also has poor weldability and wettability [West 1951], which may result in the phenomenon known as 'balling' with most parameters.

3.4.2.1 State of Al use in selective laser melting

Very recently, researchers and industrial companies have carried experimental investigation and commercial exploitation on SLS and SLM of certain aluminium

material. Initially aluminium was introduced into SLS via Alumide™, a 50/50 mixture of Duraform PA and aluminium powder [102]. This material improved the mechanical properties of Duraform but was still nowhere near the performance expected of an aluminium alloy (Alumide is used mainly as a more visually appealing material for rapid prototyping). Wong used 6061 Al alloy powder in the SLM process in 2007 [6] but was focussed on the production of novel heat sink designs rather than reporting the steps taken to successfully process Al alloys in SLM and resulting material microstructure and mechanical properties (see Fig. 3.20). In 2008 (a year after the start of the PhD) both the MTT Technologies Group and Concept Laser GmbH introduced their range of machines which could process limited ranges of aluminium alloys [103] based on casting grades that have low to medium mechanical strengths; an example is AlSi10Mg, which has a tensile strength of 317 MPa [39]. Compared to 7075-T6 Al alloy with a tensile strength of 524 MPa [104], AlSi10Mg only achieves 60% of the strength.

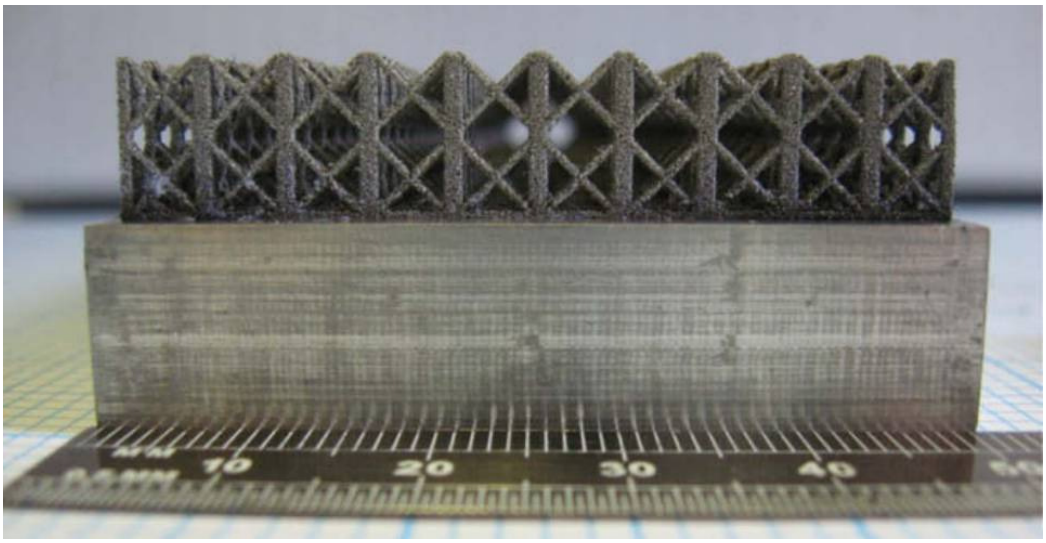

Fig. 3.20: Photograph of 6061 Al alloy lattice structure manufactured by SLM [6].

A recent work in 2011 (the last period of the PhD) published by Louvis *et al* [7] investigated the SLM of aluminum components. The work focussed on the SLM of 6061 Al alloy and was primarily concerned with the effect of changing parameters upon

density and oxide formation within consolidated material rather than the resulting microstructures.

Near the completion of the thesis presented here, the author was notified of previous work by Zhang [105] concerning the SLM of Al alloys. Zhang's PhD studied the processing of aluminium alloys in SLM, in particular AlSi10Mg, an alloy known for its casting qualities. Zhang's own results showed that al alloy powder reflectivity can vary from approximately 43 to 73 % for 10-30 μm spherical particles. Zhang also undertook numerical studies on laser reflection between particles as well as heat transfer. The numerical results showed that the first layer of particles receives the most laser light, with the second layer receiving a small fraction and the third layer receiving almost none. Numerical studies comparing aluminium and steel processing found that the resulting weld pool was a different geometry for the two materials. Steel has a 'tailing' effect causing an elongated weld pool, whereas aluminium has, for all intents and purposes, a semi-spherical geometry. Laser power was found to strongly correlate with density, in that increasing the laser power (and thus heat flux) increased density. Higher laser powers enabled faster scan speeds. Pre-heating the powder also increased density. Residual heat from the layer by layer manufacturing technique was also found to result in softening of material below the processed layer. Zhang's work made no mention of considering customised alloys or powder mixtures.

3.4.2.2 Aluminium oxide

Aluminium can form an oxide layer in exceptionally low oxygen content atmospheres and so one must accept the fact that it is in effect impossible to remove these oxides from the SLM process (a view shared by Louvis [7]). Hence, it is necessary to study how alumina may affect consolidation.

Molina [106] has reported that alumina is responsible for inaccurate measurement of the surface tension of molten aluminium. During this investigation, it was found that temperature has an effect upon molten Al wetting of alumina. Initially, at temperatures close to the melting point of aluminium, it was found poor wetting was demonstrated, but raising the temperature to approximately 1350 K shifted the aluminium to better wetting.

Incidentally, molten aluminium wetting of alumina is also affected by the crystallinity of the alumina [Shen 2003]. However, it is currently unknown if the

alumina can be controlled in this way during SLM processing or during the production of aluminium powder.

PART II: EXPERIMENTAL STUDIES AND APPLICATION

4. Experimental equipment - MTT SLM Realizer

Fig. 4.1: Photograph of the SLM Realizer installed at the University of Exeter.

The SLM machine available for use at the University of Exeter is actually a prototype MTT (formerly MCP) Realizer [62], as shown in Fig. 4.1.

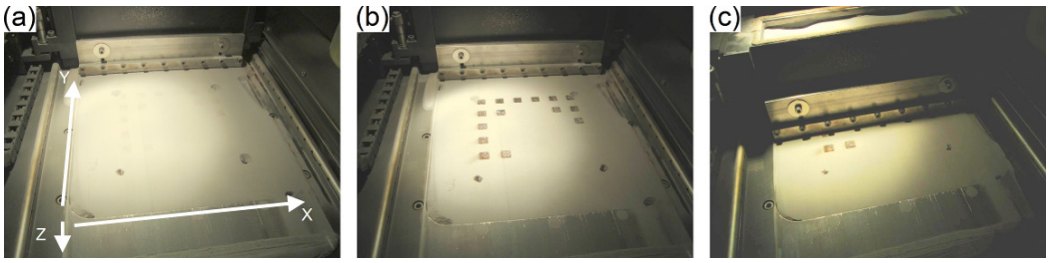

Fig. 4.2: Photographs of the SLM process in action: (a) a deposited powder layer, ready for lasing; (b) lasing of cross sectional area of part(s); (c) build is lowered one layer thickness, deposition mechanism dispenses and levels powdered material for the next layer. The sequence described repeats until the build is complete.

The Realizer has a 250×250 mm build area with filleted corners (approximate radii of 50 mm) and can build to a height of 300 mm. The build process has already been described in Chapter 2, but a visual representation is shown in Fig. 4.2.

4.1 Machine characterization

4.1.1 Laser

The laser in the Realizer is an IR fibre laser, operating continuously at a wavelength of 1064 nm (no pulsed modes are available): the beam is unpolarised. The minimum lasing power was measured to be approximately 5W and the maximum possible was 120W, though this was over the laser's rated capacity of 100 W and therefore only used in experiments with a short running time. Using ZAP-IT laser paper [108], the smallest possible spot diameter was 160 µm, achieved using a focus length of 60 mm.

During production of parts, it was observed that the SLM Realizer was prone to 'back reflection'. Back reflection refers to the undesirable situation in which a laser beam is reflected back into the laser cavity, which can result in permanent damage [109]. The laser unit of the SLM Realizer has a safety mechanism which deactivates the laser; unfortunately this is not communicated to the control software of the SLM Realizer and so the machine keeps depositing powder layers. Fortunately, using the default settings provided for stainless steel and CoCr by MTT meant back reflection was a rare occurrence when processing the aforementioned materials. It should be noted that commercial SLM machines are fitted with optical isolators and polarising filters - equipment that stops a back reflected beam from entering the laser cavity. Purchasing an optical isolator and polarising filters for the SLM Realizer was investigated but found to be prohibitively expensive.

Laser eclipsing, though previously mentioned as important to consider, is not expected to impact consolidation to any noticeable degree since the length of the beam from the galvanometer to the powder bed surface is greater than 500 mm; considering that the area used for experimentation is 140 mm × 140 mm at the centre of the bed, the laser energy flux will not drop by more than a percent (see Fig. 3.5).

4.1.2 Laser scanning

An analogue mirror galvanometer is installed in the Realizer, allowing the laser spot to be moved and positioned by the control software. Due to the nature of the galvanometer, a single value for laser scan speed isn't given: instead, two parameters control the scan speed: *point distance* and *dwell time*. The author found that point distance and dwell time could be increased incrementally by 5 µm and 20 µs respectively. Theoretical scan speed can therefore be calculated by dividing point distance by dwell time; in reality the scan speed may differ slightly due to the workings of the galvanometer. It was found that the laser could be moved at a maximum scan speed of 250 mm s^{-1}. Hatching spacing/distance, like point distance, is also increased incrementally by 5 µm but has a minimum value of 25 µm. See Fig. 4.3 for a visual explanation.

When producing parts, the control software can employ a boundary scan of the cross section currently being processed in order to improve surface quality. Additionally, the software can allow a fill contour to be employed between the boundary scan and the internal hatching. However, for samples produced in following chapters, only hatching scans were used to eliminate variables in investigations.

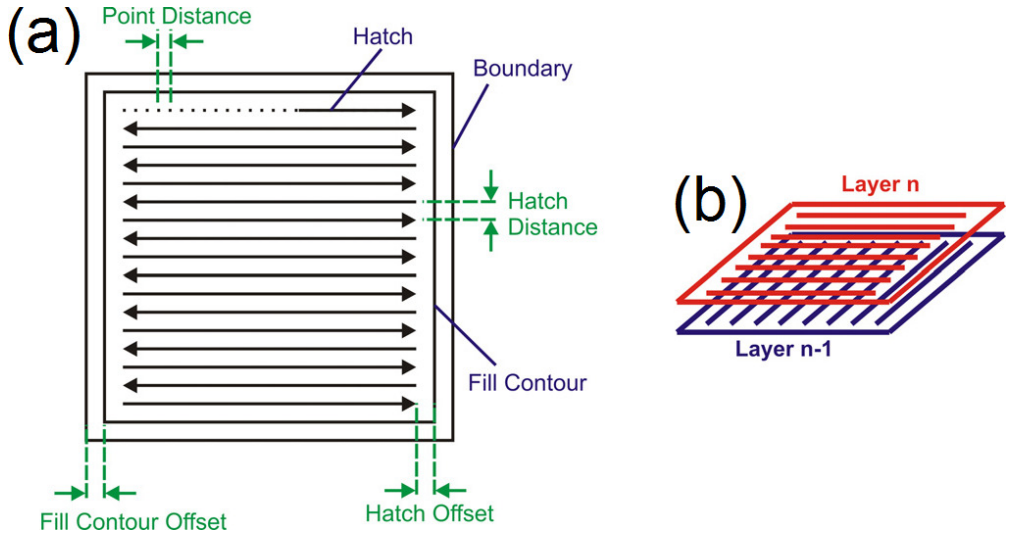

Fig. 4.3: Schematic of scanning parameters for SLM: (a) parameters relevant for each layer; (b) perpendicular scanning method for alternating layers [7].

4.1.3 Powder deposition mechanism

Powder deposition is handled by two systems, referred to as 'loader 1' and 'loader 2' (Fig. 4.4). Loader 1 is simply a large tank on the back of the machine that feeds loader 2 with powder, allowing large builds to be processed without the need for refilling. This is achieved by moving loader 2 to the back of the machine (under Loader 1) and depositing powder into the top of Loader 2 via a turning slotted shaft, shown in Fig. 4.5.

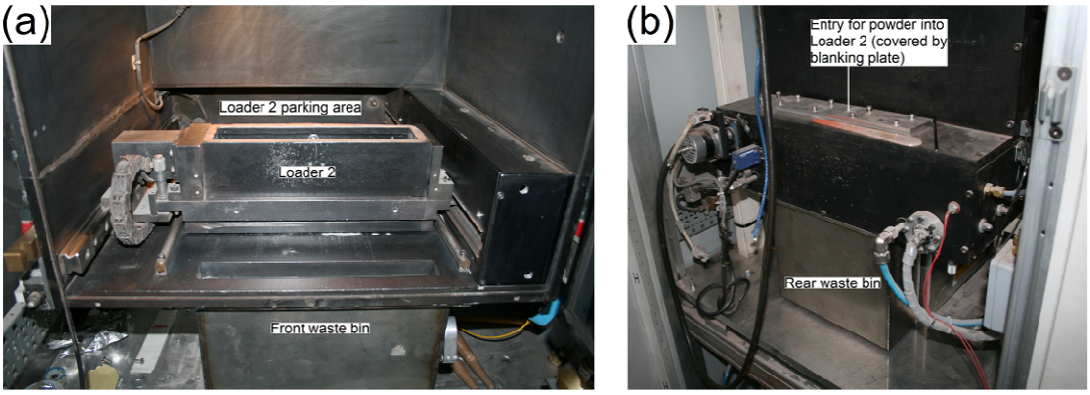

Fig. 4.4: Photographs of the powder deposition mechanism in the SLM Realizer: (a) front view showing the main deposition mechanism referred to as 'loader 2'or the 'wiper'; (b) rear view, showing the entry point that allows loader 1 to deposit into loader 2.

Loader 2, also called the 'wiper', is responsible for depositing the powder. Loader 2 is moved along rails by a servo motor; a slotted shaft, similar to the one used in loader 1, is used to deposit powder directly onto the bed. To level the powder, a fixed blade with a replaceable silicon rubber edge is used. To ensure satisfactory powder coverage for each layer, a surplus of material always has to be deposited. The excess powder is swept into the waste bins, though owing to the nature of deposition, it is the rear waste bin that receives the majority of the waste powder.

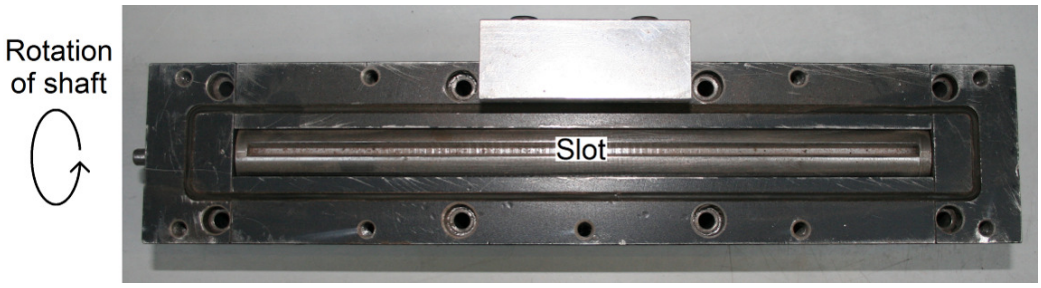

Fig. 4.5: Photograph of example of a shaft with slots, used to deposit powder in loader 1 and 2.

4.1.4 Inert atmosphere control

The Realizer uses Ar gas to inert the build chamber with a positive pressure, which is maintained by a simple inlet valve that can monitor gas flow rate. Pressure is read by an internal sensor and there is also an analogue gauge attached to the outside of the build chamber. Although not ideal (and a result of the machine being a prototype), the Ar was allowed to leak out of the machine through any imperfect seals. Over the course of a build, the gas flow needed to maintain a satisfactory pressure decreased, presumably due to powder particles settling in the leak sites (confirmed by a notable concentration of material at points around the seal.

The Ar gas was also constantly filtered by a pump system attached to the build chamber. This was to remove floating powder particles and vaporised material.

4.2 Computer hardware and software capabilities

The Realizer utilises custom software to drive the machine. The software can process STL files as well as support files generated by 'Magics', specialist software developed by Materialise [110]. The software 'slices' the inputted CAD model(s) and generates a file for each layer that contains coordinates for scanning as well as other key parameters such as laser power, dwell time and point distance.

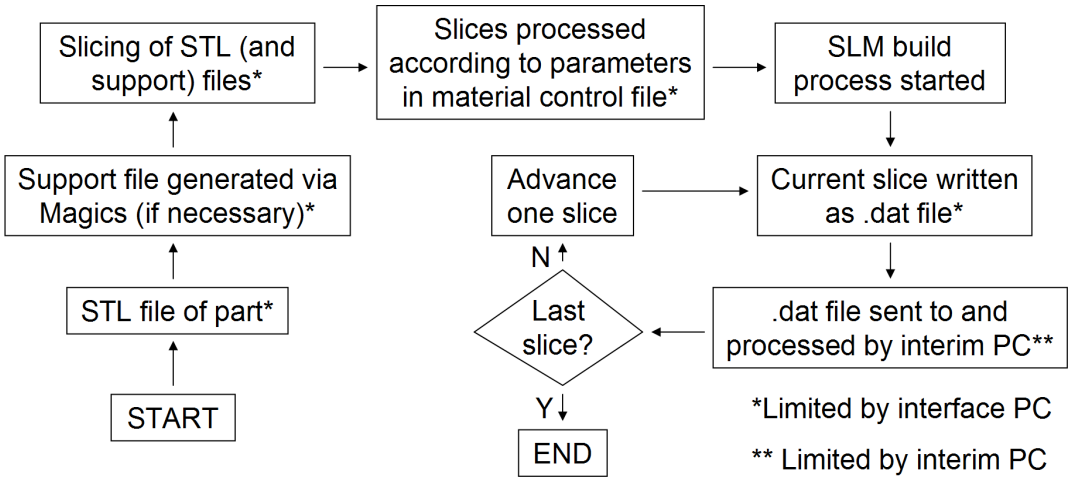

Fig. 4.6. Flow chart of software behaviour in the SLM Realizer.

The Realizer has two computers (PCs) that run the software; one that the user directly interfaces with (designated the 'interface PC') and another that acts as an interim between the interface PC and the Realizer hardware (designated the 'interim PC'). It was found that the interim PC was comparatively limited in its specification, meaning that some builds attempted were unable to be computed due to lack of system resources. The interface PC also had limitations in that if an STL file was too large (memory wise) that the software was not able to cope and could not generate the required files. A flow chart showing the software cycle and limitations is shown in Fig. 4.6.

During the course of the PhD study, proprietary software was developed by Dr Neil Sewell that allowed grids of rectangular samples to be made with varying parameters. The author would like to extend his thanks to Neil for the software, which saved time and effort for sample production.

5. Experimental investigations into the selective laser melting of mono, mixed and hybrid stainless steels

5.1 Introduction

As discussed in Chapter 3, steels are currently a dominant material within SLM, which (in effect) makes them the most understood material for processing [58, 98, 111-113]. Since the author had no prior experience with SLM, it was decided to perform the first group of experiments using steels; this would give an insight for processing more advanced materials. Running tests would allow comparison to previous work, which allows the author to verify the manufacturing of samples.

316L and 17-4PH stainless steels demonstrate good weldability and since SLM is essentially similar to laser welding [58], they are the two most common steel grades used in commercial SLM systems: the two steels are also used in aerospace applications [97]. Some previous studies have used the SLM process to consolidate these two stainless steels separately and have investigated the effects of processing parameters on the density and mechanical properties of the consolidated parts [98, 112, 113]; however, little research has been done in the way of detailed microstructure evaluation in 316L and 17-4PH parts consolidated by SLM. There has also been no investigation into the potential to tailor the microstructures and properties of parts by SLM of a mixture of two stainless steel grade powders, which may allow hybrid material parts with tailored properties to be manufactured. Much research has attempted to improve the capability of the SLM process to produce high performance metallic composite parts with desired or tailored properties [58]. The exploitation of such new capabilities drives significant research activities to understand the fundamental consolidation mechanisms governing the microstructure evolution of metallic materials and interactions between the elements of composite materials during SLM processing.

This chapter looks at three topics. Firstly, the effects of changing SLM parameters (specifically laser power and scan speed) on the consolidation of single layer mono stainless steel samples are investigated. Secondly, an investigation into the consolidation of mixing two stainless steel powders and resulting changes in the final material. Thirdly, an insight into the difference between manufacturing parts with two metals (stainless steel and CoCr) with comparison between samples of pure metals,

samples with defined metal regions and samples manufactured from a powder mixture of the two metals.

5.2 Powder characterisation

Two grades of stainless steels, 316L and 17-4PH were purchased from Sandvik Osprey [114] and EOS GmbH [115] respectively. Prior to experimentation the powders were analysed using scanning electron microscopy (SEM) to analyse particle geometry and laser diffraction to determine particle distribution. Typical particle geometry is shown in Fig. 5.1 and powder size distribution is shown in Fig. 5.2. The elemental composition of the powders is detailed in Table 5.1.

Table 5.1: Elemental composition of 316L and 17-4PH stainless steel used during experiments [114, 115]

Element, wt%	**C**	**Cr**	**Cu**	**Fe**	**Mn**	**Mo**	**Nb**	**Ni**	**Si**
316L	0.03	17	N/A	Balance	1.8	2.6	N/A	11	0.8
17-4PH	max 0.07	14-15.5	2.5-4.5	Balance	1 Max	0.5 Max	0.15-0.45	3.5-5.5	1 Max

Fig. 5.1 shows that the stainless steel powders have a spherical nature, which is to be expected from the gas atomisation manufacturing process [116]. Particle size, shown in Fig. 5.2, follows a fairly typical Gaussian distribution for volumetric distribution: 316L has a modal particle size of 32±1 μm and a maximum of 50±2 μm; 17-4PH has a modal particle size of 28±1 μm and a maximum of 47±1 μm. The number of particles ratio, which has been derived from the volumetric distribution, shows that there is a significant amount of smaller particles, which should contribute to better particle bed packing [117]. Both powders showed no signs of agglomeration, which allowed them to be easily poured and deposited during the experiments.

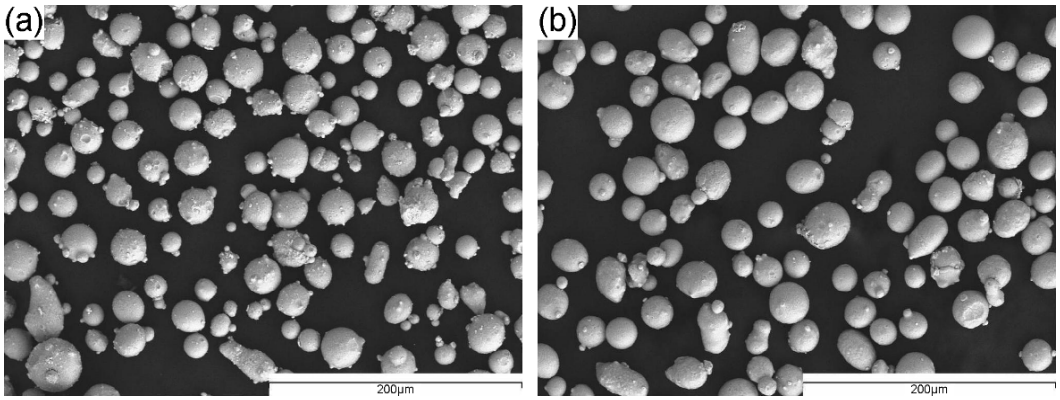

Fig. 5.1: Scanning electron micrographs of stainless steel powders showing typical particle geometry: (a) 316L; (b) 17-4PH.

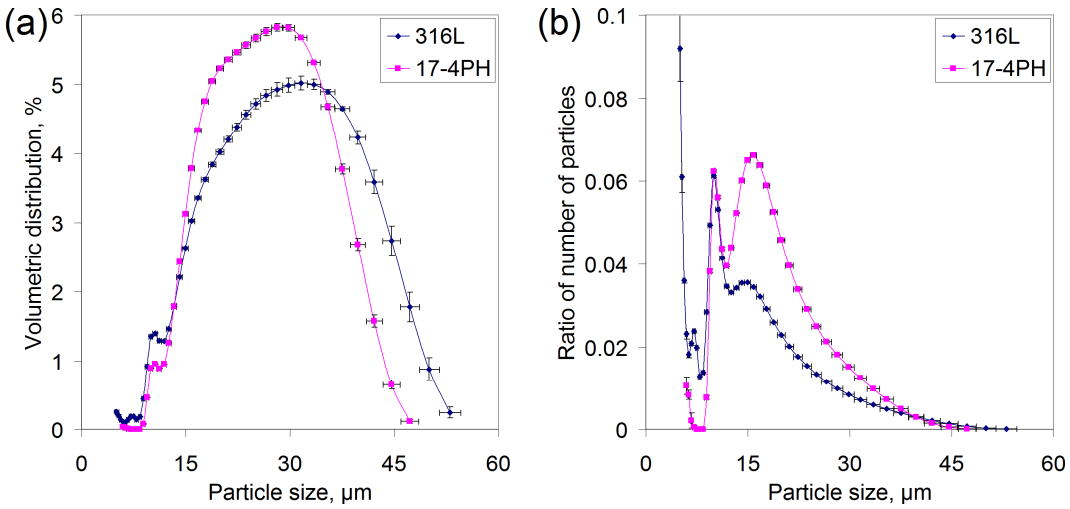

Fig. 5.2: Graphs of particle distributions determined by laser diffraction for 316L and 17-4PH stainless steel powders: (a) volumetric distribution; (b) comparative ratio of number of particles (ratio of number of particles is derived from volumetric distribution).

Magnetic behaviour was also tested, simply by pushing a magnet into the powders. It was found that the 316L was largely non-magnetic, though a few particles were attracted to the magnet (no doubt due to the fact that austenitic steels retain small amounts of martensite); 17-4PH particles were attracted to the magnet which was to be expected due to its martensitc nature.

5.3 Mono-material single layer samples

5.3.1 Introduction

A standard practice within the SLM field is to consolidate single layer samples of material on the top of a powder bed when embarking on the processing of a new material. The resulting single layer samples produced allow an insight into the consolidation behaviour and microstructural evolution of the material when subjected to melting by laser. Also, the single layer experiment allows the comparison analysis with previous work [98] as well as the selection of suitable parameters for the experimental study to build multi-layer parts.

5.3.2 Experimental method

For each test run, a 140×140 mm powder bed 10 mm deep was prepared in the Realizer's build chamber and the wiper of the dispenser mechanism was used to level and bring the powder to the correct zero position. Following this, the build chamber was then inerted using Ar gas to ≤0.8% oxygen; the oxygen level would decrease during processing to a minimum of 0.2%.

5 × 5 arrays of 20 × 10 mm mono- 316L and 17-4PH stainless steel single layer stainless samples were produced by scanning the surface of the powder with the laser. The scanning method was a raster scan (25 µm hatching spacing) with the scan lines being parallel to the shortest edge of the samples. Laser power and scan speed were varied with the range of 6 – 120 W and 50 – 250 mm/s respectively.

5.3.3 Results

Through initial experimentation, it was found that the density of a sample could be gauged by analysing the porosity of the lased surface. The lased surface was in turn affected by the scan speed and laser powder. Fig. 5.3 shows the affects of increasing laser power; as laser power increases the reduction in porosity is evident. The lowest setting, 20 W, appears to only effect a weak solid state sintering effect: 26.4 W starts to

initialise melting, probably liquid phase sintering and a transition to full melting occurs at in the range of 39.6 to 46.3 W.

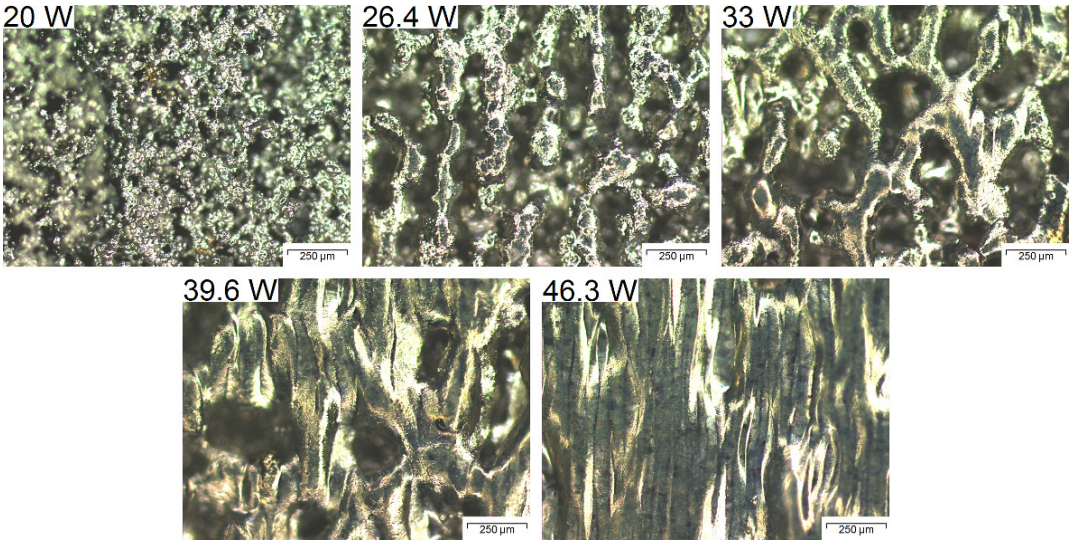

Fig. 5.3: Optical microscopy of influence of laser power on the lased surface of single layer 316L stainless steel samples (hatching spacing 25 µm, scan speed 250 mm s^{-1}). Note that 46.3 W shows a fully melted surface whereas lower powers have porosity.

Increasing laser scan speed (shown in Fig. 5.4) seems to have a less obvious effect upon consolidation than laser power. Balling phenomena become more exaggerated on the single layer samples when a slower scan speed was used, especially with the lowest scan speed of 50 mm s^{-1}. Regardless, increasing laser power while reducing scan speed increased consolidation density of samples (Fig. 5.5). This is attributed to increasing energy making it possible for molten steel to draw in surrounding powder.

The surface morphology of samples was also affected by overall energy supplied. Fig. 5.6 shows the surface morphology of 316 L and 17-4PH single layer samples processed at the highest laser power (120 W) and the lowest scan speed (50 mm s^{-1}), the highest energy density used in the SLM process. For 316L, the higher the energy used to consolidate the sample, the smoother the surface was. 17-4PH on the other hand always produced a notably higher surface roughness compared to 316L, forming visible 'ridges'.

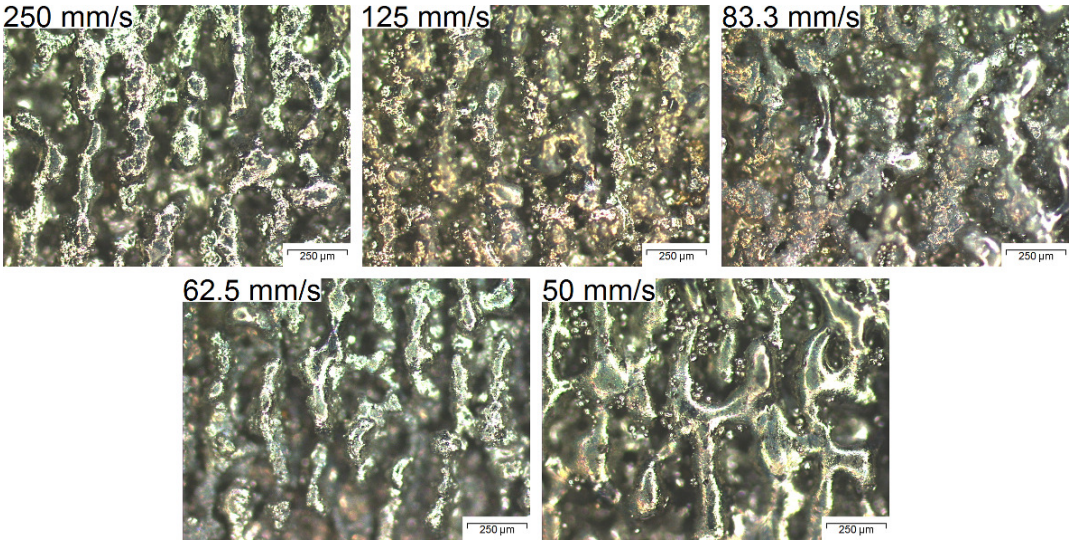

Fig. 5.4: Optical microscopy of influence of scan speed on the lased surface of single layer 316L stainless steel samples (hatching spacing 25 µm, laser power 26.4 W).

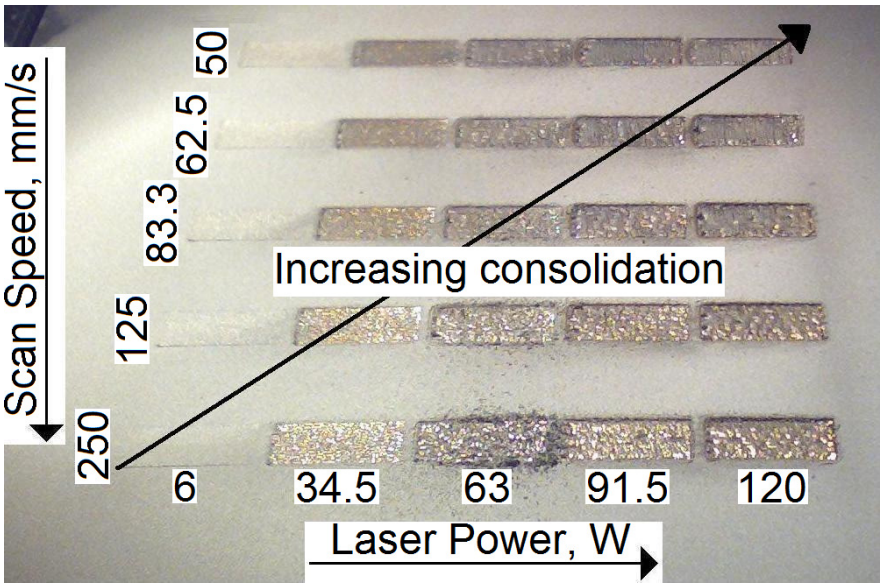

Fig. 5.5: Photograph of SLM fabrication of single layer 316L stainless steel samples.

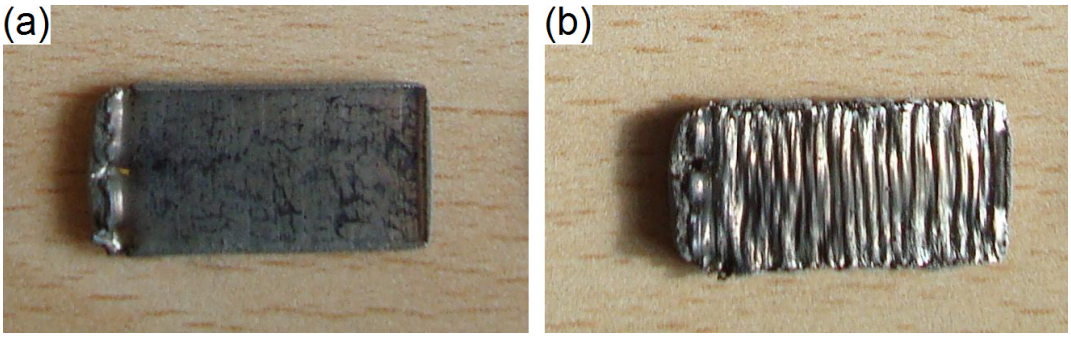

Fig 5.6: Photographs of 20×10 mm single layer stainless steel samples produced at a laser power of 120 W and a scan speed of 50 mm s^{-1}: (a) 316L; (b) 17-4PH.

Fig. 5.7 shows a cross-section of two consolidated samples. As can be seen, the 316L sample shows a fully dense region until approximately half the depth of the sample with a less dense and porous region occupying the bottom half. The fully dense region results from a full melting mechanism as the laser delivered enough heat to fully melt the powder at the top of the layer. The porous region at the bottom half of the samples has a sintered appearance. The 17-4PH sample shows full consolidation throughout most of the cross-section of the sample, with porosity evident only on the underside.

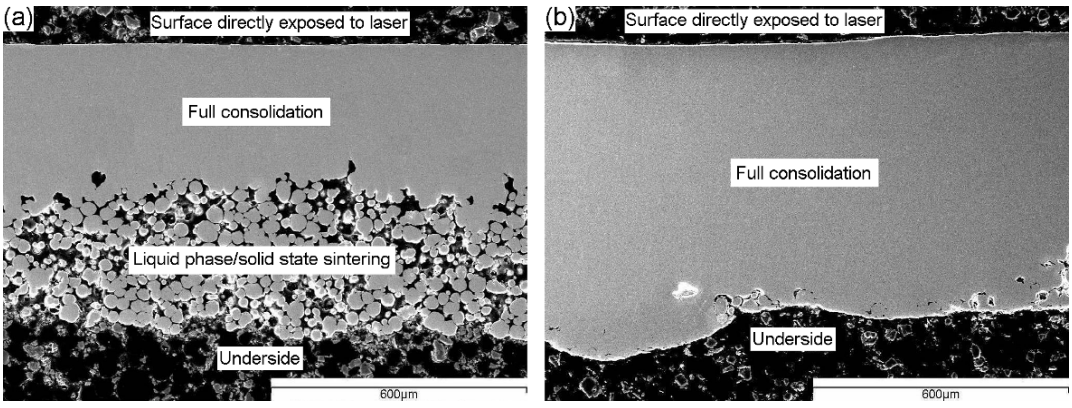

Fig. 5.7: Scanning electron micrographs of cross-sectional consolidation of single layer stainless steel samples produced at a laser power of 120 W and a scan speed of 50 mm s^{-1}: (a) 316L; (b) 17-4PH.

5.3.4 Discussion

Initial experimentation (Figs 5.3 and 5.4) revealed that a minimum laser power of approximately 46 W (for a spot size of 160 μm was required to achieve full melting of the stainless steel powders to consolidate single layer samples at the fastest possible scan speed. This can be explained by the thermal balance during processing: below a certain power (or rather, heat flux) the steel would dissipate the heat generated before full melting is achieved. This would also explain why scan speed does not seem to be so influential a parameter: it cannot change the heat flux of the laser. On the other hand, scan speed seems to influence the balling behaviour of the material, which would be due to the increased time the material spends molten, allowing surface tension forces more time to pull the liquid into a volume with minimum surface area.

In regards to the cross-sectional consolidation (Fig. 5.7), the 316L result is more expected as the heat energy supplied by the laser dissipates with depth, meaning that buried particles beneath the incident surface absorb comparatively less energy and bond via different consolidation mechanisms, specifically liquid and solid state sintering. However, 17-4PH shows almost full density. The full consolidation of 17-4PH samples is attributed to the copper addition that triggers the full melting and flow of the melted steel powders. Copper melts at ~1080 °C, whereas 17-4PH melts at ~1400 °C [118]. The copper could be flowing in a liquid phase between powder particles due to capillary forces [58] which creates a region that contains heat more effectively due to copper's thermal characteristics [119].

5.4 Selective laser melting of mixed stainless steel single layer samples

5.4.1 Introduction

Although both 316L and 17-4PH stainless steels are used extensively in industrial applications, there is a demand for steel parts consisting of two grades with differing properties [120]. As such, bi-grade or graded steel composites can be processed to produce high-performance functional products with tailored mechanical and/or magnetic properties; techniques such as metal co-injection moulding are currently the chosen processing routes [121, 122]. One advantage of powder metallurgy processes is

that various metallic powder grades can be mixed to produce desired properties for specific parts and varied composition ratios can be placed in different regions of the part to produce desired anisotropic properties [123]. Joint sintering of 316L and 17-4PH via hot isostatic pressing (HIP) was investigated by Simchi *et al* [121] to create discrete austenite or martensite regions in parts. This research reported the detection of a ferritic phase forming between austenitic and martensitic regions rather than a continuous martensitic/austenitic structure that can combine the benefits of the two grade materials and avoid the strain incompatibility when 316L is sintered or welded to 17-4PH. The biaxial stresses at the interface produced as a result of the strain incompatibility led to a higher densification rate but posed the danger of interface cracking and part warpage [121]. It is noted that current HIP processing lacks the flexibility and capability to create and control mixed material phases or graded material phases within produced parts. Furthermore, it is also difficult for HIP processing to produce components with complex shapes and/or geometries.

5.4.2 Experimental method

Three powder mixtures were prepared; 25, 50 and 75 wt% 17-4PH with the balance made up with 316L for the purpose of fabricating single layer samples. The powders were poured separately into a specially designed mixing canister (see Fig. 5.8) which was left to rotate along its axle at 47 rpm on a lathe for at least 45 minutes. Analysis of the post mixing powder was attempted but due to the similarity in elemental composition of the blended powders it was found that confirmation of homogenous mixing would be a difficult task. Instead, homogeneity of resulting microstructures was used to assess the powder mixing, which was found to be satisfactory.

Five single layer samples measuring 20×10 mm were produced for each powder mixture (including the 0 and 100 wt% 17-4PH powders). These samples were produced with the parameters found most successful in prior mono-stainless steel experiments: laser power of 120 W, laser scan speed of 50 mm s^{-1} and hatching spacing of 25 µm. Three of the five samples from each powder mixture were used for evaluating microstructural, hardness, and magnetic properties with the other two being used to investigate the consolidation of the cross-section. To examine resulting microstructures, the top of samples were ground and polished, then etched using Kalling's no. 1 reagent,

an etchant that shows up austenitic, martensitic, and ferritic phases [124]. Optical microscopy was used to evaluate the microstructures.

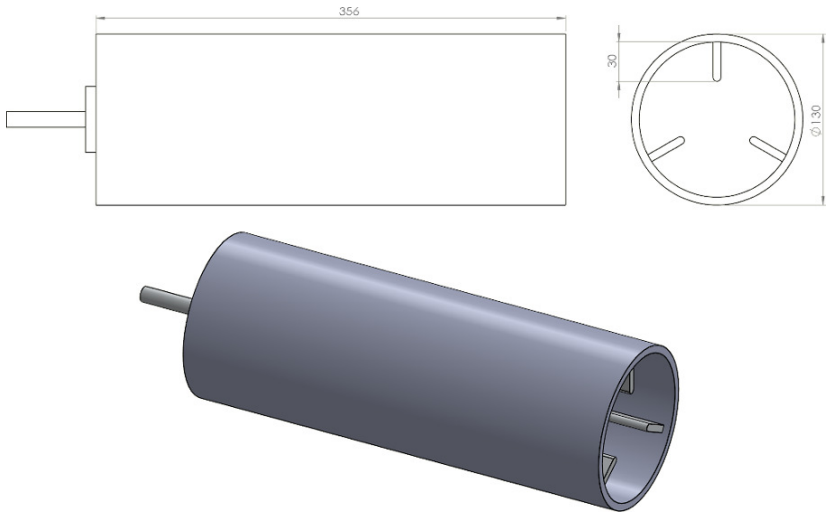

Fig. 5.8: Schematic of custom mixing cylinder used to blend powders.

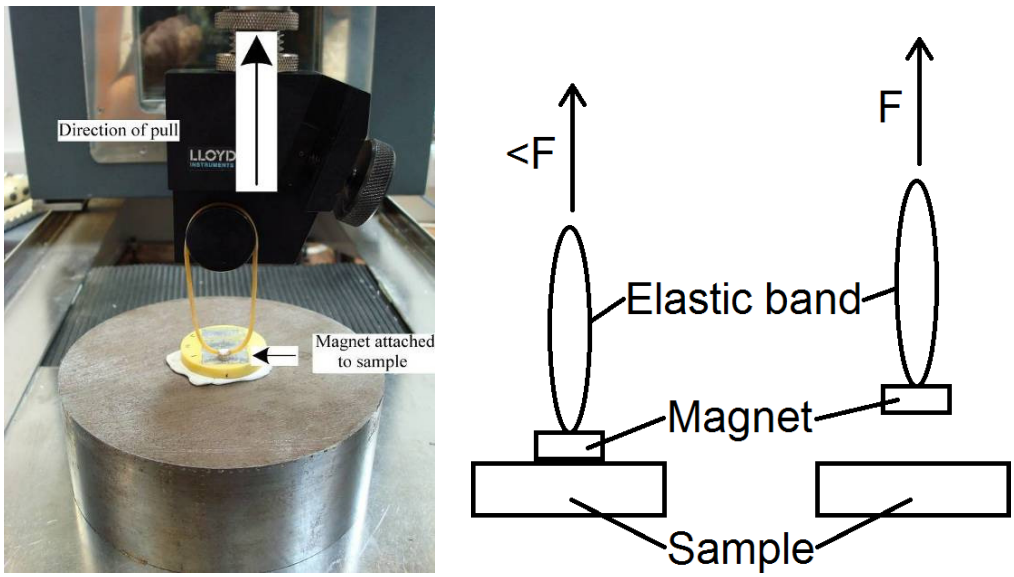

Fig. 5.9: Photograph and schematic of experimental setup for testing of magnetic properties of single layer stainless steel samples (both pure and mixed varieties). The tensile testing machine allows the reading of the tension of the rubber band, which immediately falls to zero upon the magnet pulling off (the tension required to pull the magnet off is designated '*F*').

To compare the magnetic behaviour of SLM fabricated samples, a rudimentary test that could be easily set up was desired. A small earth magnet was attached to an elastic band that in turn was attached to a tensile testing machine [125] fitted with a 50N load cell (the setup can be seen in Fig. 5.9). The tests began with the elastic band under no mechanical force with the magnet sat flat on the sample. The machine then pulled the elastic band into tension at a rate of 1mm/s and the highest force recorded during the experiment was taken as the force required to remove the magnet from the sample. All results are compared to the consolidated powder mixture requiring the most force to remove the magnet, being rated at 100 per cent 'magnetic adherence'.

5.4.3 Results

Fig. 5.10 shows the consolidation of a 25 wt% 17-4PH sample, with 0% 17-4PH (100% 316L) and 100% 17-4PH samples shown for reference. It is interesting to note the much improved consolidation of the 25 wt% 17-4PH sample over the 0 wt% 17-4PH sample; few pores can be found in the bottom region of the 25 wt% sample. The 50 and 75 wt% 17-4PH samples were effectively identical to the 25 wt% 17-4PH sample in terms of consolidation (samples are not shown due to similarity).

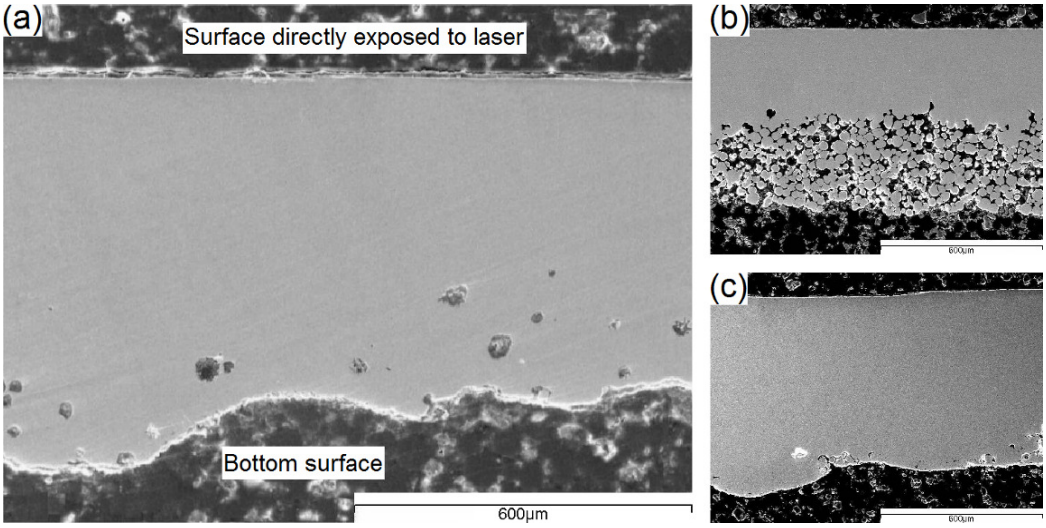

Fig. 5.10: Scanning electron microscopy of change in consolidation of single layer stainless steel samples produced at a laser power of 120 W and a scan speed of 50 mm/s: (a) 25 wt% 17-4PH; (b) 0% 17-4PH (100% 316L); (c) 100% 17-4PH.

The 316L steel with 0 wt% 17-4PH sample shows a very clear consolidated austenitic microstructure in Fig. 5.11a [126]. It is encouraging to see that the SLM process can produce a widely recognized and fully dense microstructure from powdered steel. The 25 wt% 17-4PH microstructure appears dendritic in nature and has more in common with that of cast A356 aluminium alloy [126]. The high cooling rate of the SLM process could be responsible for the fine dendrites just as in the casting of aluminium alloys. The structure is still austenitic but demonstrates more defined grain boundaries compared to the 0 wt% 17-4PH samples. This could result from α-phase ferrite and cementite (Fe_3C) precipitating out of solid solution due to an interface between austenitic and martensitic grains [121]. Also, the addition of copper via 17-4PH into austenitic steel could cause precipitation in the grain boundaries that reinforcing the steel. At 50 wt% 17-4PH the austenitic 316L still dominates the microstructure but the apparent precipitation of α -phase ferrite and cementite is more apparent. The 75 wt% 17-4PH microstructure appears to consist of elongated austenite grains laminar in nature with small regions of martensite forming. It appears that a critical value has been reached that allows martensite to form as grains. Exaggerated grain boundaries again indicate a-phase ferrite and cementite precipitates. The 100 wt% 17-4PH sample shows a typical lath martensite microstructure that has been tempered [121]. Like the 0 wt% 17-4PH sample it is good that the SLM process can take a maraging steel powder and keep the microstructure of the material. The tempered effect may also be considered a benefit as it is standard practice for conventionally produced martensitic steels to be tempered to give a higher ductility at a cost of reduced hardness [127]. The tempering could be an effect of the multiple passes of the laser over the material. Given the hatching spacing and diameter of the laser beam spot (25 and 160 μm respectively), a point on the sample would be heated by the laser approximately six or seven times. There was also evidence of a trailing heat effect; that is all samples would have a patch that continued to glow yellow for a small amount of time after the laser had passed, followed by cooling to a red glow that would hold until the sample had been processed.

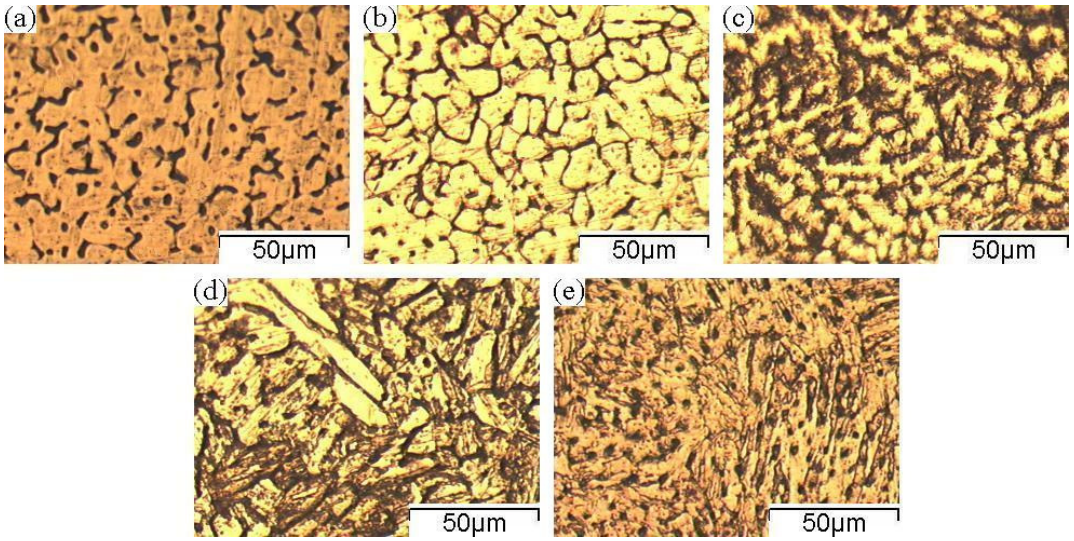

Fig. 5.11: Optical micrographs of etched microstructures taken from 316L stainless steel samples with varying 17-4PH content: (a) 0 wt% 17-4PH; (b) 25 wt% 17-4PH; (c) 50 wt% 17-4PH; (d) 75 wt% 17-4PH; and (e) 100 wt% 17-4PH.

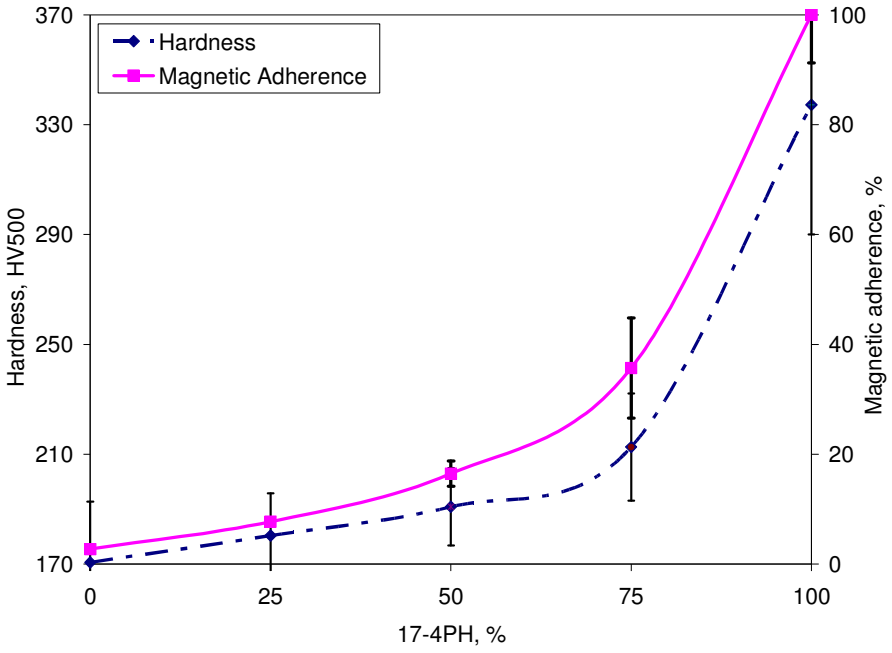

Fig. 5.12: Graph of 17-4PH content (316L as the remainder) *versus* mean values of Vickers hardness and magnetic adherence.

5.4.4 Discussion

The first phenomenon encountered was the increase in consolidation for mixed powder samples compared to pure 316L stainless steel samples. Though 17-4PH has a slightly higher thermal conductivity than 316L, this minor difference should not be the main cause of variation in the consolidation across the depth of the sample. As can be seen from Table 5.1, 316L has 0 wt% copper and 17-4PH has 2.5 to 4.5 wt% copper. It is thought that the superior consolidation of 316L samples containing 25 wt% 17-4PH is due to the copper addition that triggers the full melting and flow of the melted steel powders. Copper melts at 1080 °C [119] whereas 316L tends to melt at 1375 °C (17-4PH at 1400 °C). The copper could be flowing in a liquid phase between powder particles due to capillary forces which would create a region that contains heat more effectively due to copper's thermal characteristics [119]. The results indicate that the addition of 17-4 PH powder into 316L even at a low ratio could significantly improve consolidation and help to improve the SLM process.

The graph in Fig. 5.12 shows the initial value of 316L with 0 wt% 17-4PH to have a hardness of approximately 170 HV, over 10 per cent higher than if conventionally manufactured (148 HV [128]). This indicates that laser processing introduced hardening effects to the 316L samples due to rapid heating in a localized area followed by a cooling rate that allows a small amount of martensitic transformation. This laser hardening effect is typically seen in medium carbon steels such as 316L with carbon content between 0.3 – 0.5 wt% [129]. When the samples consist of 100 wt% 17-4PH, the hardness is approximately 337 HV, slightly lower than conventional values (349 HV [128]). This is due to the overlapping multiple laser scanning passes which lead to a tempering effect in 17-4PH and reduce its hardness to a small extent [129]. This confirms that tempering occurred for 17-4PH during the SLM process. These values show that the hardness of the samples produced by SLM is satisfactory; moreover, a slight beneficial effect can be added to both 316L and 17-4PH by SLM. What is interesting is the results in between 0 and 100 wt% 17-4PH as the hardness does not increase proportionally with the 17-4PH content. Up to 50 wt% 17-4PH, the hardness increases linearly but only at a rate of 0.4 HV (or a 0.235 per cent increase in hardness) per weight per cent 17-4PH added. This is due to a linear increase in a martensitic phase but an austenitic microstructure is still dominating the consolidated material. Between 50 and 75 wt% 17-4PH, the graph begins to stop showing signs of linear behaviour, culminating in a sudden increase between 75 and

100 wt% 17-4PH. The magnetic values determined experimentally show a striking similarity to the results found for hardness. The 100 wt% 17-4PH samples show the strongest affinity for magnetic adherence whereas the 0 wt% 17-4PH samples only have trace values. This matches with the magnetic permeability of the materials (1.02 for 316L, 95 for 17-4PH [128]). Just like the hardness values, the increase in magnetic adherence does not follow a linear trend throughout the whole range of values. Up to 50 wt% 17-4PH the magnetic adherence increases linearly, gaining ~0.28 per cent magnetic adherence per weight per cent 17-4PH. At >50 wt% 17-4PH content, the magnetic adherence increases disproportionately. Given the evidence of the hardness and magnetic values in Fig. 5.12, it appears that the samples consist of primarily austenitic phases until a 75 wt% martensite fraction is reached at which point the hardness and magnetic adherence increase dramatically. As seen in Fig. 5.11, this correlates with a dramatic change in microstructure. The increases in magnetic adherence seen in Fig. 5.12 may be attributed to ferrite forming (due to its ferromagnetic nature [128]) and cementite would increase hardness (cementite being a brittle ceramic [128]).

Investigation into the ability of SLM to consolidate 316L and 17-4PH stainless steel powder mixtures and variation of mixture ratios showed an effective means to tailor the mechanical and magnetic properties of stainless parts made by SLM. This opens up opportunities to produce new stainless steel alloy parts with specifically designed properties using the SLM process to meet various requirements and applications. Moreover, the findings are valuable for future research to develop SLM to fabricate functionally graded stainless steel materials with combined properties of two or more materials. Due to the nature of SLM processing, it is possible to change the mixture ratio of the deposited powder from layer to layer to form graded materials, therefore allowing the material properties to be altered in the z-axis of the build. The feasibility of this approach has been proved in the selective laser sintering process [130], but not yet attempted for SLM processing. The development of SLM and stainless steel based gradient materials will make it possible to generate a graded magnetic material with reduced strain incompatibility between steels. There is also scope for other functionally graded materials to be developed, such as titanium alloy implants with localized cobalt chromium bearing surfaces [131]. Due to the complexity involved in making functionally graded parts, it is likely that initial parts will be bespoke products. Over time, as the procedure becomes more accepted, small batches of high-value parts may become the normal method of production.

5.5 Production of 316L and CoCr tensile test parts

5.5.1 Introduction

As mentioned in Section 5.4.1 there is a demand for parts produced of two different materials [120]. Having demonstrated the potential of mixing 316L and 17-4PH stainless steels for single layer samples, the next logical step would be to produce multilayer samples with discrete or graded 316L/17-4PH powder mixtures, to examine changes in microstructure and magnetic behaviour through a sample.

Owing to a limited budget, producing multilayer samples of 316L/17-4PH mixtures was not possible since depositing varying powder mixtures would result in mixing that would not allow the separation of powders, effectively denying recycling of powders. Fortunately another SLM project was in progress during the author's tenure, called 'selective laser melting for functionally graded material' (SLAMFunc), which was investigating the mixing of powders with the intent of producing multi-material parts [132]. SLAMFunc was interested in the potential of stainless steel and CoCr and so the author collaborated to study the effects of multi-material multi-layer parts.

5.5.2 Experimental method

Parameters used for the SLM of 316L and CoCr tensile test parts were recommended by the equipment provider (MTT). These settings were: layer thickness of 75 µm; point distance of 80 µm and dwell time of 320 µm (theoretical scan speed of 250 mm s^{-1}); laser power of 100W; hatching spacing of 130 µm; one scan per layer with alternating XY hatching each layer; and a pre and post perimeter scan. Mixing of powders was achieved using the same method as with mixing the stainless steel. For 316L/CoCr hybrid samples produced with discrete material volumes, the bottom half of samples were manufactured using 316L; the process was then paused, the 316L powder was replaced with CoCr powder and manufacturing then continued. Laser diffraction analysis of the CoCr powder found that particle size distribution was similar to 316L and 17-4PH (Fig. 5.2)

Dumbbell-type tensile test samples (shown in Fig. 5.13) were produced based on ASTM guidelines [133]. Four sample material variants were fabricated: pure 316L, pure

CoCr, a 50/50 316L/CoCr powder mixture; and samples produced with two discrete material sections (the interface between the two materials ran parallel to the sample central axis). Samples were sand blasted but not subjected to any other finishing techniques. Since experimentation had to be as material efficient as possible, samples produced using CoCr were only produced in the XY plane (i.e. no samples orientated in the Z axis to minimise material use).

5.5.3 Results

Fig. 5.13: Example of tensile testing samples produced for 316L stainless steel, CoCr and combinations thereof. Note that for samples containing CoCr, only samples built in the XY plane were produced.

The tensile test data of SLM fabricated 316 L and CoCr parts shown in Fig. 5.14 shows strengths that would be expected from conventionally produced CoCr and 316L stainless steel materials; 316L stainless steel is much more ductile compared to CoCr. When the dumbbell samples are made with the 316L stainless steel/CoCr materials in separate sections (50/50 volume with an interface halfway through) the overall elongation length is reduced, though tensile strength is increased. Mixing the CoCr and 316L stainless steel powders prior to SLM processing results in a material that has a

better elongation tolerance as well as a tensile strength halfway between 316L stainless steel and CoCr. Elastic modulus is similar for all materials except the CoCr, which is stiffer.

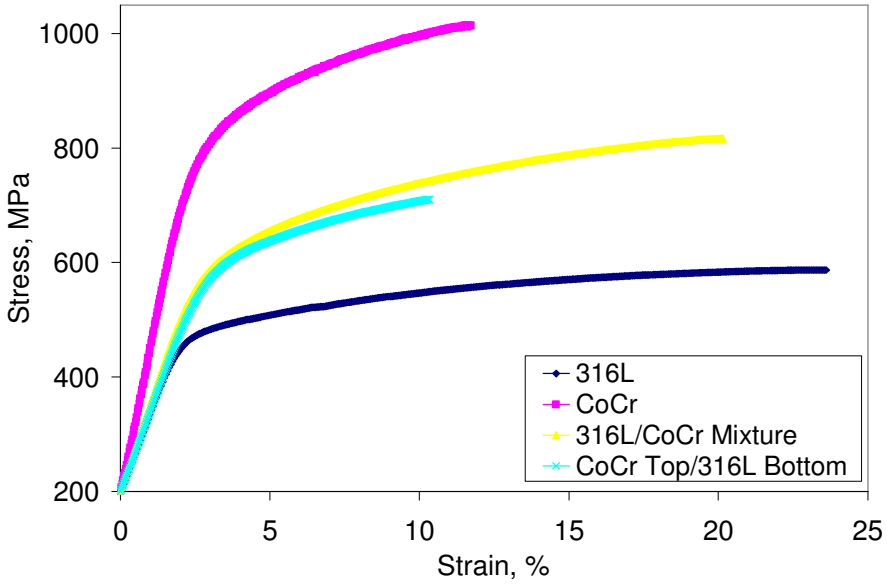

Fig. 5.14: Graph of strain *versus* stress for SLM parts fabricated from 316L stainless steel, CoCr and hybrid materials thereof (samples all in XY plane).

5.5.4 Discussion

The CoCr samples made by SLM exhibit higher strength but lower ductility compared to the 316L samples. The relatively low elongation of samples produced with discrete 316L and CoCr material volumes at 50% by 50% percentage can be explained by strain incompatibility. The higher elastic modulus of the CoCr infers that the CoCr half of the samples would be subjected to higher stresses than the 316L half; biaxial forces at the materials' interface would further increase resultant forces. By combining the 316L and CoCr materials via powder mixing at same 50/50 volume ratio, the resulting material would be more homogeneous, which would negate the strain incompatibility. Results showed that mixing 316L stainless steel and CoCr produced samples that had improved mechanical performance compared to the samples produced with separate materials that have a sudden change in material properties. This can be explained by the fact that

strain incompatibility and any resulting biaxial forces are nullified by mixing of materials. This demonstrates the ability of SLM to manufacture parts with a graded material composition, allowing the fabrication of hybrid and functionally graded materials. FGMs have the potential to be used to reduce strain incompatibility between interfacing materials.

6. Selective laser melting of single layer samples using pure aluminium and 6061 Al alloy

6.1 Introduction

Aluminium is a versatile material. The range of physical and mechanical properties that can be achieved from pure aluminium and its alloys is vast and as a result finds use in many applications, not just aerospace. Pure aluminium is known for its corrosion resistance (owing to an oxide layer formed through passivation) and low density (2.7g/cm3 [134]), as well as being attractive in appearance. Aluminium also displays excellent electrical and thermal conductivity and lends itself well to most forms of fabrication. Aluminium surfaces can be highly reflective to radiant energy, visible light, radiant heat and electromagnetic waves.

Processing aluminium powder is potentially difficult due to several properties of the material. Perhaps the primary disadvantage of aluminium powders is the oxide layer that will form upon exposure to air. Current machines that are able to process aluminium alloys reduce this problem by keeping the powder in an inert atmosphere at all times, even from the point of manufacture of the actual powder itself. This oxide may, however, increase absorption which leads onto another issue: the reflectivity of aluminium. Since aluminium is highly reflective, the laser power and/or energy density needed to process the powder may be increased compared to that of, for example, steel. Aluminium also has poor weldability and wettability [101], which may result in the phenomenon known as 'balling' with most parameters.

As discussed in Chapter 5, before embarking on the processing of a new material in SLM, it is common practice to produce single layer samples of the material to anticipate its behaviour. With this in mind, it was decided to analyse the behaviour of pure Al as a control material, with 6061 Al alloy also being investigated due to its relatively high Al content and weldability [135, 119] as well as its previous successful use in SLM [6].

There has been little to no research on the SLM of pure aluminium, probably due to the fact that pure aluminium itself is mechanically weak compared to other materials and therefore not suitable as a structural material. An investigation into the SLM of pure aluminium will allow a deeper understanding of the thermodynamic and

consolidation mechanisms involved; through this it is planned to open the way for more successful consolidation of Al alloys in SLM processing.

6.2 Powder characterisation

Two types of powder, pure Al and 6061 Al alloy, were purchased from Alpoco [136]. Prior to experimentation, the powders were analysed; typical particle geometry is shown in Fig. 6.1 and powder size distribution is shown in Fig. 6.2. The elemental composition of 6061 is shown in Table 6.1.

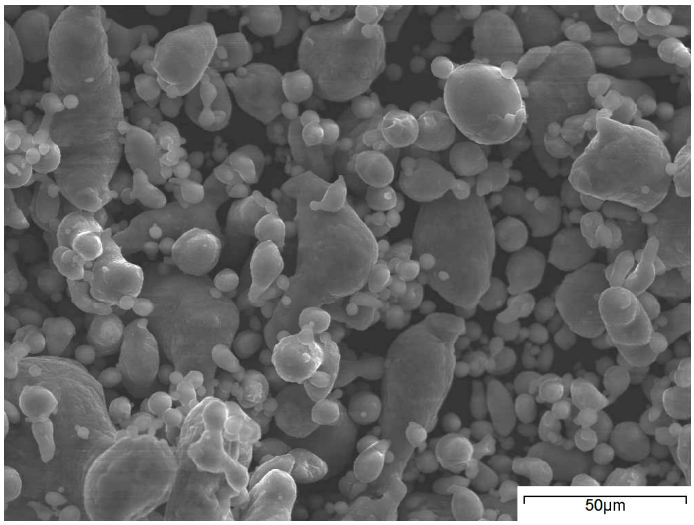

Fig. 6.1: Scanning electron micrograph of 6061 Al alloy powder showing typical geometry; pure Al powder was found to be similar.

Table 6.1: Elemental composition of 6061 Al alloy [134]

Element, wt%	Al	Cr	Cu	Fe	Mg	Mn	Si	Ti	Zn	Max other (each)	Max other (total)
6061	**Balance**	**0.04-0.35**	**0.15-0.4**	**0.7 max**	**0.8-1.2**	**0.15 max**	**0.4-0.8**	**0.15 max**	**0.25 max**	**0.05**	**0.15**

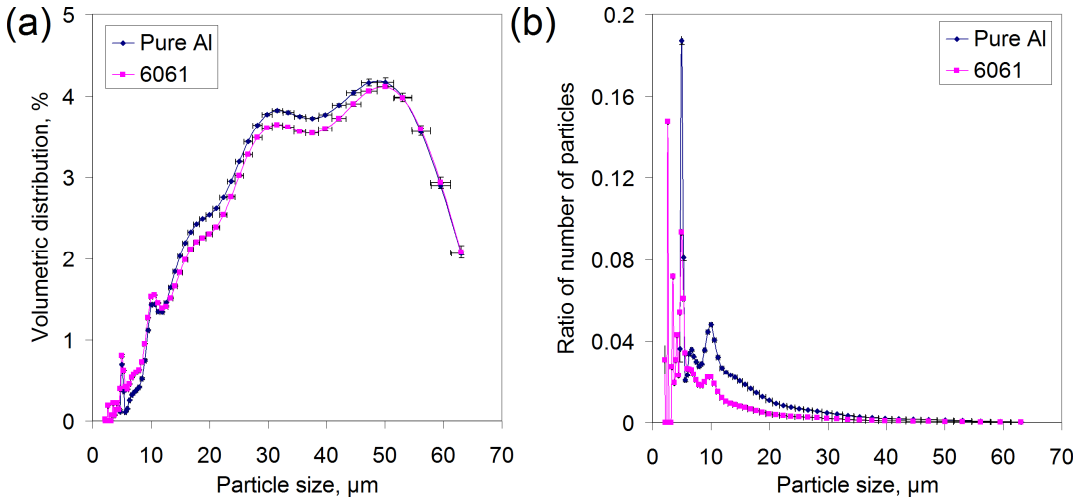

Fig. 6.2: Graphs of particle distributions determined by laser diffraction for pure Al and 6061 Al alloy powders: (a) volumetric distribution; (b) comparative ratio of number of particles (ratio of number of particles is derived from volumetric distribution).

Fig. 6.1 shows that the powders have a mixture of different geometries, apparently dependent on particle size; smaller particles are mostly spherical whereas larger particles seem distorted or stretched; it also seems that the Al based powders have a tendency to agglomerate but this is expected due to very strong inter-particle cohesion mainly ascribed to van der Waals forces [137]. Particle size, shown in Fig. 6.2, follows a somewhat Gaussian distribution for volumetric distribution indicating the powders have been sieved to a maximum of 63 μm: both pure Al and 6061 Al alloy have a modal particle size of 50±2 μm, The number of particles ratio, which has been derived from the volumetric distribution, shows that there is a significant amount of smaller particles of 10 μm in size or less, which should contribute to better particle bed packing [117].

6.3 Selective laser melting of single layer samples

Sample production was similar to the method used to produce the single layer stainless steel samples in Chapter 4, but a 7×7 grid was used instead. Samples were fabricated with varying laser power and scan speed (see Fig. 6.3): hatching spacing was kept at 25 μm and a conventional raster scanning technique was used. The following materials were used: unexposed pure Al powder (powder that was kept in an argon atmosphere

from manufacture to processing); exposed pure Al powder (powder that had been sieved in air and left to stand for approximately 16 hours); unexposed 6061 powder; and exposed 6061 powder. In the case of samples made with powder unexposed to air prior to processing, a sealed container containing the powder was put in the build chamber before flushing with argon; once the oxygen level had dropped to less than 1% the container was opened and the powder deposited.

6.4 Analysis

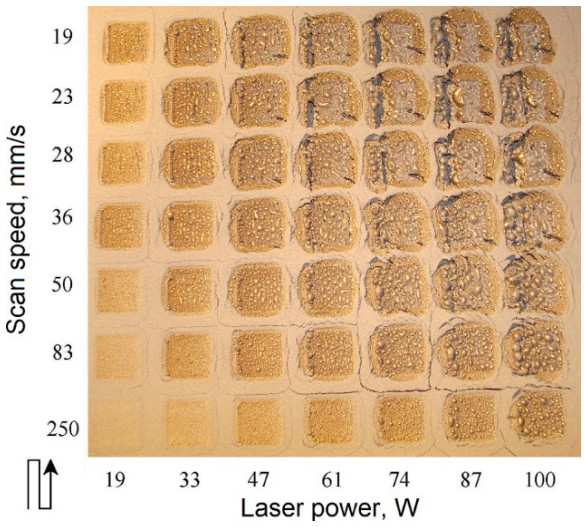

Fig. 6.3: Photograph of resulting samples from a single layer scan onto a pure aluminium powder bed. The arrow in the bottom left corner represents the scanning orientation; each sample is the result of a 10×10mm raster scan.

The SLM of pure Al powder formed large globules of material that contained evidence of microporosity (see Fig.6.5); this was unaffected by whether the pure Al powder had been exposed to air prior to processing or not. Samples varied in thickness depending upon the energy density; the thinnest sample that could be measured (33 W, 250 mm s^{-1}) was approximately 1mm thick whereas the thickest sample (100 W, 19 mm s^{-1}) was approximately 9mm thick. As shown in Fig. 6.5, the largest globules formed at the surface of the samples with the globule size generally decreasing with the depth of the sample. At greater magnification pores become evident within globules. The pores

formed in every globule of every sample and ranged in size downwards from approximately 9 µm; image analysis revealed that pores could account for approximately 20 vol% of a globule. SEM of samples did not yield any results that were not evident with optical microscopy. The pure Al samples were deemed unsuitable for further testing due to poor consolidation properties: excessive balling prevented a solid sample forming, instead forming a lightly sintered agglomeration of aluminium 'balls' that could easily be crumbled by hand.

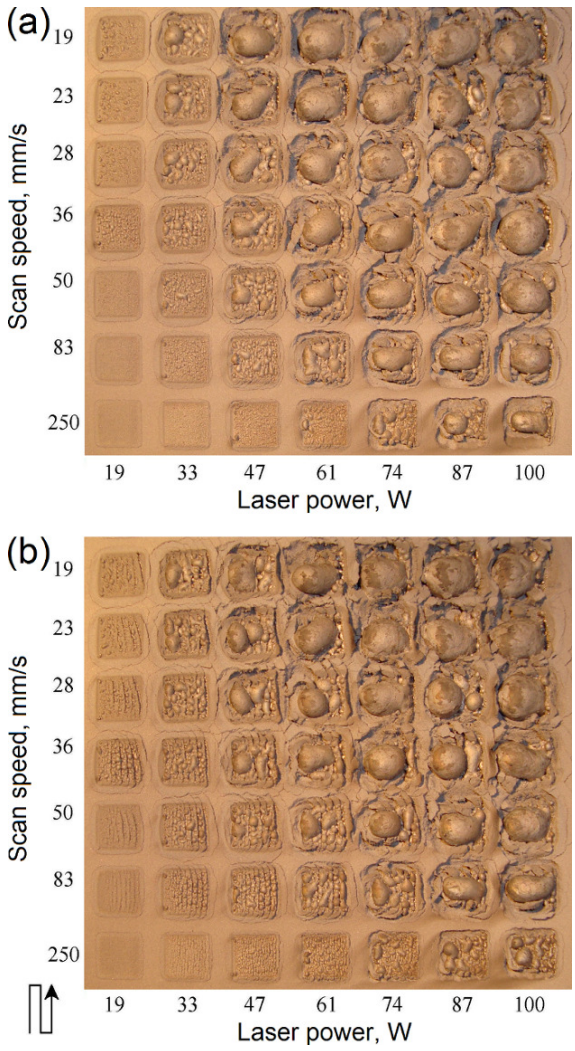

Fig. 6.4: Photograph of resulting samples from a single layer scan onto a 6061 aluminium alloy powder bed: (a) powder not exposed to air prior to build; (b) powder exposed to air prior to build. The arrow in the bottom left corner represents the scanning orientation; each sample is the result of a 10×10mm raster scan.

Hardness testing was undertaken on 6061 samples that were durable enough, using a Vickers indenter with a load of 20 Kg and a dwell time of 30 s. The unexposed 6061 had a hardness of 55.8 HV (standard deviation 5.1 HV) and the exposed 6061 had a hardness of 49.6 HV (standard deviation 4.4 HV). This was independent of processing parameters.

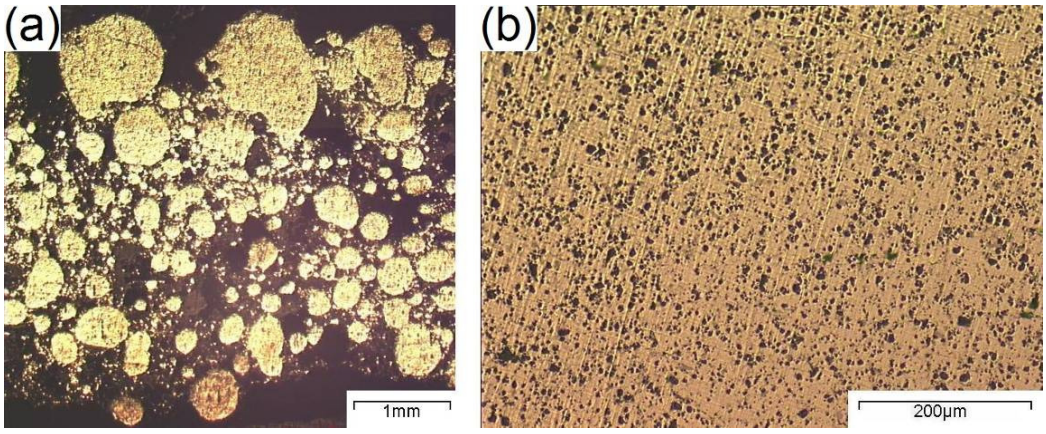

Fig. 6.5: Optical micrograph of a typical cross-section of a processed pure Al sample: (a) overall view; (b) pore formation.

The 6061 Al alloy was found to have superior consolidation compared to pure Al, enabling SLM production of large samples. For microstructural analysis, an etchant consisting of 46.2cc HF (40% conc.), 7.6cc HCl (37% conc.) and 46.2cc distilled water was used as recommended in the Metals Reference Book [124]. The microstructures of the samplses produced from 6061 Al alloy are shown in Figs 6.6 and 6.7. As seen, samples produced using only 6061 Al alloy show a dendritic structure; exposing the powder to air prior to processing increases segregation between dendrites. EDX analysis revealed that the dendrites themselves consisted of 100 % Al; interdendritic regions also contained Al, the additional elements of the alloy and oxygen. Exposed 6061 had higher oxygen content in the interdendritic regions compared to unexposed 6061.

Some of the exposed and unexposed 6061 Al alloy samples were machined into a cuboid approximately 3×2×2 mm. These cuboids were then weighed to compare density: assuming 2.7 g cm-3 for 6061 Al alloy, both exposed and unexposed 6061 achieved 96 ± 0.5 % density.

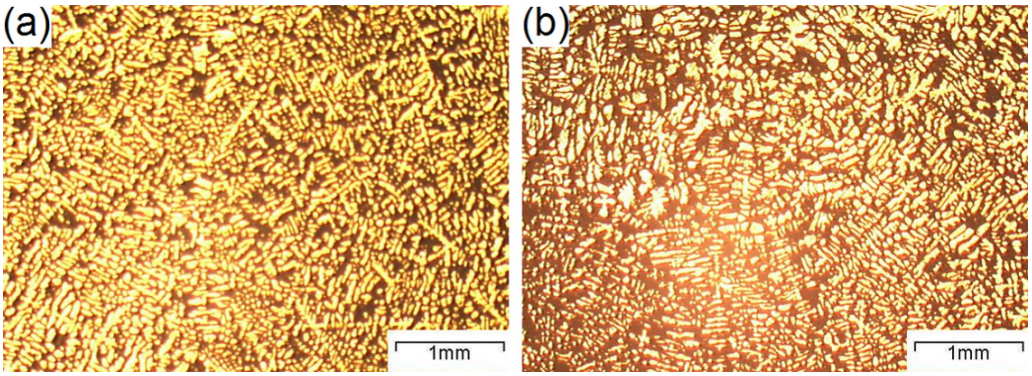

Fig. 6.6: Optical micrographs of typical microstructures in single layer 6061 Al alloy samples: (a) powder kept under inert atmosphere; (b) powder exposed to air prior to processing.

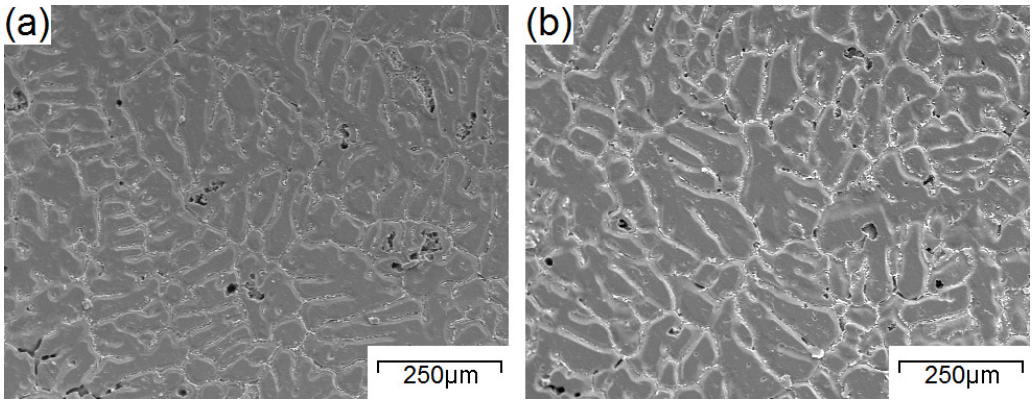

Fig. 6.7: Scanning electron micrographs of consolidated and etched single layer 6061 Al alloy samples: (a) powder kept under inert atmosphere; (b) powder exposed to air prior to processing. Dark grey areas are pure Al whilst lighter grey areas are interdendritic spaces and contain other alloying elements, as well as oxygen.

6.5 Discussion

6.5.1 Sample macrostructure

Surface analysis of produced samples show that pure Al powder is highly susceptible to the balling phenomenon when subjected to SLM processing. To be able to successfully

consolidate pure Al powder, a solution to reduce balling must be found. One effective approach is to find a way of increasing the surface wetting of molten aluminium. It is possible to do this by adding other elements or compounds [99] but the aluminium would no longer be pure and the resulting material would be an alloy. Alternatively, a double scanning strategy might be used as was demonstrated in a previous study to prevent the balling effect in the SLM of a ceramic and stainless steel mixture [138]. In addition, a laser more powerful than 100 W might have to be used in order to break down the oxide film more effectively in order to encourage the fusion of the melted aluminium [7].

The 6061 powder clearly shows a far superior consolidation compared to pure Al, which can be explained by the additional elements present (mainly silicon and magnesium); these materials account for the better weldability of the alloy [134]. However, exposing the 6061 powder prior to producing samples has a more visible effect upon consolidation compared to pure Al.

6.5.2 Microstructure

Pores are a typical flaw from welding Al and its alloys [139]. Since SLM can be considered to be a large scale welding process [58], it is not surprising that the Al that has melted together shows evidence of pores and possibly a complex network of microporosity [140]. During welding of Al, hydrogen is readily absorbed by the molten metal and forms pores. Water (which can be in the form of humidity in the environment) reacts with Al to form Al oxide and hydrogen. Even if not directly forming a pore, hydrogen can be stored atomically within the Al and released when the metal is melted [139]. The high power of the laser could be producing temperature gradients on the order of 10^6 °C which leads to Marangoni convection, with surface velocities approaching 1 m s^{-1} [85, 128]. Convection dramatically affects the geometry of the weld pool and can therefore modify (amongst other defects) porosity. Bearing this in mind, the Prandtl number, Pr_m, (kinematic viscosity/molecular diffusivity) of a material therefore can mean the difference between a deep, narrow spherical weld pool and a wide, shallow elliptical weld pool [141]. Al has a low Pr_m of 0.02 compared to, for example, steel with a high Pr_m of 0.1 which means that Al laser welding is dominated by conductive heat transfer. Cavitation could also be a factor in forming the pores due to the combination of Marangoni convection and the high energy of the laser.

This could be enough to activate microbubbles left in the material from processing or even to form microbubbles of Al vapour.

For the 6061 samples, there is no evidence of microporosity at the same level of magnification as observed in Figs 6.5 (b) and 6.7. Both exposed and unexposed microstructures show a rapidly cooled dendritic structure that is commonly seen in Al alloy casting [135]. However, exposure to air prior to production of samples has resulted in a slight change to microstructure, which can be attributed to the formation of oxide on the surface of the 6061 powder particles. Oxides can move to interdendritic spaces during SLM, increasing dendrite segregations and reducing mechanical properties. This explains the presence of oxygen in white grain boundaries in Fig. 6.7 and is also why a slightly lower hardness is achieved for exposed samples than that of unexposed ones.

6.6 Conclusion

This study shows that pure Al and 6061 Al alloy can be fully melted in the SLM process, but the molten material tends to agglomerate into globules due to the balling effect and possibly the existing oxide layer. Globule size is generally increased with increasing energy densities used in the SLM process. The poor wetting, poor absorption and the high thermal conductivity of pure Al and the oxide layer on the pure Al particles are primary reasons governing the agglomerations that result in the poor necking and fusion of the melted particles. Pores are formed within consolidated globules of pure Al, an effect seen in welding. If this is an inherent nature of aluminium when being processed via SLM, it is possible that aluminium alloys currently available may show the same behaviour. This will have negative effects on the mechanical properties of produced parts. Results also show that 6061 Al alloy powder consolidates better if kept under an inert atmosphere from production to SLM processing.

7. Selective laser melting of single layer samples using pure aluminium and 6061 Al alloy with copper

7.1 Introduction

The research described in the last chapter has demonstrated that (SLM) is capable of consolidating commercially available 6061 Al alloy. However, the use of existing Al alloys in the SLM process that show suitability for welding might not provide the high mechanical performance required for aerospace applications. There is also the fact that the high temperatures attained in SLM could lead to cracking in produced parts [135]. Owing to the layer-by-layer consolidating nature of SLM, there is not the same extent of heat treatment control as there is in more conventional alloy manufacturing techniques; that is to say, whilst there has been research into the simulation of heat transfer in SLM processing [142], there is no escaping the fact that a laser must form the part by continually raster scanning a cross-section. Hence, rather than try and impose a potentially advanced scanning method that may or may not work depending on geometry, it makes sense to instead investigate new Al alloy compositions with a proper additive to produce a material that could play to the strength of the thermal nature of the SLM process.

The Al alloys currently available in SLM are based on casting alloys [39] due to the combination of weldability and material molten flow behaviour; there is a growing consensus [143] that SLM may need specific, customised Al alloys that have not been considered viable previously in conventional processing. As discussed in Chapter 1, the main Al alloys in use in aerospace applications are the 2000 and 7000 series, with the 8xxx series becoming a material of interest. Consider the aforementioned Al alloys: the 2000 series uses Cu as the main alloying element; the 7000 series uses Zn; and the 8000 series uses Li. Since the materials used in SLM have to be in powder form, the health and safety risk of using fine Zn and/or Li powder is greatly exacerbated from what already would be considered dangerous materials. This leaves Cu as the only viable option as Cu powder is inert [144] and suitable to be added in Al alloy for SLM development. This research is to investigate the use of customised Al-Cu alloy powders in the SLM process to tailor their consolidation behaviours and improve mechanical properties of the resulting parts.

7.2 Manufacturing of single layer samples

7.2.1 Powder mixture characterisation

High purity Cu powder was purchased from Sandvik Osprey. Prior to mixing, the powder was analysed; typical particle geometry is shown in Fig. 7.1 and powder size distribution is shown in Fig. 7.2.

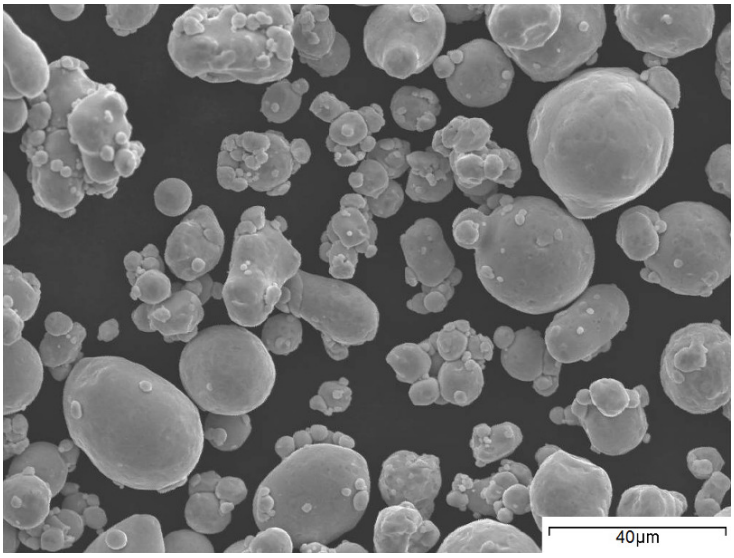

Fig. 7.1: Scanning electron micrograph showing typical geometry of copper powder.

Fig. 7.1 shows that the Cu powder has a spherical nature, which is to be expected from the gas atomisation manufacturing process [116]. Particle size, shown in Fig. 7.2, follows a fairly typical Gaussian distribution for volumetric distribution; Cu has a volumetric modal particle size of 28 ± 1 µm and a maximum of 50 ± 2 µm. The number of particles ratio, which has been derived from the volumetric distribution, shows that there is a significant amount of smaller particles. The number of particles ratio, which has been derived from the volumetric distribution, shows that there is a significant amount of smaller particles but also shows a comparatively high proportion of particles in the 18.8 ± 1 µm range when compared to the 6061 Al alloy powder. The Cu powder showed no signs of agglomeration when being poured.

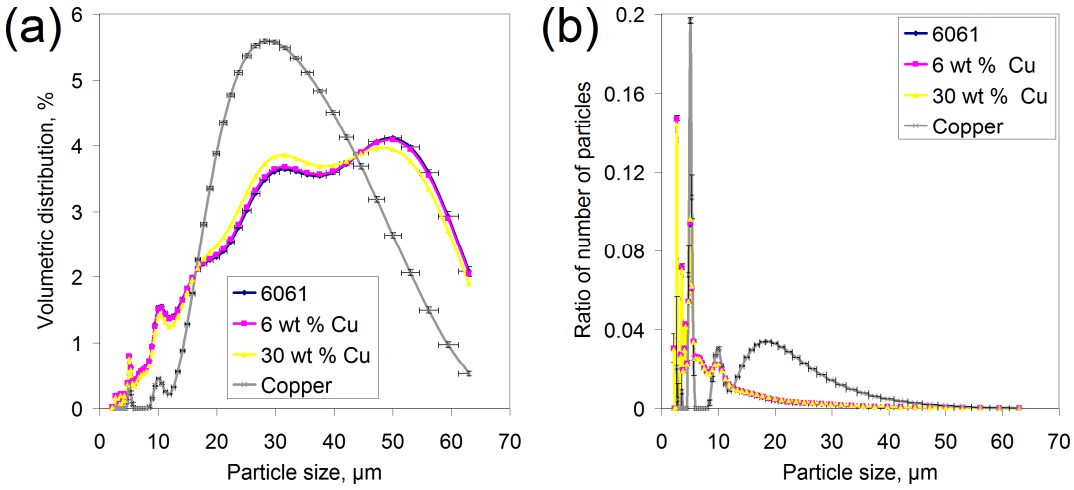

Fig. 7.2: Graphs of particle distributions determined by laser diffraction for 6061 Al alloy and copper powders: (a) volumetric distribution; (b) comparative ratio of number of particles (ratio of number of particles is derived from volumetric distribution).

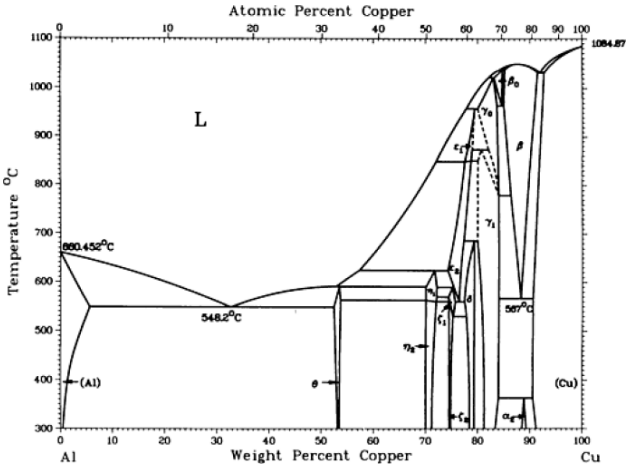

Fig. 7.3: Aluminium - copper binary phase diagram [145]

Two 6061 Al alloy-Cu powder mixtures were prepared: 6 wt% Cu and 30 wt% Cu. These values were chosen due to the nature of the Al-Cu binary phase diagram (Fig. 7.3): 6 wt% Cu represents the triple point that occurs at 548 °C, 30 wt% Cu represents the eutectic point of the two materials.

Mixing 6061 and Cu powder was found to reduce agglomeration of the base 6061 powder resulting in better pouring flow. As for the new particle distribution of the

mixed powders, this has been calculated in Fig. 7.2. Even though the Cu particle distribution is notably different from that of the 6061 powder, the relatively high volumetric ratio of 6061 to Cu (51.8:1 for 5 wt % Cu, 7.7:1 for 30 wt % Cu) means that overall distributions are not significantly different from the base 6061 powder.

7.2.2 Sample production

Powder mixtures were prepared in the same manner as the stainless steel powder mixtures were in Chapter 4; successful mixing was confirmed through EDX on consolidated samples. Due to the method of mixing and limited resources, it was impossible to keep the powders under an inert atmosphere; hence, all powders are considered 'exposed' as discussed in Chapter 6.

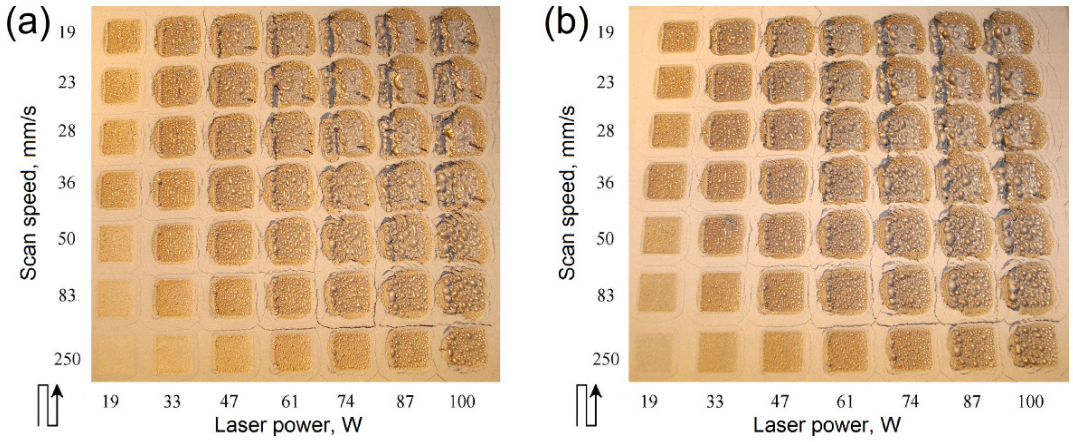

Fig. 7.4: Photographs of consolidation of single layer pure Al powder samples: (a) pure Al; (b) pure Al powder with 6 wt% Cu. Note the lack of any visual differences; cross-sectional consolidation was also similar.

Sample production was identical to the method used in Chapter 5, excepting the fact that in these instances powder mixtures of 6061 Al alloy and Cu were used. Pure Al with 6 wt% Cu samples were produced to see if adding Cu powder would help consolidationbut no difference was found compared to previous results in Chapter 5 (as demonstrated in Fig. 7.4). As such, pure Al powder investigation was halted in order to

focus on 6061 mixtures. However, for 6061, it was noted that introducing Cu powder improved consolidation (Fig. 7.5).

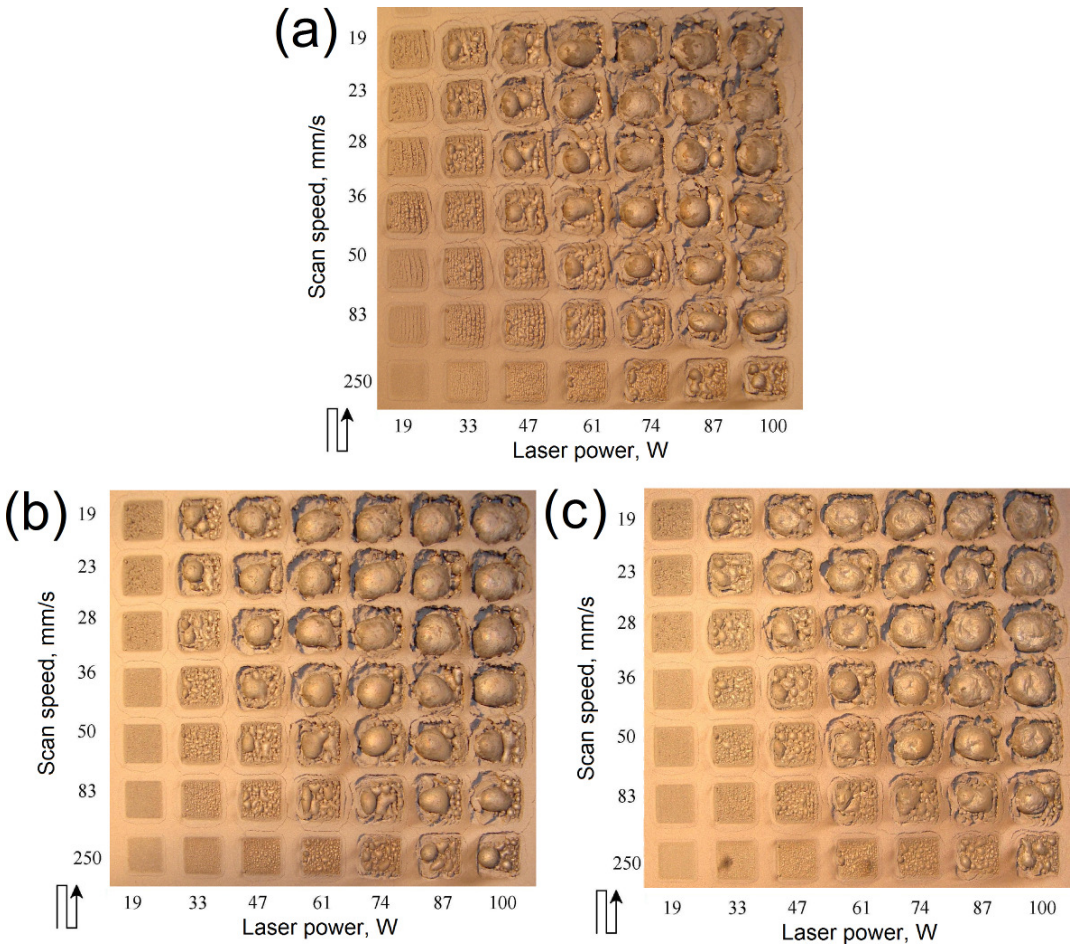

Fig. 7.5: Photographs of consolidation of single layer 6061 Al alloy powder samples: (a) pure 6061 Al alloy (exposed); (b) with 6 wt % Cu; (c) with 30 wt % Cu.

7.3 Analysis

Samples were etched with the same etchant used in Chapter 5, although it was found polishing the 30 wt% Cu sample with isopropanol as a lubricant gave a satisfactory etching that was used in for SEM analysis (isopropanol reacts with aluminium). As in Chapter 5, hardness testing was undertaken on samples using a Vickers indenter with 20 Kg load and a 30 s dwell time.

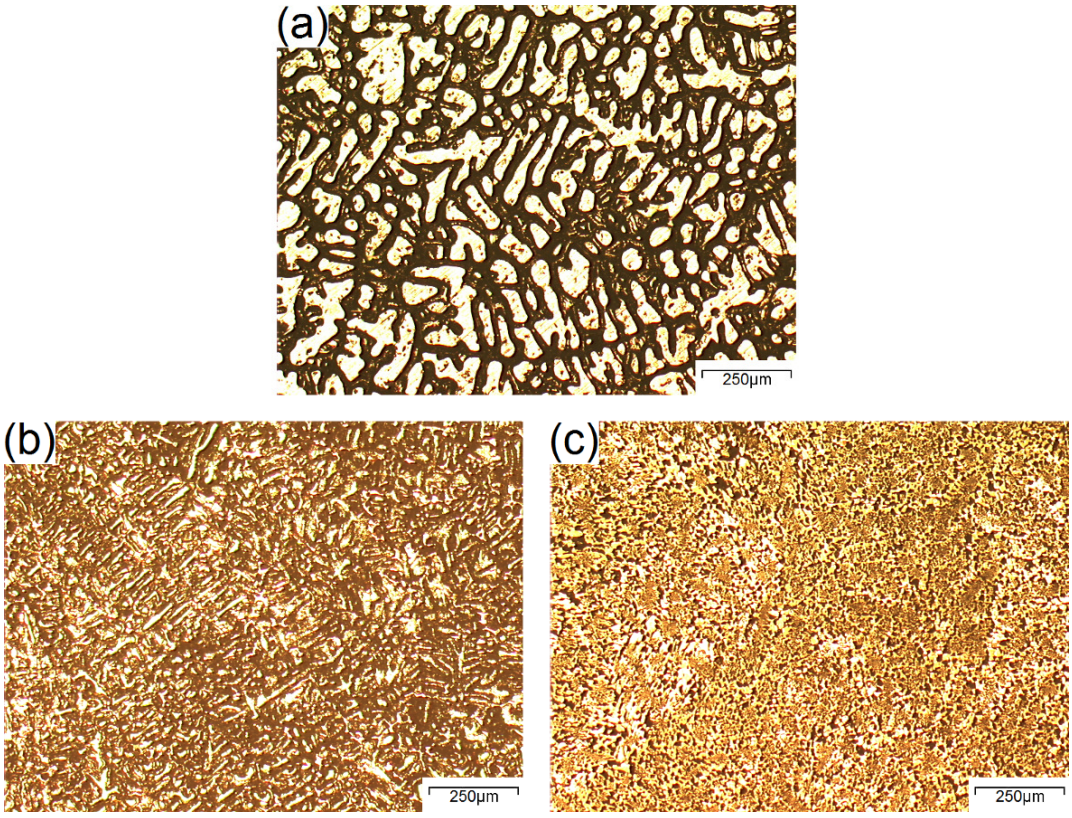

Fig. 7.6: Optical micrographs of etched 6061 Al alloy single layer samples (100 W, 19 mm s^{-1}): (a) pure 6061 Al alloy; (b) with 6 wt% Cu; (c) with 30 wt% Cu.

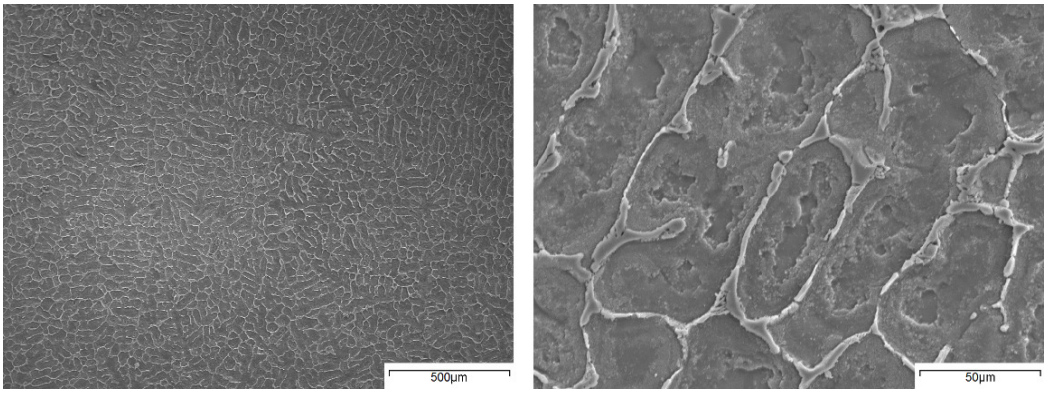

Fig. 7.7: Scanning electron micrographs of an etched 6061 Al alloy/6 wt% Cu single layer sample (100 W, 19 mm s^{-1}). Darker areas consist of approximately 95.1 wt% Al (remainder Cu); lighter areas consist of approximately 41.2 wt% Al, 51.6 wt% Cu and 5 wt% oxygen, remainder alloying elements (determined by XRD).

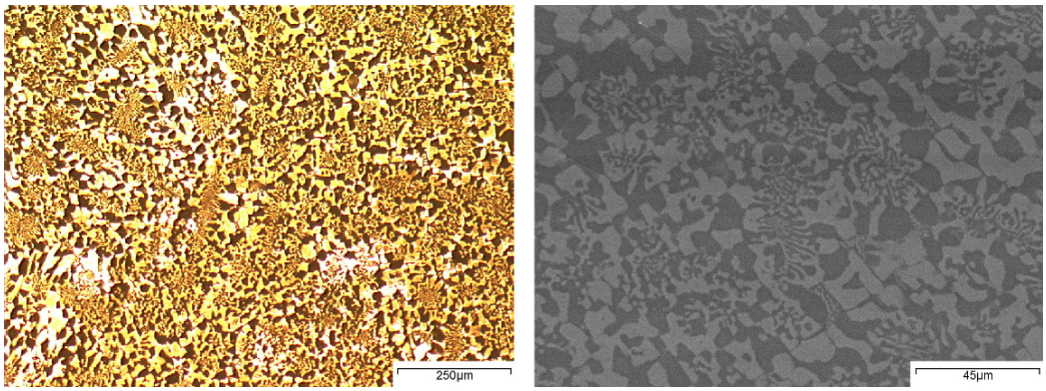

Fig. 7.8: Optical (left) and scanning electron (right) micrographs of an etched 6061 Al alloy/30 wt% Cu single layer sample (100 W, 19 mm s^{-1}). Darker areas consist of approximately 86 wt% Al (remainder Cu); lighter areas consist of approximately 43 wt% Al (remainder Cu).

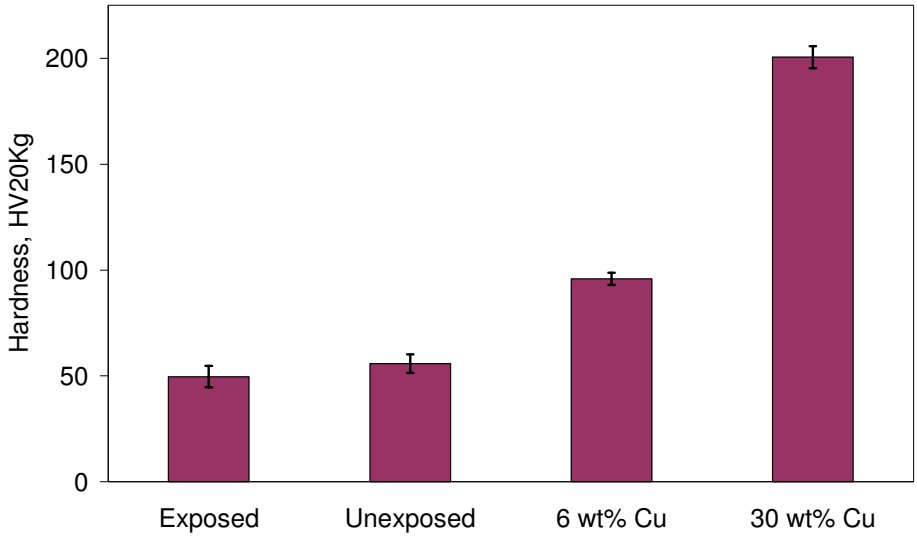

Fig. 7.9. Bar graph of hardness for single layer 6061 Al alloy samples with and without Cu (100 W, 19 mm s^{-1}).

A sample was taken from each experiment (100 W, 19 mm s^{-1}) and machined into a cuboid approximately 3×2×2 mm. This cuboid was used to calculate density: all samples appeared to be 96.5±0.5% dense.

7.4 Discussion

7.4.1 Microstructure analysis

The addition of Cu powder to 6061 dramatically changes the resultant microstructure (Fig. 7.6). In the case of adding 6 wt% powder, the microstructure has been considerably refined leading to an appearance of broken dendrites. Fig. 7.7 and relevant EDX results illustrates that these broken dendrites are in fact a combination of mainly Al (formed as dendrites) and Al-Cu intermetallics (formed in between dendrites), although interdendritic regions contain excess oxide from the exposed 6061 powder. These observations can be explained according to the Al-Cu binary phase diagram (Fig 7.3). Al dendrites primarily form in liquid while small amounts of remaining liquid contains Al and Al_2Cu. However, the energy supplied by the laser is not sufficient to properly dissolve Al_2Cu into Al liquid, leading to solidification of these phases instead of forming a solid solution. This results in Al solidifying as dendrites and Al-Cu intermetallics solidifying in between dendrites. The chemical composition results from brighter areas in Fig. 7.7 confirms this hypothesis where the chemical composition is almost the same as Al_2Cu (Al_2Cu contains about 53 wt% Cu [145]). These Al-Cu intermetallics can restrict the growth of dendrites leading to finer dendrites and subsequently higher mechanical properties. It should be noted that oxides on the powder particle surfaces tend to move short distances to fill gaps and are the last locations which solidify, therefore they mainly appear in between dendrites.

Adding 30 wt% Cu to 6061 Al alloy further changes the microstructure, resulting in a lamellar eutectic structure [126] plus Al and Al-Cu intermetallics, according to EDX results in Fig. 7.8. In fact, it seems that Al-Cu intermetallics (perhaps Al_2Cu) are mixed with Al but, as with the 6 wt% Cu samples, the energy supplied by the laser is not sufficient to properly dissolve to them into a complete solid solution. Thus, as the alloy is near the eutectic point and it should solidify at once, partially mixed liquid form lamellar eutectic phase from Al and Al_2Cu and the rest solidifies as it was. The result is altogether formation of darker (mainly Al) and brighter (mainly Al-Cu intermetallics) grey areas in the form of lamellar eutectics and droplets (Fig. 7.8). The lamellar nature of the eutectic phase can impede dislocation movement leading to higher material strength, but this heterogeneous microstructure may lead to flow localisation and is not desirable. Accordingly, it is suggested that molten alloys should

homogenised during SLM processing at high temperature which can be achieved by methods such as slower scanning speeds and/or higher laser energy fluxes.

7.4.2 Hardness

The hardness results (Fig. 7.9) compare pure 6061 Al alloy (exposed and unexposed) to the customised 6061/Cu alloys. As is expected, adding Cu improves the hardness of the resultant material by formation of strong Al-Cu intermetallics as secondary phases. For example, addition of 6 wt% Cu approximately doubled the hardness whereas addition of 30% Cu effectively quadrupled the hardness of the base alloy. In the case of the 6 wt% Cu mixture, this can be attributed to solid solution strengthening and dendrite refinement; for the 30 wt% Cu mixture, the combination of a fine eutectic structure and the formation of Al_2Cu intermetallics will cause the increase in hardness. Compared to a conventional 2000 series Al alloy such as 2024-T6 with a hardness of 142 HV [104], 6 wt% Cu attains 70% of the hardness which would imply a similar comparison in strength; 30 wt% Cu manages an improvement of 41% on the hardness, but as a eutectic material will be more brittle. It may be that optimising the Cu content could result in an Al alloy of at least an equivalent strength.

7.4.3 Elemental Composition

Fig. 7.7 shows the result of etching a 6061 Al alloy with 6 wt% Cu. The grains (darker areas) consist of pure Al with approximately 4.9 wt% Cu, which implies a solid solution forming. On the other hand, the grain boundaries contain 51.6 wt% Cu, 65 wt% Al and 5 wt% oxygen; the remainder being the alloying elements. Compared to 6061 Al alloy samples in Chapter 5, this shows a reduced oxygen content. Increasing the Cu content to 30 wt% removes any traces of oxygen altogether (Fig. 7.8).

This oxygen reduction phenomenon may be explained by the fact that Cu prefers to bond with Al rather than Al_2O_3 [146]. The Cu could be desorbed through any Al_2O_3 films that exist and, once in the molten Al, push the Al_2O_3 to the grain boundaries and outside of the sample.

7.5 Conclusion

The work presented in this section has set out to show the advantages of customised alloy usage in SLM, demonstrated by the improved consolidation behaviours of powder mixtures of 6061 Al alloy and Cu; on the other hand, pure Al does not respond so well to Cu additions (tested at 6 wt% Cu). The results show that by picking a base alloy that has a high weldability and sensible additive, customised alloys become a logical and proper choice in the SLM process. 6061 and its mixtures with Cu show promise to be successfully processed by SLM, while the addition of Cu has a positive influence on samples' hardness and reduces oxygen content. The improvement in hardness was related to the ability of Cu to alter the resultant microstructure. Microstructural analysis of samples revealed that Cu additions can restrict the growth of dendrites leading to a finer microstructural characteristic; Al-Cu intermetallics are also produced, appearing inside the matrix and increasing the strength of the alloy. The positive influence of Cu on strength by forming Al-Cu intermetallics was more pronounced especially in higher Cu percentages near eutectic compositions. However, it was suggested that homogenising the microstructure of this series of alloys might provide even more benefits.

8. Selective laser melting of Al and Al-Cu alloy multilayer samples

8.1 Introduction

Having undertaken an investigation into the effect of adding Cu powder to 6061 Al alloy powder and consolidating single layer samples in the previous chapter, the research was carried further to produce multilayer samples to illustrate the capability of the SLM process for the fabrication of net-shape or near net-shape parts. Various multilayer samples were produced from pure 6061 powder as well as 6061/Cu powder mixtures of differing ratios. As discussed in the previous chapter, Al-Cu alloys are prominent in aerospace material usage and the ease of handling Cu powder compared to other alloying elements (Zn and Li) makes researching Al-Cu alloys a sound starting point for the investigation of customised alloys produced by SLM.

Up to this point, work has focussed on single layer samples, though multilayer stainless steel and CoCr samples have been demonstrated in Chapter 4; these multilayer samples were produced using recommended parameters from MTT. It was quickly found that multilayer SLM processing of 6061 based materials was considerably more demanding than the aforementioned materials and naturally required more in-depth experimentation. The first round of experiments focussed on the production of 6061 samples. This allowed settings to be found that could then be used to produce samples from 6061/Cu powder mixtures.

The objective of the research presented in this chapter are therefore threefold: firstly, to find suitable parameters that allow SLM processing of 6061 and 6061/Cu powder mixtures; secondly, to examine sample properties in an effort to understand material and process phenomena occurring; and thirdly, to choose a satisfactory 6061/Cu powder mixture ratio to use in the production of a demonstration part (covered later in Chapter 9).

It needs to be mentioned that attempts were made to produce multilayer pure Al samples, however it was found that pure Al powder was unable to be deposited due to considerable agglomeration (a well known characteristic of Al powder [137]) despite varying deposition parameters. For practical reasons, experimentation on pure Al was abandoned.

8.2 6061 Al alloy

Since 6061 Al alloy is the base material used for the experiments outlined in this chapter, it was necessary to study the effect of SLM processing on the pure powder. This allows an insight into the effects additional Cu has on 6061 and will also allow reference for further work for improving consolidation.

8.2.1 Multilayer selective laser melting of 6061 Al alloy

As mentioned in Chapter 3, there was little previous research reporting findings on the SLM of Al alloys, let alone recommended settings for the production of parts out of specific alloys. Hence, same procedures used to process stainless steels as a starting point (see Chapter 3) in order to fabricate samples with a 10×10 mm cross section with the height limited by the maximum amount of powder the wiper unit could hold. It was found that processing the 6061 Al alloy in SLM was more difficult compared to steels. A trial and improvement method of experimentation was therefore undertaken to identify suitable operating parameters. Eventually the parameters that could make multilayer 6061 samples were found to be within a very small 'processing window'. Steels processed by SLM can tolerate comparatively large deviations of parameters while still being able to build a part [71], albeit with flaws such as increased porosity. 6061 was found to be extremely intolerant of varying parameters which are discussed in this section.

8.2.1.1 Powder deposition

The 6061 Al alloy powder was handled in the manner described in Chapter 6. Powder deposition was immediately found to be unsatisfactory with the default wiper speed (60 mm s^{-1}) and loader two deposition (150 steps), with the 6061 powder either not depositing at all or depositing unevenly leaving areas of the powder bed uncovered; increasing the number of steps loader two deposited did not improve the situation. Fortunately it was found that at a wiper speed of 15 mm s^{-1} or below, the wiper was prone to vibration which could lead to far better powder deposition, resulting in an apparently even powder layer. The wiper was run at a speed of 15 mm s^{-1} with loader

two depositing 120 steps per layer for all experiments hereafter; slower wiper speeds were not investigated as the powder deposition was deemed to be satisfactory and the comparatively slow wiping process was significantly prolonging the build time. With the deposition settings used, it was found that when the wiper was filled with powder to full capacity, a powder bed up to 7 mm deep could be deposited with the deposition settings used.

8.2.1.2 Base plate adhesion

Multilayer production was first attempted using a steel base plate as it was thought that an Al alloy base plate would conduct a large amount of the heat generated by the laser, possibly resulting in poor consolidation. However, the 6061 Al alloy powder was found to not bond with the steel, resulting in poorly formed samples. An Al alloy base plate was then used; initially the powder seemed to consolidate well but after a few layers the consolidated material would peel off the base plate; the peeling affect is shown in Fig. 8. 1. A sufficient bond was not established between the laser consolidated layers and the base plate surface as it was not receiving enough energy.

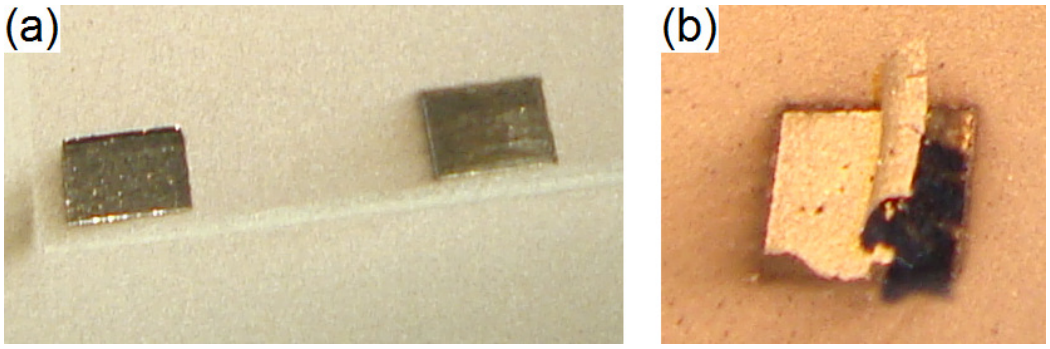

Fig. 8.1: Photographs of initial attempts at producing 6061 Al alloy multilayer samples (10×10 mm) on an unheated Al alloy base plate: (a) samples would begin satisfactorily provided parameters were suitable; (b) after a few layers samples would peel off.

To supply additional energy, a heating unit was installed to be in direct contact with the base plate to raise its surface temperature (see Fig. 8.2). After discussion with

MTT engineers and studying the isothermal transformation diagram for 6061, a base plate temperature of 150 °C was chosen. This would prevent precipitation (the formation of fine particles of a secondary phase) yet still supply significant heat. With this modification, the samples achieved satisfactory bonding to the plate i.e. laser consolidated layers would not peel off as they had done with a room temperature base plate.

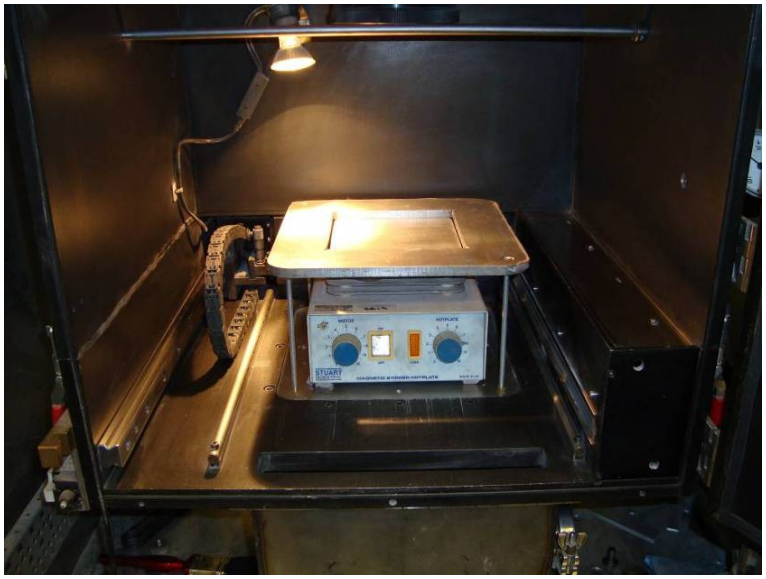

Fig. 8.2: Photograph of the installation of the heating unit in the Realizer. Al alloy base plates were placed on the top of the hot plate and held in place by an Al alloy 'ring'.

Prior to any build, the build chamber was inerted with Ar (as was the case with previous experiments), after which the heating unit was then switched on for three hours to allow the base plate and surrounding material to reach an even temperature.

8.2.1.3 Laser back reflection

Back reflection (discussed in Chapter 3) was prevalent, which was expected due to aluminium's highly reflective nature. Initially, this severely hindered experiments but after repeated observations, it was found that certain areas of the bed were more liable to cause back reflection, specifically near the centre. This is most likely caused by the

fact that the laser lens is directly above the centre of the bed, encouraging the beam to 'double back' on itself. Not only that, dropping the laser power to approximately 90W also seemed to reduce the number of back reflection incidents. Additional situations such as relative higher layer thickness or wider hatching spacing could also reduce the likelihood of back reflection occurring.

8.2.1.4 Layer thickness

Layer thicknesses of 25, 50 and 75 µm were investigated; all layer thickness achieved a satisfactory deposition. Sample production with 25 µm layers was found to be highly susceptible to back reflection, making manufacturing samples of any significant height extremely difficult. A 50 µm layer thickness was found to allow the build of relatively high multilayer samples with a significant reduction in back reflection occurrences: most builds completed without a single back reflection incident. SLM with a 75 µm layer thickness did not suffer from back reflection incidents but resulted in excessive balling that would not bond and cause the build to fail after a few layers, as shown in Fig. 8.3. Hence, all sample builds used a 50 µm layer thickness.

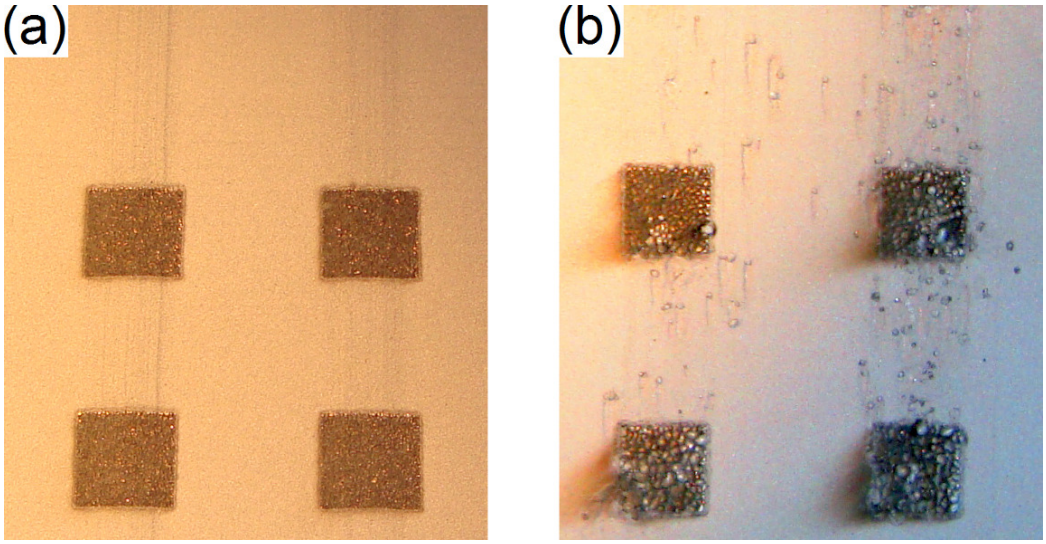

Fig. 8.3: Photograph of the effect of layer thickness on consolidation of 6061 Al alloy powder (10×10 mm squares): (a) 50 µm layer thickness (successful consolidation); (b) 75 µm layer thickness (failed consolidation).

8.2.1.5 Laser power

Since the Realizer had a laser spot size of 160 µm and a maximum laser power of 100 W, it was considered unable to supply enough energy flux for the satisfactory consolidation of Al alloys [7]. Hence the laser was run at the highest setting possible, which due to back reflection (which has already been discussed) was limited to 90 W. Running at lower powers resulted in balling effects similar to those seen in Fig. 8.3.

8.2.1.6 Scanning speed

In previous chapters concerning single layer sample production, it was found that decreasing the scanning speed improved sample consolidation; this is generally regarded to hold true for the SLM of multilayer steel parts as well [71]. In the case of 6061 Al alloy this was not found to be the case.

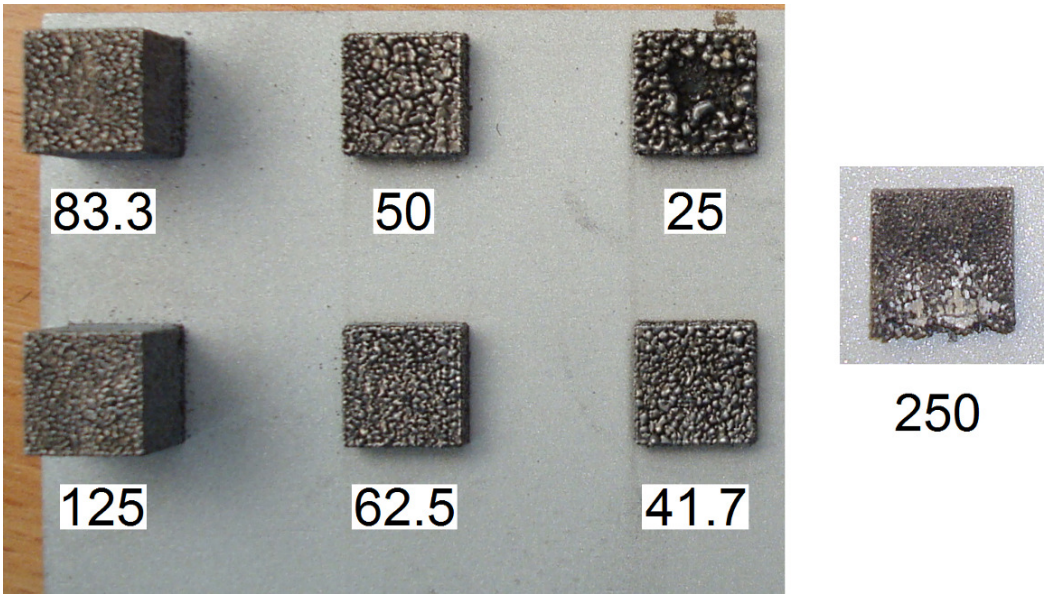

Fig. 8.4: Photographs of examples of the effect of scan speed upon consolidation of 6061 Al alloy powder (values in mm s^{-1}): 90 W, 50 µm layer thickness, 50 µm hatching spacing, 4 scans per layer. Balling on the top surface visibly increases with decreasing scan speed (samples 10×10 mm).

Fig. 8.4 shows the results of altering scanning speed. The fastest scan speed available (250 mm s^{-1}) resulted in 'overbuilding', that is to say the material consolidated into geometry higher than the layer thickness. Continuing a build using the fastest scan speed resulted in the wiper jamming.

The next lower scanning speed (125 mm s^{-1}) showed good consolidation, as did 83.3 mm s^{-1} though the top surface appeared to suffering from balling compared to samples produced with 125 mm s^{-1}. Further reductions in scan speed resulted in balling that worsened with decreasing scan speed. The effects of scan speeds used here for SLM consolidation agree with results published by Louvis [7].

8.2.1.7 Multiple scans per layer

Multiple scans per layer has been demonstrated by others to provide benefits such as improved consolidation and reduced residual stresses [67]. During experimentation, multiple scans per layer was investigated and appeared to have a positive effect on consolidation compared with a single scan per layer, so the multiple scanning strategy was investigated further. Scanning orientation of the following scan was perpendicular to the previous scan.

8.2.1.8 Wiper wear

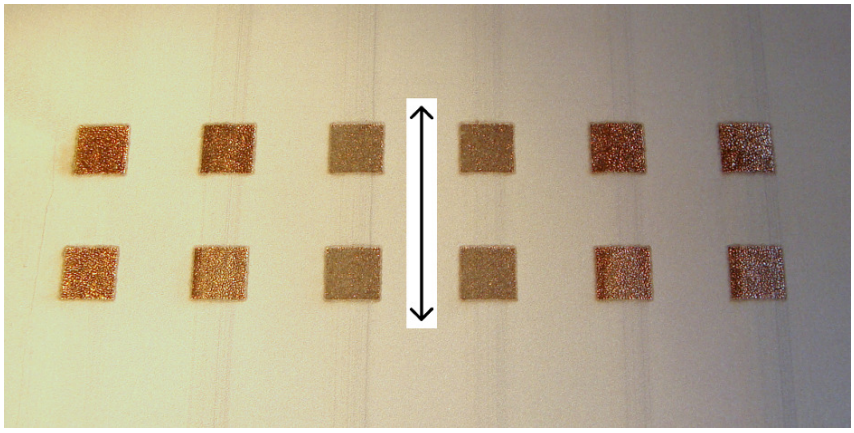

Fig. 8.5: Photograph of example of wiper wear that would occur during a build (arrow indicates wiper movement). Sample layout can be seen in Fig. 8.6.

As optimal settings for successful sample fabrication were set, it was found that the silcone rubber wiper would show signs of wear where it had passed over the samples (see Fig. 8.5). Wear would develop rapidly within the initial layers of a build, then appear to reach a stable point where no more material was removed from the wiper.

Wiper wear could not be eliminated from any build, though it was found that the left most samples in a build appeared to show almost no signs of wear.

8.2.1.9 Fabrication of multilayer samples

By taking all the factors discussed into account, multilayer samples of 6061 Al alloy were produced, as shown in Fig. 8.6. Optimum parameters were found to be: laser power of 90 W; base plate temperature of 150 ºC; 50 µm layer thickness; and 50 µm hatching spacing. Laser scan speeds of 125 mm s^{-1} and 83.3 mm s^{-1} were found to be able to produce samples; scan speeds were limited to the aforementioned values due to the point distance of 5 µm used (see Chapter 3). Multiple scanning per layer was also implemented for some samples to study any beneficial effects.

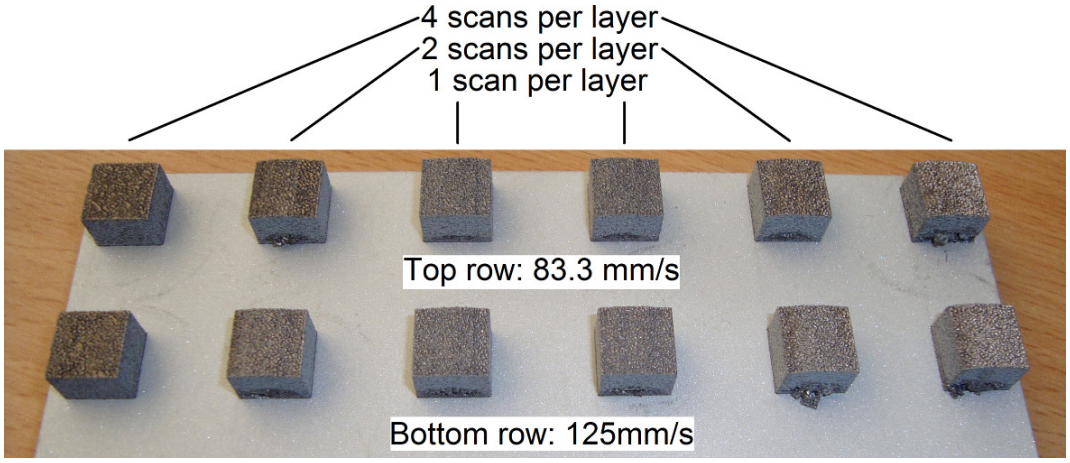

Fig. 8.6: Photograph of successfully consolidated multilayer samples of 6061 Al alloy (90 W, 150 ºC base plate, 50 µm hatching). Samples have a cross section of 10×10 mm.

It was found that even with optimised parameters samples would differ in appearance and consolidation depending on their position on the base plate. The effect

was repeatable, implying that whatever was causing the difference between samples was inherent to the SLM Realizer machine platform itself rather than differences in preparation. In particular, it was found that samples on the right side of the build plate had visibly poorer consolidation.

8.2.2 Characterisation

The SLM multilayer samples (see Fig. 8.6) were cut off the plate and subjected to surface roughness evaluation. Samples were then cut in half: one side was used for cross-sectional analysis perpendicular to the base plate and the other side for cross-sectional analysis parallel to the base plate. Additionally, a couple of earlier samples (see Fig. 8.4) were left attached to a portion of the base plate but cut perpendicular to the base plate to allow analysis of the bond between the base plate and samples.

8.2.2.1 Base plate bonding

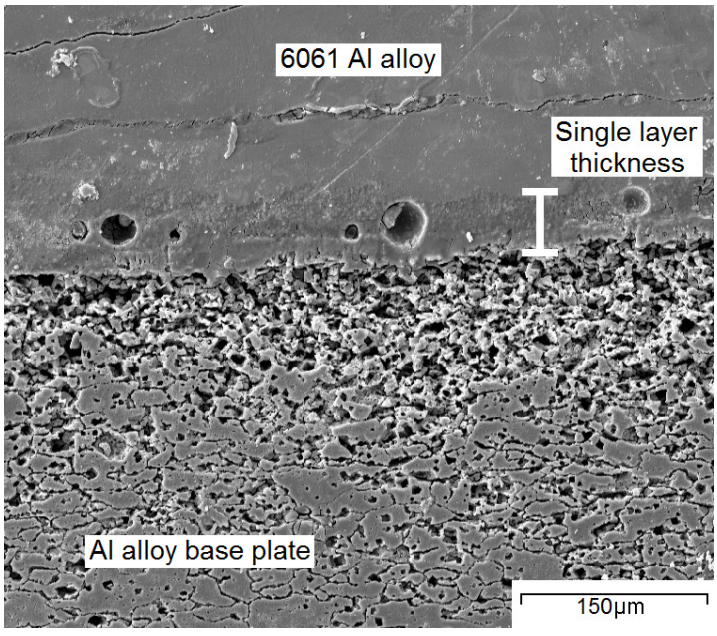

Fig. 8.7: Scanning electron micrograph of the interface between an Al alloy base plate and a 6061 Al alloy multilayer sample (etchant has been used). The area denoted as 'single layer thickness' represents the first layer of the build and is therefore 50 µm deep.

Fig. 8.7 shows an example of the interface between a consolidated 6061 Al alloy sample and the Al alloy base plate it was built on. The etchant (the same used to etch Al alloy samples in previous chapters) has attacked the microstructure of the base plate revealing elongated grains which is typical of rolled alloys [147]. The consolidated 6061 however shows little, if any, signs of etching except within the first layer of material. Even then, the darker region that is the first layer has no microstructure and implies diffusion of elements either from the base plate to the 6061 or vice versa; likewise the base plate material adjacent to 6061 shows increased signs of attack implying diffusion in either direction. One last feature to note is the formation of spherical pores that appear within the 6061 diffusion zone.

8.2.2.2 Consolidation

Consolidation of a typical 6061 Al alloy sample is shown in Fig. 8.8. Solid material has formed into a porous part with an ordered consolidation of columns that grow at approximately 45 º to the base plate.

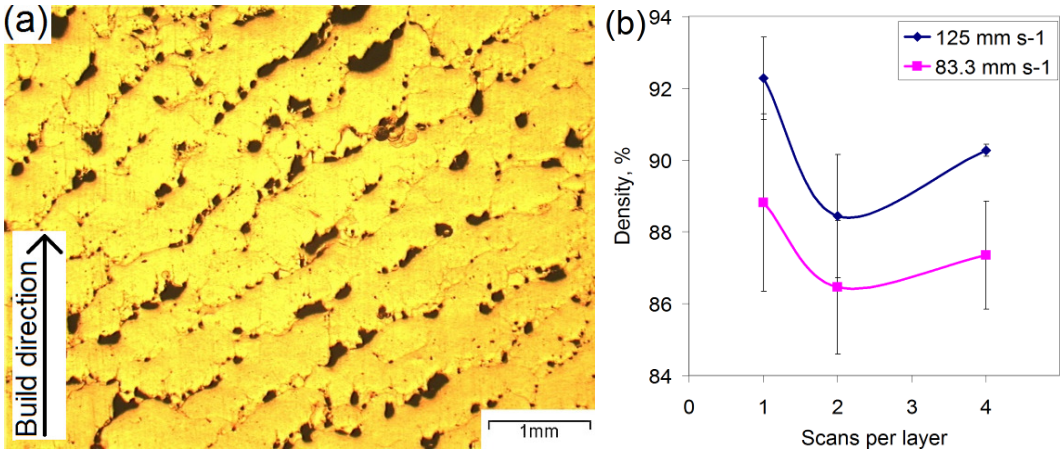

Fig. 8.8: (a) Optical micrograph of an example of cross-sectional consolidation in a 6061 Al alloy multilayer sample; (b) graph of scans per layer *versus* density at different scan speeds. (90W, 50 µm hatching, 50 µm layer thickness).

Density was calculated by dividing the cross section into five areas which were then evaluated individually for porosity: from this the mean value and standard deviation was derived: note that this is not a standard technique and was implemented to save time. Samples produced with a faster scan speed (125 mm s^{-1}) show better consolidation, peaking at 92.3±1.1 % density for one scan per layer. Scanning twice per layer reduces density by approximately 3.9 %; scanning four times per layer improves consolidation compared to two scans per layer but still reduces density by 2 % compared to one scan per layer, though seems to dramatically improve the deviation of density over the area analysed, implying a more uniform consolidation.

8.2.2.3 Microstructure

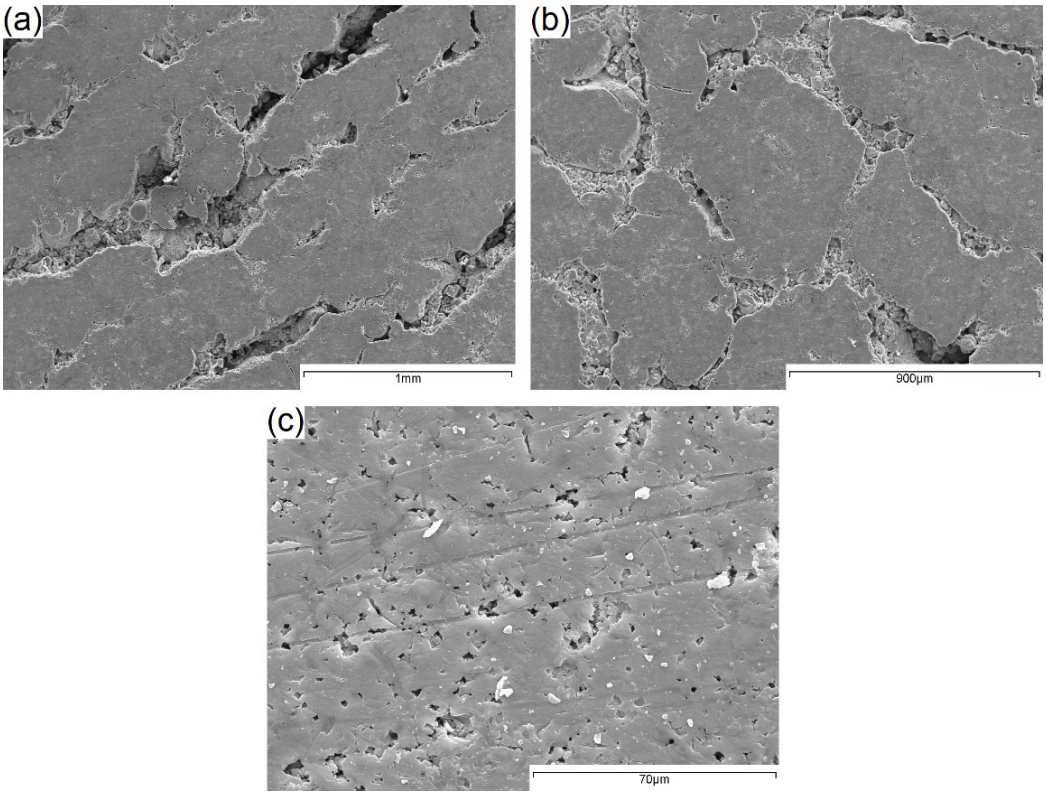

Fig. 8.9: Scanning electron micrographs of an etched 6061 Al alloy multilayer sample: (a) cross section through a sample parallel to laser; (b) cross section through a sample perpendicular to laser; (c) example of porosity in a sample (pores approximately 2 µm in size).

Etching of 6061 samples (Fig. 8.9) was attempted using the same etchant described in Chapter 5 but the samples were found to be resistant to etching. As has been discussed, the etchant is known to be effective since it etches the base plate (Fig. 8.7) therefore the consolidated 6061 demonstrates an anti-corrosional characteristic. On the other hand, boundaries between consolidated solids were more exaggerated as were small pores; the pores were approximately 2 µm in size. EDX analysis showed that oxygen levels were higher in the regions between solid material, indicating oxide formation and/or accumulation.

8.2.2.4 Surface roughness

Prior to analysis, samples were air blasted to remove loose powder without removing material that was loosely bonded. Surface roughness was measured on the same side for all samples, using a laser surface profiler [148]; results are shown in Fig. 8.10. Using a slower scan speed (83.3 mm s^{-1}) resulted in an approximate 2 µm increase in surface roughness compared to the faster (125 mm s^{-1}) scan speed, regardless of the amount of scans per layer. Multiple scans per layer were found to have a linear increase in surface roughness, with four scans per layer increasing surface roughness by 56 and 61.7 % compared to one scan per layer for the faster and slower speeds respectively.

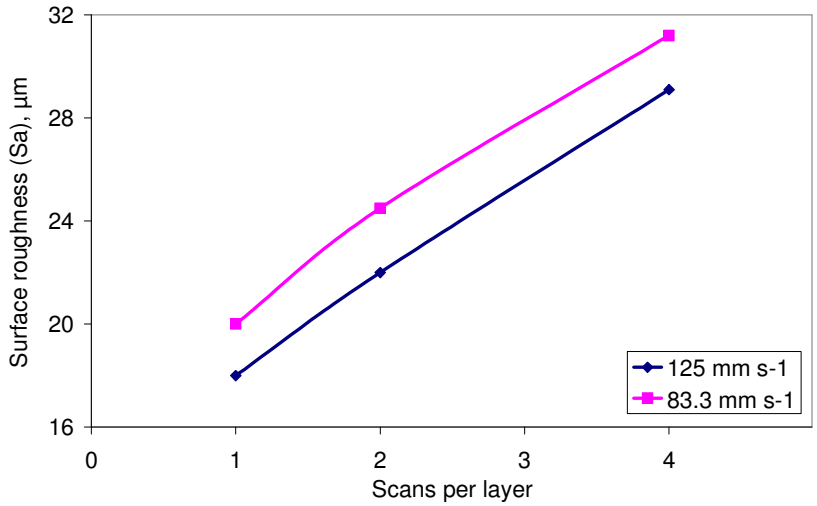

Fig. 8.10: Graph of scans per layer *versus* surface roughness for 6061 Al alloy samples (side of sample).

8.2.2.5 Hardness

Like previous chapters, hardness testing was undertaken on samples using a Vickers indenter. However, due to the comparatively poor consolidation, smaller indents had to be made using a 500 g load and a 30 s dwell time. Results can be seen in Fig. 8.11.

The hardness results follow a similar trend to the density of the samples (see Fig. 8.8), though scan speed does not seem to be so influential. However, in the case of hardness, four scans per layer was found to increase hardness compared to a single scan per layer by 7.8 and 12.1 % for 125 mm s^{-1} and 83.3 mm s^{-1} scan speeds respectively.

The hardness of the multilayer samples are superior to that of single layer 6061 Al alloy samples (see Chapter 6). A single layer sample produced with 6061 powder that has been exposed prior to processing has a hardness of 49.6 HV and the maximum hardness attained by a multilayer 6061 sample is 86 HV: this equates to a 73.4 % increase.

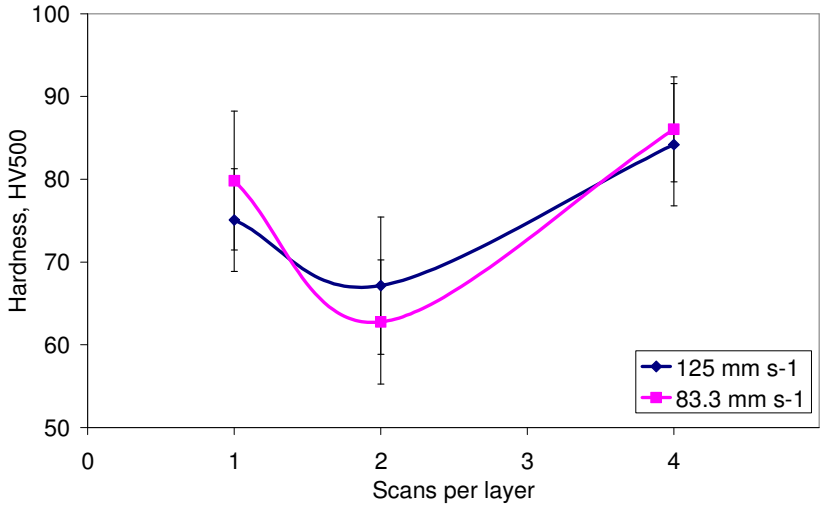

Fig. 8.11: Graph of scans per layer *versus* hardness for 6061 Al alloy multilayer samples.

8.2.2.6 Top surface analysis

As seen in Fig. 8.12, multiple scans per layer resulted in a striped pattern appearing on the lased surface, which matches with the 50 µm hatching spacing used to produce

samples. SEM analysis revealed scanning tracks perpendicular to the optically visible tracks, as expected from the scanning strategy used. The re-melted track width (i.e. where the laser had rescanned the surface) was approximately 27 µm: far smaller than the laser spot size (160 µm).

An EDX line analysis across a track width revealed that oxides were reduced to negligible levels on the surface of the track but peaked at the sides.

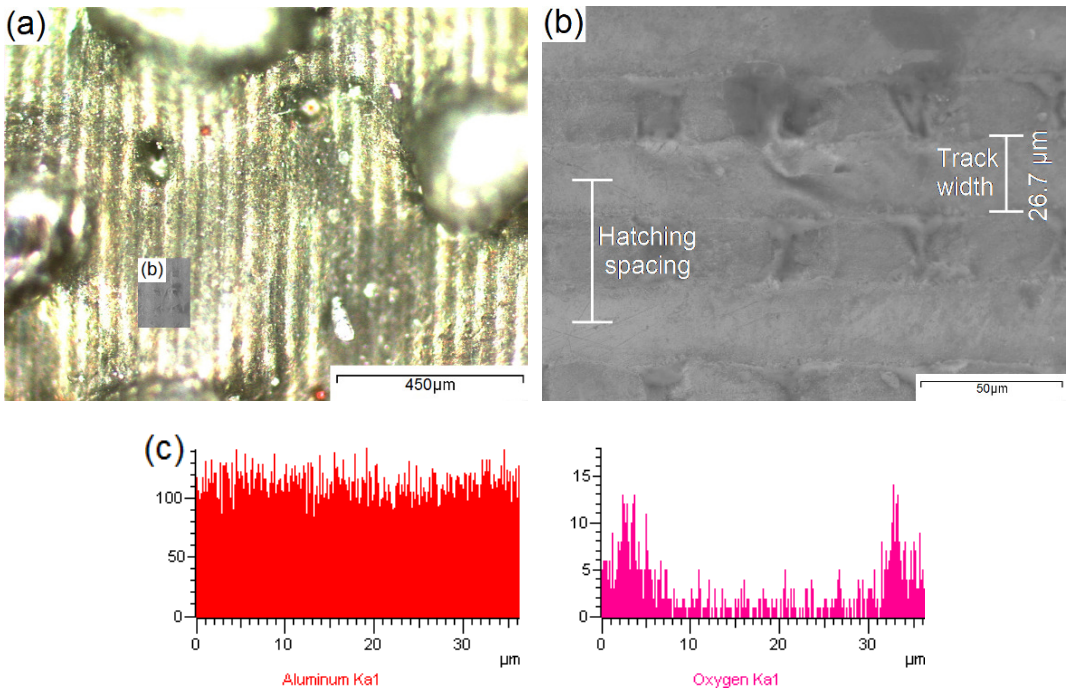

Fig. 8.12: Effect of multiple scanning on the top surface of a 6061 Al alloy multilayer sample: (a) optical micrograph showing visual effect of laser scan and showing location of (b); (b) scanning electron micrograph of the top surface, showing hatching spacing (50 µm) and re-melted track width; (c) EDX line scan across a re-melted track width, showing oxygen displacement to the edge of the track

8.3 6061 Al alloy and copper

With the successful fabrication of 6061 Al alloy samples, experimental study and analysis was then carried to produce customised Al-Cu alloys using 6061 as the base material.

8.3.1 Multilayer selective laser melting of Al-Cu alloy

Samples were fabricated in an identical fashion to the pure 6061 Al alloy samples to maintain consistency between the sample groups. Since materials were in short supply, the powder from the previous build was sieved to 63 µm, mixed with more Cu powder (and more 6061 powder if necessary) to meet the correct Cu content and then used in the next build. EDX was used to confirm elemental composition of the last samples after SLM fabrication, which matched with expectations. Powder mixtures were prepared in the same way as has been described in previous chapters. Examples of samples are seen in Fig. 8.13. As before, sample height was limited to the maximum capacity of the wiper producing samples up to 7 mm tall.

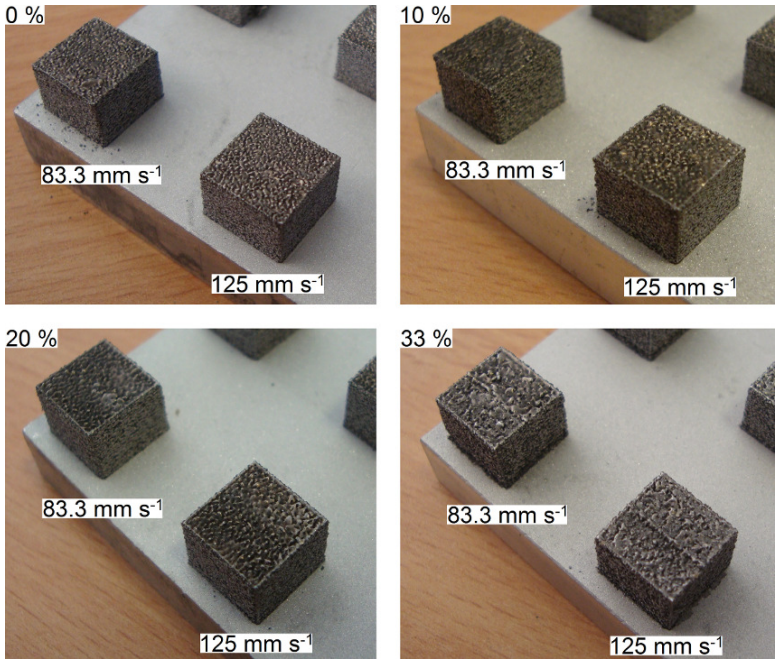

Fig. 8.13: Photographs of examples of multilayer samples produced with 6061 Al alloy/Cu powder mixtures. Values are in wt% Cu, with relevant scan speeds given; all featured samples have been produced with four scans per layer. As with the pure 6061 Al alloy samples, samples are produced with a 10×10 mm cross section.

After an initial batch of samples had been manufactured, some samples approximately 80 mm tall were manufactured by refilling of loader 2 to test height

building capabilities using what was deemed to be the best powder mixture ratio and the best parameters available (see Figs 8.14 and 8.15). This would allow some compression samples to be made as well as more accurate measurements of density.

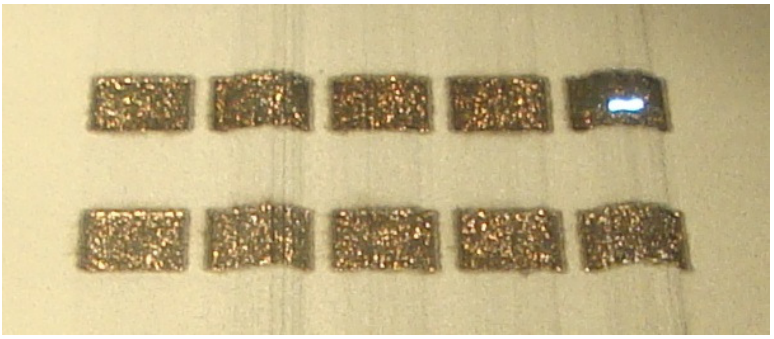

Fig. 8.14: Photograph of fabrication of 20 wt% Cu multilayer samples towards the end of the build (90W, 125 mm s^{-1}, 50 µm hatching, 50 µm layer thickness, four scans per layer). Note that two columns (second from the left and the furthest on the right) show signs of increased wiper wear despite identical parameters for all samples.

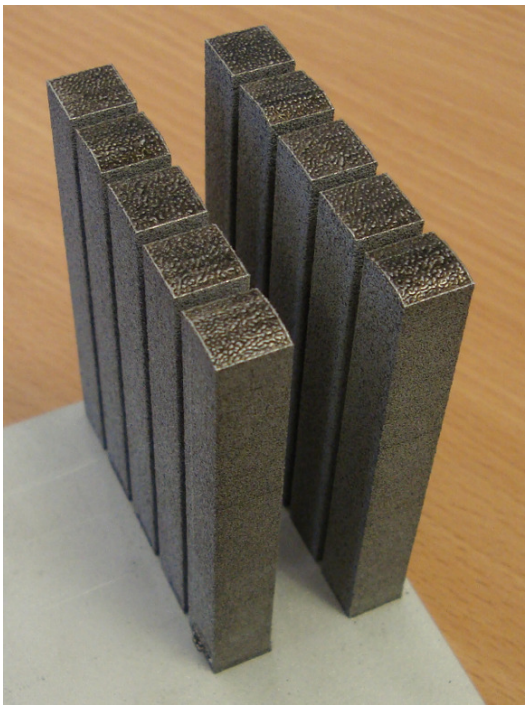

Fig. 8.15: Photograph of completed 20 wt% Cu multilayer samples, 10×10×80 mm each.

8.3.2 Characterisation

Samples were treated in an identical fashion to the pure 6061 Al alloy samples for analysis; results are presented below:

8.3.2.1 Surface roughness

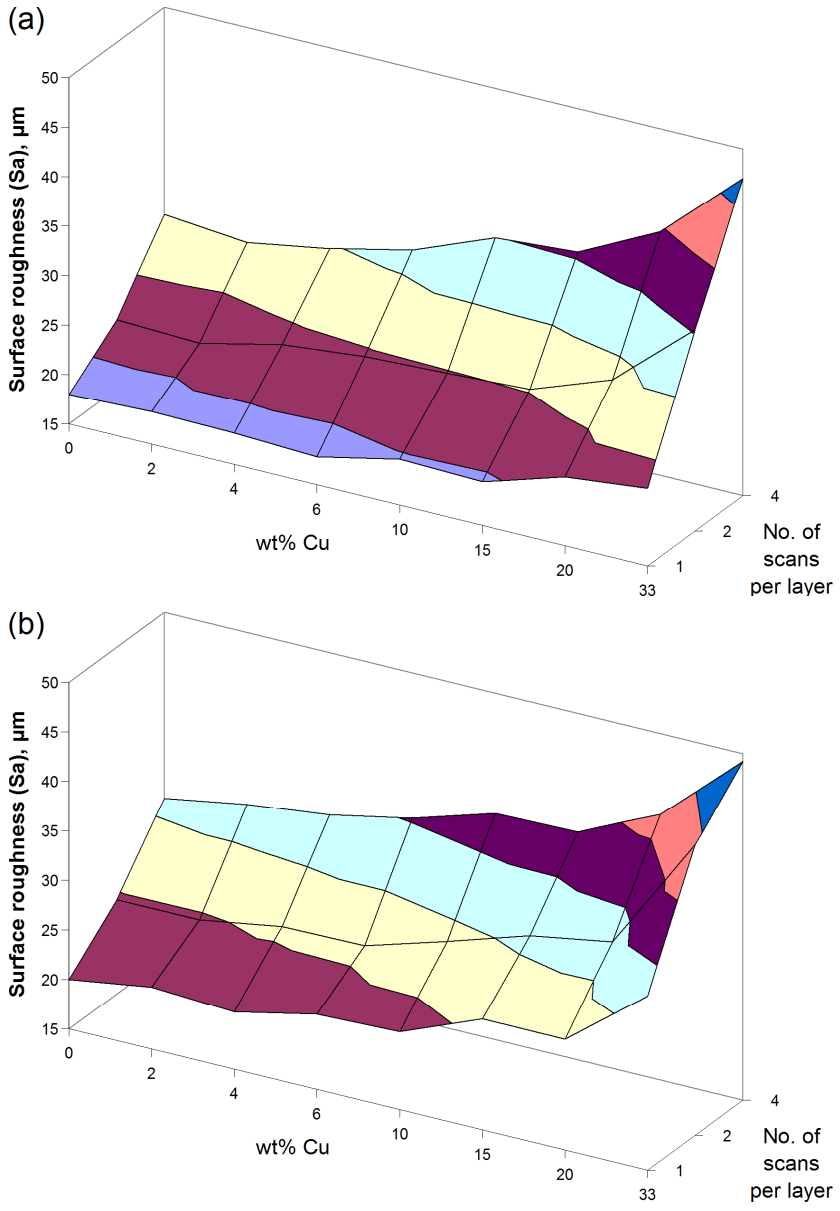

Fig 8.16: Graphs of wt% Cu *versus* surface roughness *versus* number of scans per layer for varying scan speeds: (a) 125 mm s^{-1}; (b) 83.3 mm s^{-1}.

As with the 6061 Al alloy samples, surface roughness readings were taken from the same side of each sample using a laser surface profiler. These results are represented as three-axis graphs in Fig. 8.16.

The trends observed for the pure 6061 samples occur for the Cu containing samples as well in that a lower scan speed and increasing number of scans per layer increase the surface roughness of consolidated samples; in addition, increasing Cu content also increases surface roughness, though it does not appear to have a significant effect until approximately 15 wt% Cu is reached. The effects are accumulative with pure 6061 (one scan per layer, 125 mm s^{-1} scan speed) showing the lowest surface roughness and 33 wt% Cu (four scans per layer, 83.3 mm s^{-1} scan speed) showing the highest.

8.3.2.2 Consolidation and density

Fig. 8.17 shows a graph of density *versus* Cu content. Fig. 8.18 shows the cross-sectional consolidation of 6061 Al alloy samples with varying Cu content. The sections are taken approximately half way through the samples, perpendicular to the base plate.

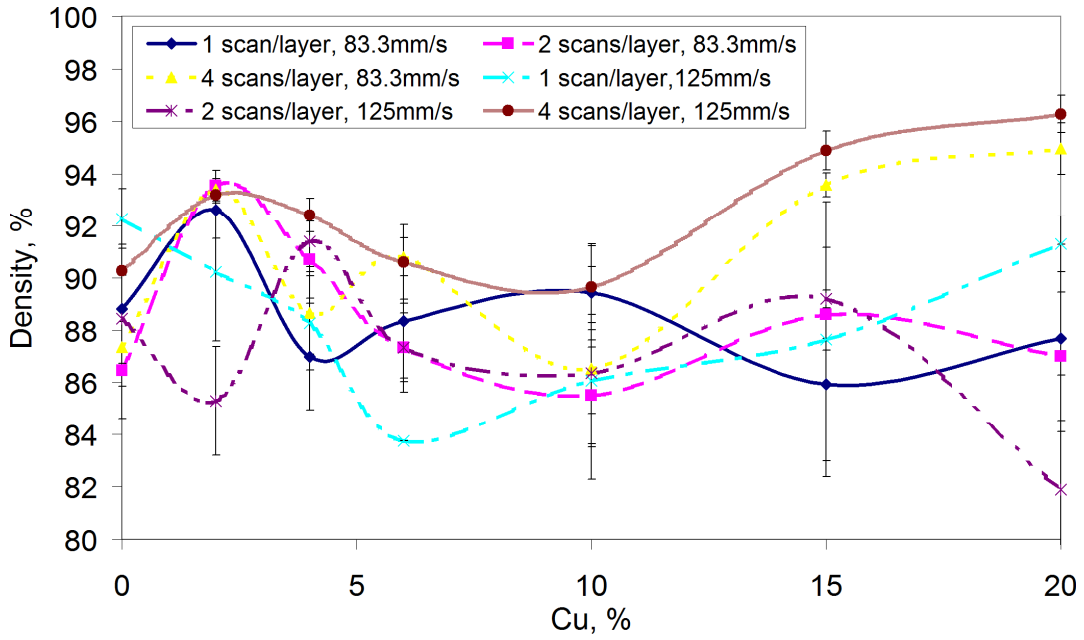

Fig 8.17: Graph of Cu content *versus* density for multilayer samples (density estimated from cross-sectional analysis).

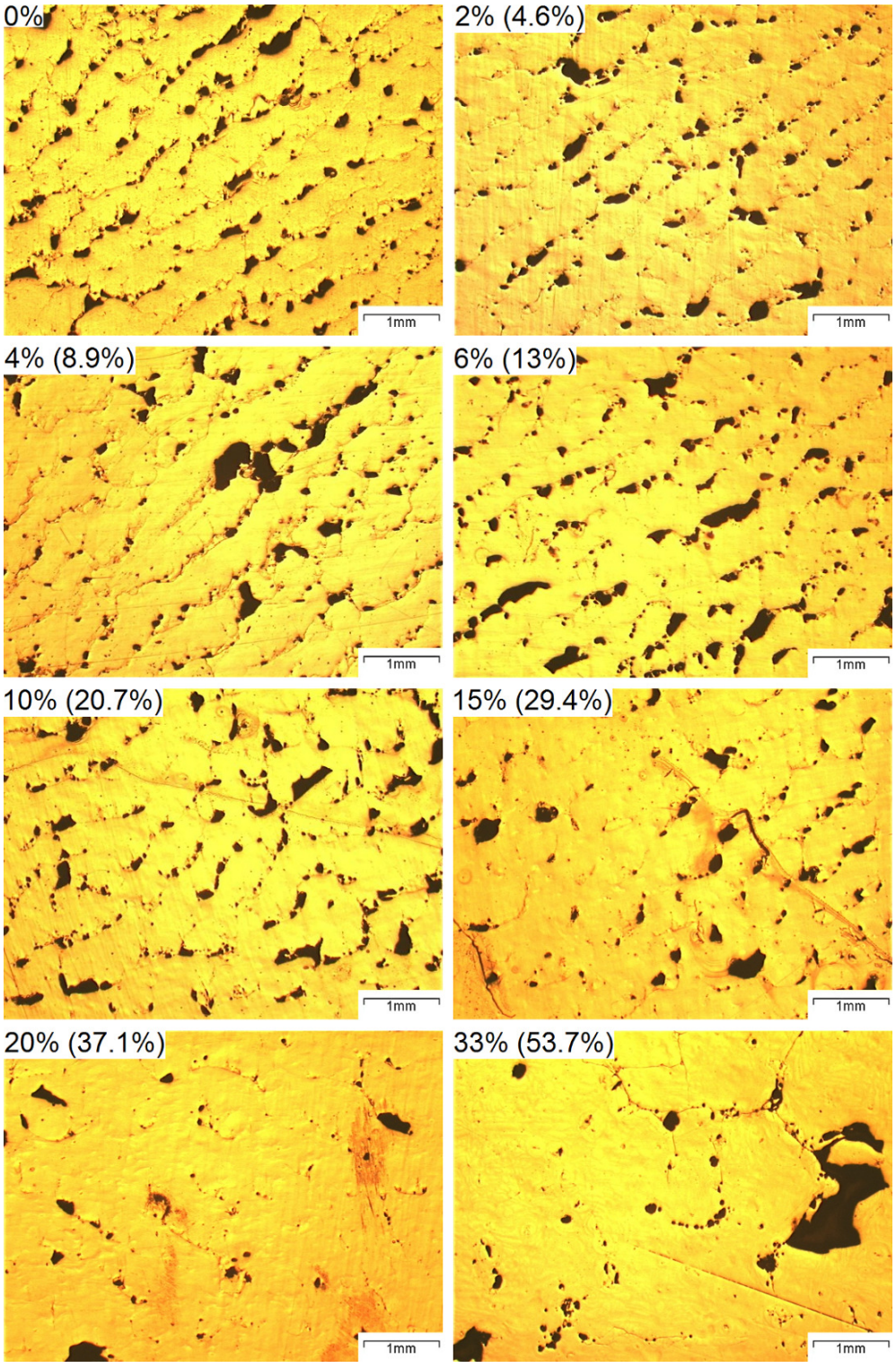

Fig. 8.18: Optical micrographs of cross-sectional consolidation of multilayer samples using 6061 Al alloy with varying wt % Cu (numbers in brackets represent at % Cu). All samples produced at: laser power of 90 W; scan speed of 125 mm s^{-1}; hatching spacing of 50 µm; 4 scans per layer; layer thickness of 50 µm; and a base plate temperature of 150 °C. Build direction is vertical to the page.

Consolidation was found to show the same trend of ordered consolidation of columns that grow at approximately 45 ° to the base plate for samples up to and including 10 wt% Cu. 15 wt% Cu however shows a change in consolidation, with the column effect less visible. The 20 wt% Cu samples reduce this effect even further and the 33 wt% Cu samples show almost no sign of it. It was noted that during removal from the base plate, the 33 wt% Cu samples were exceptionally brittle in nature; in fact, the sawing process seemed to rely on continuously breaking off of material rather than typical sawing deformation. The brittle nature of the 33 wt% Cu samples also prevented satisfactory analysis as machining resulted in chips of material being removed from the surface, resulting in an appearance of having large pores.

Density analysis revealed no apparent trend to results, though using parameters of 4 scans per layer and 125 mm s^{-1} always resulted in better densities, particularly with Cu contents of 15 wt % and above.

8.3.2.3 Microstructure analysis

Samples were etched with the same etchant used for etching the pure 6061 Al alloy samples: results are shown in Fig. 8.19. It was found that samples were highly resistant to etching, even after prolonged exposure (potency of the etchant was also still found to be satisfactory by the re-etching of a single layer sample). As a result, there were no discernable structures to comment on for 0-20 wt% Cu samples, though the 33 wt% Cu samples started displaying faint, fine dendritic structures with dendrites approximately 1 µm wide. Note that although the 20 %wt Cu example may appear to have a microstructure, it is thought to actually be a mottling effect caused by corrosion, brought about by the tendency of Cu to reduce the corrosion resistance of an Al alloy.

The addition of Cu to 6061 appears to dramatically reduce the amount of pores in the consolidated material. 6061 seems to be dominated by pores whereas the lowest Cu containing samples (2 wt% Cu) appear to an effective absence of pores.

EDX scans revealed that oxygen was present, though it was unable to determine which form any oxide took: it is assumed that Al_2O_3 was the form of the oxide, since Al is more reactive than Cu. The oxide was present in the form of irregular particles. Samples typically never had a mean oxygen content greater than 2 wt% which was irrespective of Cu content.

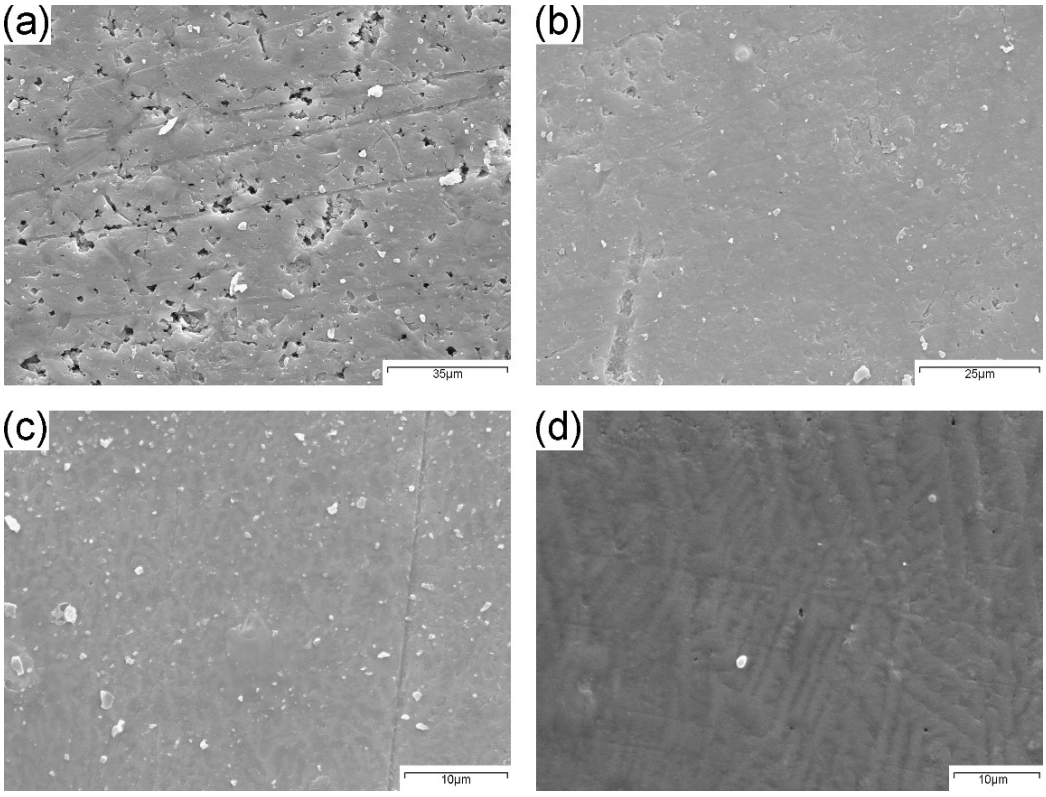

Fig. 8.19: Scanning electron micrograph of typical etched structures of: (a) pure 6061 Al alloy; (b) 2 wt% Cu; (c) 20 wt% Cu; (d) 33 wt% Cu multilayer samples.

8.3.2.4 XRD analysis

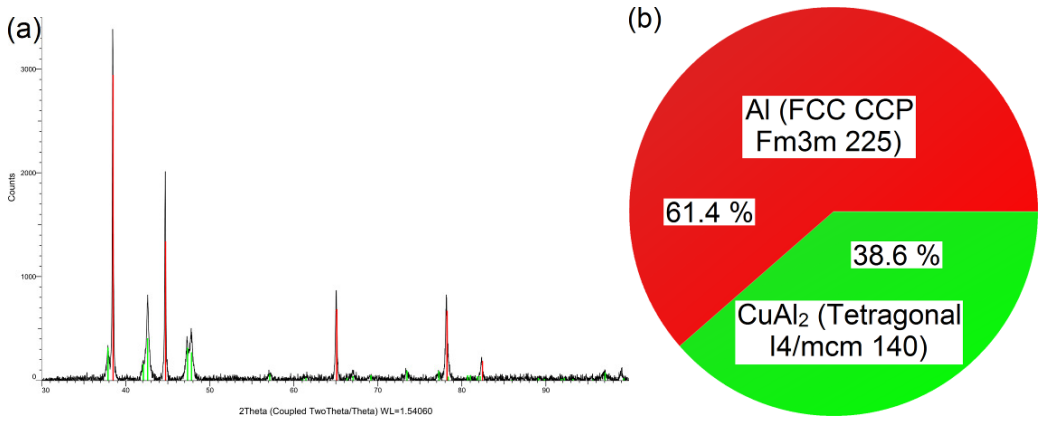

Fig. 8.20: X-ray diffraction results for a 20 wt% Cu multilayer sample: (a) the peaks recorded; (b) pie chart of composition (wt%).

Owing to budget restraints and availability of equipment, only 20 wt% Cu samples were analysed by XRD. Results are shown in Fig. 8.20.

The XRD revealed that the resultant material had two determinable crystalline formations. The majority formation (61.4 wt%) consisted of Al in a Face Centered Cubic (FCC) Cubic Close Packing (CCP) Fm3m (225) structure; the remainder consisted of Al_2Cu in a tetragonal I4/mcm (140) structure which was identified as khatyrkite by the XRD analysis software available. Values reported agree with calculated values for an Al alloy consisting of 20 wt% Cu where essentially all Cu has formed an intermetallic (Al_2Cu). Representations of the structures can be seen in Fig. 8.21.

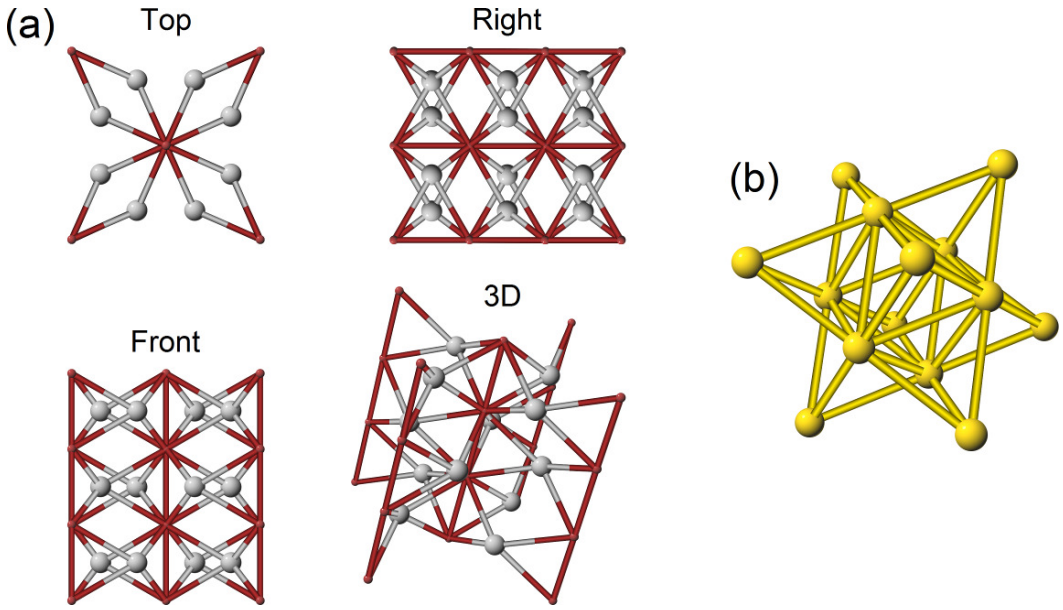

Fig. 8.21: Schematics of crystal lattice structures of (a) Al_2Cu (Tetragonal I4/mcm 140) and (b) Al (FCC CCP Fm3m 225). Note that the top, right and front views in (a) are third angle projection. Structures generated by the Naval Research Laboratory [149].

8.3.3 Mechanical testing

Originally, it was planned to run a full suite of mechanical tests but owing to a limited budget (both in time and budget) only two types of testing were undertaken: hardness and compression.

8.3.3.1Hardness testing

The procedure for hardness testing was as it had been for the pure 6061 samples. Results in Fig. 8.22 show an overall linear increase in hardness for an increase in Cu content, inicating a composite-like behaviour. However, in the range of 15 to 20 wt% Cu, samples fabricated using 4 scans per layer and 125 mm s^{-1} scan speed appear to perform above the average hardness.

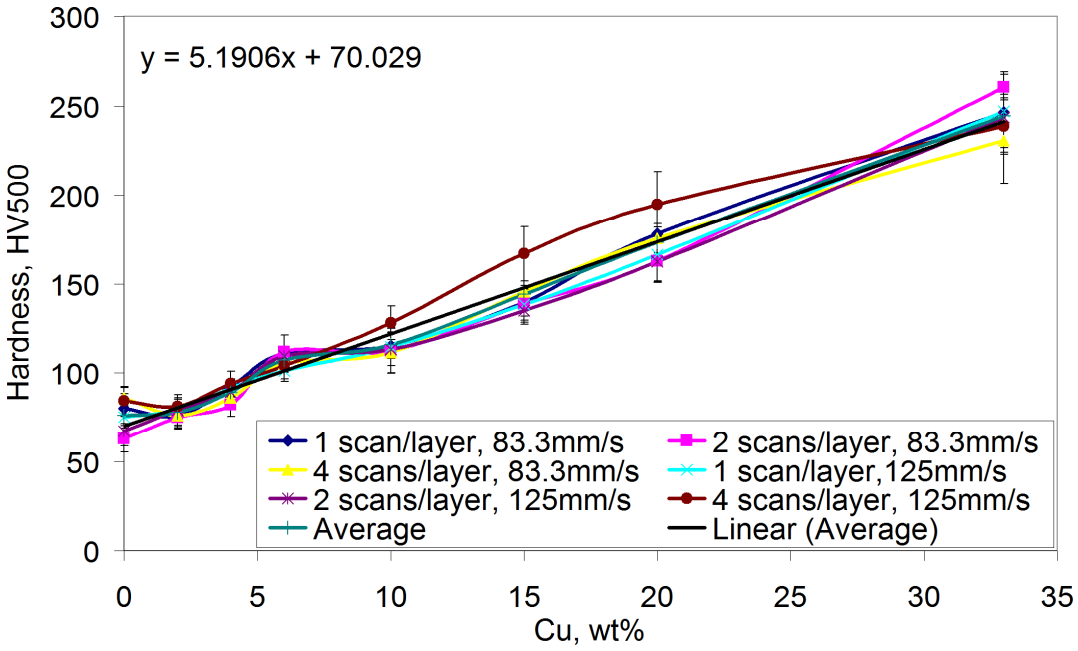

Fig. 8.22: Graph of Cu content *versus* resulting hardness for consolidated Al-Cu Alloy multilayer samples (laser power of 90 W, hatching spacing of 50 µm, 50 µm hatching spacing and 150 °C base plate).

8.3.3.2 Compression testing

Initially, it was planned to produce tensile samples from the tall 20 wt% Cu parts but it was expected that the evident porosity would give poor results that were not indicative of true performance. Instead, compression testing was used as the porosity was deemed to have less effect in a compression load scenario.

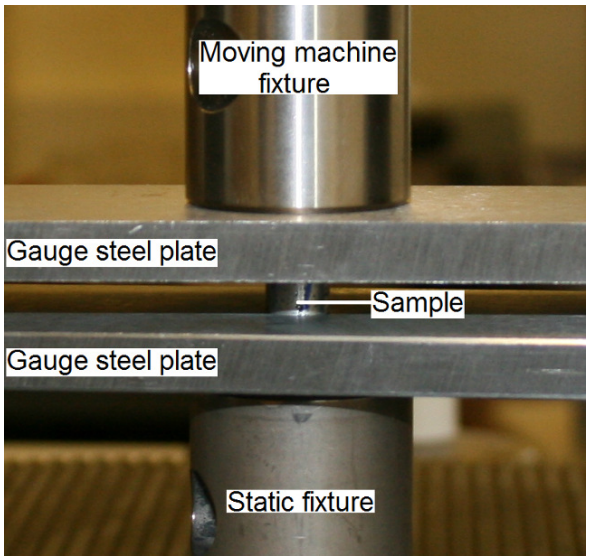

Fig. 8.23: Photograph of an example of compression testing of 20 % Cu/6061 multilayer samples that have been machined into cylinder form.

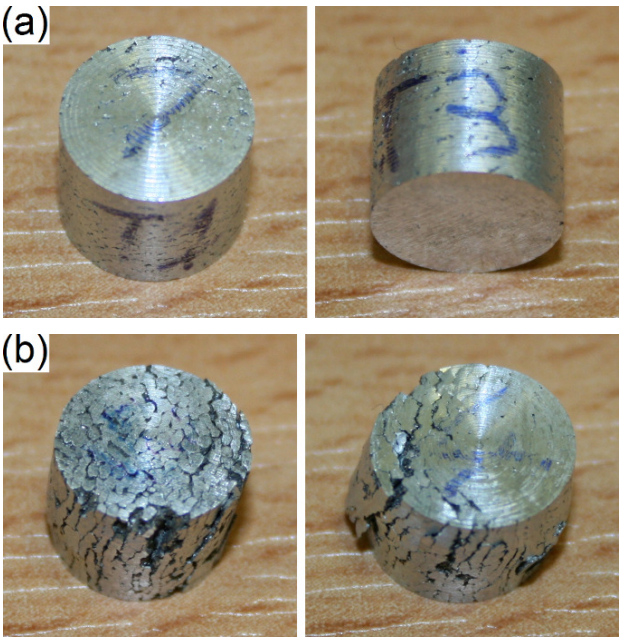

Fig. 8.24: Photographs of examples of 20 wt% Cu /6061 compression samples: (a) before testing; (b) post testing (failed).

Samples were machined as cylinders from selected tall 20 wt% Cu parts; geometry of the samples (Fig. 8.24) was based on ASTM 9 - 89a [150] and measure 9

mm in diameter and 7.2 mm in height, keeping a length to diameter ratio of 0.8. The samples were then tested in compression between two gauge steel plates, with a molybdenum sulphide based lubricant applied to reduce barreling (see Fig. 8.23). The compression rate was set at 1 mm min^{-1}. Owing to limitations of the apparatus [125] used, the maximum load that could be applied was 300 MPa. See Fig. 8.25 for results.

It was found that compression samples produced from parts with little to no sign of overbuilding did not reach their tensile limit (samples 4 and 7 in Fig. 8.25), surviving a 300 MPa load, whereas those produced from parts with more obvious signs of overbuilding did (sample 10). Samples that reached their tensile limit had obviously failed due to a separation of columnar solids, regarded earlier in Fig. 8.24.

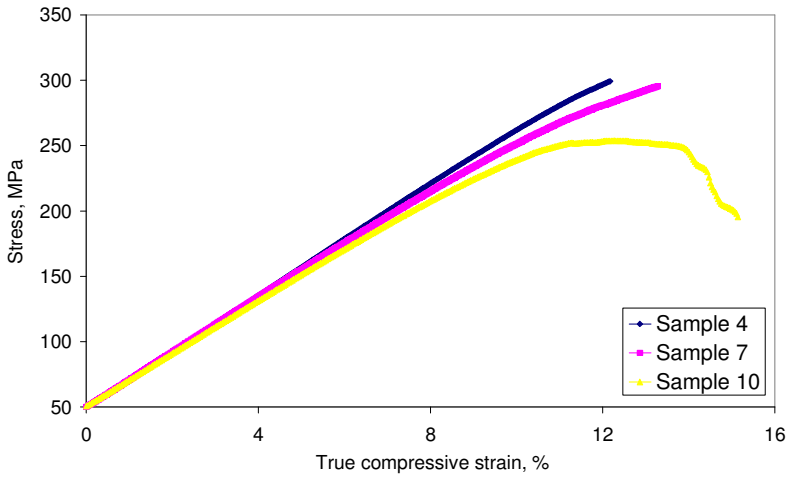

Fig 8.25: Graph of strain *versus* stress for some samples from the 20% wt Cu tall build. Note that the limit of the testing equipment meant that samples could not be tested at stresses over approximately 300 MPa.

8.4 Discussion

8.4.1 Powder deposition

The difficulty in powder deposition can be attributed to the natural tendency of Al particles to agglomerate [137]; the small funneled opening of the wiper the powder

flows through exacerbates the situation since the powder is being compacted together as it moves downwards. This vibration may also have had an effect on the powder bed, resulting in more tightly packed particles [151].

8.4.2 Base plate bonding

The failed bonding of 6061 Al alloy to a steel base plate was to be expected as steel and aluminium have no mutual conventional welding characteristics, however it was a simple experiment to confirm this. Lack of bonding can also be attributed to poor wetting of steel by the molten 6061 [152].

When produced from Al alloy, the base plate acts as a heat sink. Given Newton's law of cooling, "*the rate of heat loss of a body is proportional to the difference in temperatures between the body and its surroundings*" [153], it is unsurprising that a 'cold' base plate hinders successful bonding as the initial temperature limits the maximum steady state temperature that can be attained. Lower temperatures also affect diffusion bonding, which would allow accumulative residual stresses (see Chapter 3) to initiate the peeling effect seen in Fig. 8.1.

Pre-heating the base plate allowed bonding between the base plate and the molten 6061 Al alloy powder to occur. Fig. 8.7 shows the resultant bond, implying a diffusion bond rather than a homogeneous melting of the two alloys. The rolled structure of the Al alloy base plate is visible below what is believed to be a diffusion zone. Of particular note is the fact that the diffusion zone within the 6061 appears to be limited to the first layer of material. This may be due to the fact that the actual amount of diffusion is relatively small and therefore is limited to the first layer since the second layer either doesn't absorb significant additional material from the first layer (in the event element transfer favours movement from the base plate to the 6061) or that the first layer of 6061 did not transfer much material to the base plate. The effect of pre-heating the base plate is studied numerically in Chapter 8.

The spherical porosity evident within the first layer is theorised to be due to superior heat conduction of the base plate compared to 6061. Jiang *et al* demonstrated controlled porosity within a Cu-Mn alloy using a chiller to initiate porosity growth [154]: the mechanism is thought to be similar.

8.4.3 Surface roughness

The increase in surface roughness may be explained by the balling phenomenon: behaviour that is a result of the molten material's wetting properties (see Chapter 3). A slower scan speed allows the material to be molten for longer, allowing the liquid more time to achieve a shape that minimises surface area for a given volume. Multiple scans per layer would also lead to exaggerated balling as each reheat (and therefore re-melt) of the material would give additional time for the material to move to a lower surface energy state.

Increasing Cu content also increases surface roughness. Additional Cu alters the melting point of the resulting alloy: pure Al melts at 660 °C whereas the eutectic composition (33 wt% Cu) melts at 548 °C, with the melting temperature varying in between [155]. As such, a lower melting temperature would result in the material remaining in a molten state for a longer period and, just as with a slower scanning speed, would allow more time for the molten material to succumb to the balling phenomena.

In the SLM production of steel parts, Rayleigh instabilities (the tendency of a liquid cylinder to break up into droplets, see Chapter 3) are typically held accountable for increases in surface roughness [99, 156].

8.4.4 Consolidation

As shown in Fig. 8.8, all pure 6061 Al alloy samples showed columns of material in the side cross section, which would 'grow' at varying angles. This phenomena has not been found to be previously documented but its occurrence in stainless steel SLM parts that have been produced with an out of focus laser beam has been observed in preliminary experiments conducted by the author. This implies that the process is not achieving the laser energy flux required for better consolidation, supported by Louvis *et al* by the statement that a laser power of 150 W or greater is required to successfully process Al alloys, not to mention the use of more tightly focused laser beams [7]. Concerning the mechanism(s) governing the phenomena, it cannot be surmised exactly what is occurring. Presumably, the phenomena has been overlooked as it is non-existent in well consolidated parts.

Fig. 8.18 shows the consolidation of samples with varying Cu content, with what was considered to be optimal parameters. One notices that the angled formations seen in pure 6061 samples also appear in lower percentage Cu samples. However, it can be said that this formation phenomena starts to be visibly affected at 10 wt % Cu, with the 20 wt % and 33 wt % samples arguably being visibly free of the effect. The 33 wt% Cu samples in particular show good consolidation but, as mentioned earlier, the brittle nature of the eutectic composition lead to material breaking off during sample preparation, giving the appearance of large pores.

Rosazza Prin [157] investigated the wetting behaviour of Al-Cu alloys on an AlN substrate. In the aforementioned work, it was noted that the wetting angle varied according to the Cu content. It was found that Cu additions up to 17 at% have little effect upon wetting whereas Cu content in excess of 30 at% improved the wetting angle, which concurs with the consolidation seen in Fig. 8.18. This was explained to be due to an increase in surface energy and work of adhesion brought about by the increase in Cu content, governed by the Young-Dupré equation. Of particular note is the observation that at temperatures in excess of 1000 ºC, molten Al can 'scrub' oxidized surfaces and encourage better bonding, as well as showing an improved wetting angle - an effect also seen in the wetting of TiC by Al-Cu alloys [155].

In regards to areas that show high Cu dominance, this may be explained by the high reflectivity of Cu (see Chapter 3). An agglomeration of Cu particles that has somehow managed to collect at the lased surface may result in greater reflection of the laser energy; Cu's high thermal conductivity will further aggravate consolidation as the heat energy supplied by the laser is transferred to deeper material rather than melting the current layer.

A final point in regards to the movement of Cu and Al atoms. The movement will be Cu diffusing into the Al due to Cu having a smaller atomic radius compared to Al (2.556 Å and 2.886 Å respectively), as well as the higher melting point of Cu hindering Al diffusion and Al forming vacancies easier than Cu [158]. Diffusion is shown to rapidly increase at temperatures of 750 K or more.

8.4.5 Microstructure

It must be stated that from the outset that the microstructure formations for processed 6061 Al alloy and 6061/Cu powder mixture multilayer parts were unlike any

encountered in conventional alloy literature (conventional microstructures being demonstrated in Chapters 5 and 6. The reason for this is believed to be due to extremely high cooling rates on the order of 10^6 K s^{-1}, seen in literature [159].The cooling rates of SLM processed 6061 parts gave rise to a single nanocrystalline phase (see Fig. 8.19). Adding Cu does not change the microstructure (or lack thereof) until 33 Cu % is reached, though it may occur before since samples were not fabricated in the 20-33 wt% Cu range . This implies a 'shifting' of traditional alloy phase diagrams; an effect noted by Zimmermann *et al* [160] and represented in Fig. 8.26.

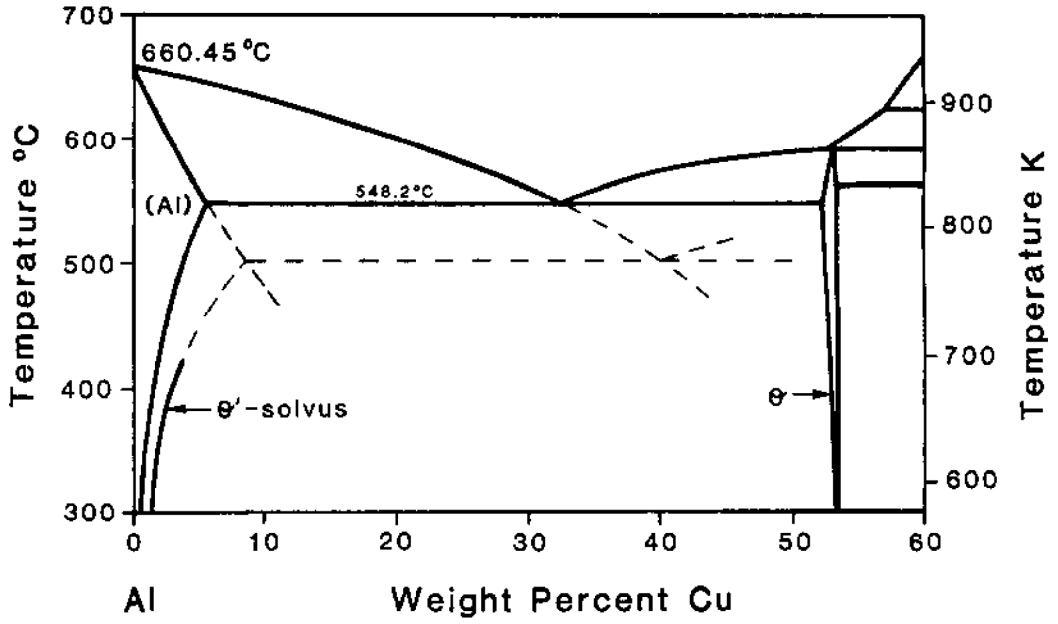

Fig. 8.26: Example of how the traditional Al-Cu binary phase diagram could shift at extremely high (10^6 K s^{-1}) cooling rates (shifted values are represented by dashed lines) [160].

From the results, it can be deduced that an amorphous super saturated solid solution is formed: the incredible cooling rates do not give enough time for nucleation sites to occur and the material effectively snap freezes. Another argument that the resulting material was amorphous is that the etchant appeared to have very little effect. Amorphous metals are known for being resistant to corrosion [161, 162]; perhaps this can be explained by the lack of grain boundaries for the etchant to attack.

The nature of the powder mixture may attribute to amorphous phases forming in 6061/Cu mixtures. Since the Cu exists as a separate material within the 6061 prior to processing, diffusion may occur between particles, given that diffusion increases exponentially with temperature. The structure seen in 33 wt% Cu samples has been observed by Contreras [155]; however in the aforementioned work, Al_2Cu intermetallics form at lower Cu concentrations compared to the work presented here, adding weight to the argument that the processed materials have snap frozen.

Currently, the only technique that can reliably identify the difference between a truly amorphous and/or nanocrystalline phase is Atomic Probe Tomography (ATP), though TEM may also be able to differentiate if conditions are suitable [163].

8.4.6 X-ray diffraction

As identified in Fig. 8.20, all Al left unalloyed is identified as an FCC structure. This can be attributed to FCC-Al precipitation occurring on a nanoscale basis [164]. The composition results show that effectively all Cu has successfully interacted with the Al to form a Al_2Cu intermetallic, identified as khatyrkite. Khatyrkite is a naturally occurring quasiperiodic crystal (quasicrystal). Quasicrystals are a crystalline structure that display rotational symmetry and do not adhere to conventional periodic crystal behaviour [165]. Quasicrystals can be formed with a wide range of quenching rates [166]. However, it is plausible that the XRD prediction of khatyrkite may be due to Al_2Cu intermetallic molecules growing in a disordered nature.

8.4.7 Hardness

The graph in Fig. 8.22 shows that the hardness of samples increases linearly with an increase in Cu content. This is believed to be due to an increase in Al_2Cu intermetallics forming in solid solution within Al dominant areas, as well as Al_2Cu growth areas. The linear nature implies a composite like material that follows the Voigt isostrain assumption [167]. The negligible difference between hardness results for scan speeds can be attributed to the fact that the cooling rate will not be significantly affected, and since cooling rate defines the resulting microstructure, the hardness will be similar due to similar microstructures.

Improvement of hardness for multilayer samples over single layer samples examined in Chapters 5 and 6 is due to different cooling rates of the molten materials: single layer samples would be effectively insulated by the powder bed below and so heat would be kept within the molten material, slowing cooling rates compared to the multilayer samples. The amorphous phase formed in the multilayer samples would have a superior hardness compared to the grain structure seen in the single layer samples [168] .

Callister [169] states that the tensile strength of a material with a conventional microstructure can be approximated as 3.45 times its Brinell hardness; in turn the Brinell hardness can be approximated as equal to Vicker's hardness (for values up to 300 HV) with an estimated error of 5 % [170]. Using this assumption, this means that the pure 6061 Al alloy when processed under ideal conditions has a theoretical tensile strength of 297 MPa, which is the equivalent of 6061-T6 [104]. Furthermore, taking into account the linear trend seen in Fig. 8.22, this would result in an increase of 17.9 MPa per wt% Cu added for the tensile strength of the resultant material. For example, a 20 wt% Cu alloy could have a tensile strength of 600 MPa. However, as previously discussed, there is evidence that the resultant materials analysed may be amorphous, nanocrystalline or an amalgam of both which may affect the relationship between hardness and tensile strength, as investigated by Brooks *et al* [168]. Brooks found that a nanocrstalline material may have strength 1.33 to 2.7 times that of the tensile strength predicted by the aforementioned conventional method. For example, pure 6061 with an amorphous/nanocrystalline structure could have a tensile strength of 395 to 801 MPa.

8.4.8 Oxide content and nature

The size of particles match up with the size of the pores in pure 6061 Al alloy samples, with Cu containing samples showing an almost complete lack of pores. This could be due to better wetting of the particles by the increased Cu content. As Cu diffuses into Al, it may be the case that regions go through a range of Cu content ratios, encouraging wetting before the Cu has fully dispersed within the Al. Improved wetting has already been discussed in ‘Consolidation’.

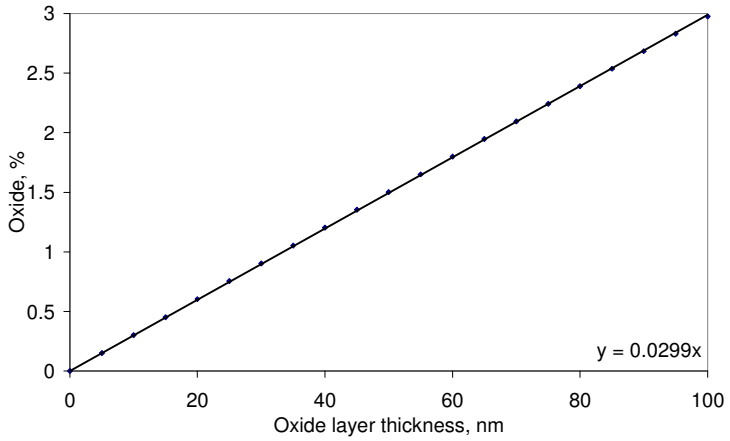

Fig. 8.27: Graph of oxide layer thickness of 6061 Al alloy *versus* consolidated oxide content (calculated from 6061 powder particle volume distribution in Chapter 6).

Fig. 8.27 shows theoretical oxide content of a consolidated Al alloy as a function of the oxide layer thickness of the particles according to the powder distribution reported in Chapter 5 for 6061 Al alloy powder. Multilayer samples never contained more than 2 % oxygen, which implies a maximum oxide layer thickness of 67 nm - a sensible value for an Al alloy [171]. From this, it can be assumed that the vast majority of oxide present comes from the particles themselves.

8.4.9 Laser scan track analysis

Studying the EDX results in Fig. 8.12, it appears that any oxides are either 'swept' to the edges of the laser scan track and/or potentially vaporized by the laser.

This could be due to Marangoni convection (see Chapter 3), that is convection within the molten material due to surface tension gradients caused by high temperature gradients. This effect is confirmed by Louvis [7].

8.4.10 Sample build position

Inconsistency between part position on a build platform and resulting properties is a phenomena commonly encountered by those who operate AM machines. Differences

are typically put down to uneven temperature distribution (both due to uneven bed pre-heating and heat added by laser), as well as the innate layout of the AM machine in question. It is typical practice for AM engineers to 'map' the build volume, producing a large build full of samples to test inconsistencies between discrete volumetric regions; these samples are usually tested for mechanical strength, surface roughness and dimensional accuracy [1].

All builds for the pure 6061 Al alloy and the 6061/Cu powder mixtures were symmetrical in nature (see Fig. 8.6). A possible explanation for discrepancies between the left and right hand samples is the gas flow of the re-circulating pump unit, which makes the Ar gas flow from left to right (see Chapter 3). This has been found to affect stainless steel samples in SLM [172].

8.4.11 Mechanical testing

Ideally, the mechanical testing of a material would ideally be performed on a fully dense sample; owing to limitations of the Realizer, fully dense parts could not be made. Inevitably, the failure mechanism for relevant samples was due to the ordered nature of porosity within samples, which was still present despite their visual appearance (Fig. 8.24). However, one may comment that the samples that survived a 300MPa compressive force show remarkable strength for what is essentially a poor internal structure for enduring loads. It is thought that a fully dense sample would demonstrate exceptional load bearing capacity.

8.5 Conclusion

The work presented shows that most aspects of SLM Al alloy processing can be considered far more difficult when compared to using steels. Compared to steel, the deposition of Al alloy powder requires more thought due to the tendency to agglomerate and the base plate must be heated to ensure a bond that will enable multilayer production. Based on the results, the processing parameter window for Al alloys within SLM is far smaller than that of steels, though the results were most likely artificially limited due to back reflection, which is also an issue compared to steel which can be attributed to Al's high reflectivity to a 1064 nm laser source.

Consolidation of pure 6061 Al alloy resulted in a columnar structure that grew at an angle of approximately 45º to the horizontal. Though no current explanation for this phenomena is forthcoming, the addition of 15 wt% Cu appeared to start reducing this effect, with 20 wt% and 33 wt% Cu significantly reducing visual evidence of the structure. The phenomena is seen as an indication of poor consolidation. Consolidation is found to be improved for three reasons: firstly, the melting point of an Al alloy is decreased with an increasing Cu content (with a limit of the eutectic point); secondly, adding Cu in sufficient quantities allows better wetting; and thirdly, Cu particles encourage diffusion into the Al alloy powder. In regards to actual parts built, there is a trade off between having higher density and hardness at the expense of increased surface roughness.

6061 Al alloy showed a lack of microstructure, implying an amorphous single phase that may or may not have nanocrystalline regions. This is believed to be a result of extraordinarily high cooling rates, which allow the material to solidify with the same composition as when in the liquid phase; in addition, the base plate was kept at a temperature under the precipitation forming ageing temperature. This may have advantages as amorphous metals have been shown to have improved properties such as wear and corrosion resistance. As such, SLM may be a viable method for the manufacture of amorphous Al alloy parts. However, the exact nature of the phase could not be identified since APT and/or TEM analysis would be required.

Given that materials displayed amorphous behaviour and demonstrated admirable compressive strength despite a detrimental ordered porous structure, it is foreseeable that the materials manufactured and studied could have use as bearing materials: that is, materials that endure wear and compressive load.

9. Demonstration part design and production

With the manufacture and analyses of multilayer test samples in Chapter 8, it was decided that the manufacturing capability of the SLM process using a custom aluminium alloy should be tested. The reasoning behind this decision was to allow observation of the production of a real part and to assess the effect of a changing geometry rather than a fixed geometry test sample, and to showcase a customised Al alloy part. Since aerospace designs tend to be closely guarded secrets, it was also necessary to design a part that gave the impression that it could be used as an aerospace part.

This chapter covers the design and manufacture of a theoretical customised Al alloy aerospace AM part. A part specification was produced with the aim of showcasing the manufacturing strengths of SLM. The specification was then used to generate a design encompassing theoretical aerospace needs and geometries. Manufacturing procedures and considerations are described, with reports of any manufacturing anomalies that affected the build. Finally, the produced part is evaluated through visual inspection and hardness testing.

9.1 Part specification and design

The aim in manufacturing a demonstration part was to produce an object which showed the benefits of the SLM process whilst eliminating or at least reducing potential manufacturing issues. With this in mind, a part specification was produced:

9.1.1 Design for additive manufacture

The part must be designed with SLM limitations in mind. All surfaces should be 45º or greater from the build plane to ensure no supports are needed [94] and features should have a suitable thickness. Powder removal must also be considered, so closed, empty volumes are not allowed.

9.1.2 Truly complex geometry

The part should be extremely difficult or impossible to build with any other manufacturing technique. This can include features such as re-entrant geometry, lofted surfaces, internal features and fine details.

9.1.3 Multiple components merging

A key advantage of AM is the ability to save assembly time by merging parts; this may also allow better tolerances as alignment of components is a non-issue (though the tolerances of the AM process are still a concern) and removes interface problems such as stress incompatibility and differences in thermal expansion. Additionally, the need for attachment methods such as bolts or adhesives is removed for the merged parts. Hence, the part should demonstrate merging of existing CAD files for previously designed parts.

9.1.4 Ability to integrate with other components

Although AM may reduce the number of parts in an assembly, most components have to attach to others through a variety of means and parts produced by AM are no exception. The nature of AM means that mechanical keys, mating surfaces or holes can be easily integrated.

9.1.5 Internal structure

AM makes adding advanced weight saving structures possible and, as opposed to conventional manufacturing methods, may save manufacturing time due to a reduced material volume. This means that (perhaps ironically) an internal structure can be introduced with no foreseeable disadvantages - rather, there is actually an incentive to increase the complexity of a part in this way. Additionally, less material usage means more material that can be recycled for further use. Therefore, an internal structure capable of supporting itself during manufacture should be demonstrated.

9.1.6 Functional grading

An ability to change material properties throughout a component is something that AM can put into effect more easily than other processes. At this point it is necessary to stress that an FGM does not necessarily have to be implemented by changes in material elemental composition alone: changing processing parameters may result in changes in material properties.

9.2 Design

Given the criteria described, a theoretical aerospace component was designed using SolidWorks [173] (see Fig. 9.1). The component successfully integrates all the criteria, discussed below.

9.2.1 Helical gear

SolidWorks has a CAD library of standard components such as bolts, nuts and gears. Conventionally, an engineering solution would need to purchase these parts separately if needed but the nature of AM means that a component can simply be added in and become part of the model. Hence, it was decided to use a gear to demonstrate the ease of adding in a relatively complex geometry; the gear was of a helical variety since the additional geometry complexity compared to a spur gear made no theoretical difference for SLM processing.

9.2.2 Advanced geometry

Conventional manufacturing typically relies upon simple geometries e.g. planar surfaces and revolved profiles; combinations of simple geometries allow a more complex part to be manufactured. To allow even more complex geometries to be formed, five axis machining process can be utilised, though software is expensive and can require some effort to generate a successful tool path - which naturally can only be created if it is actually possible [174].

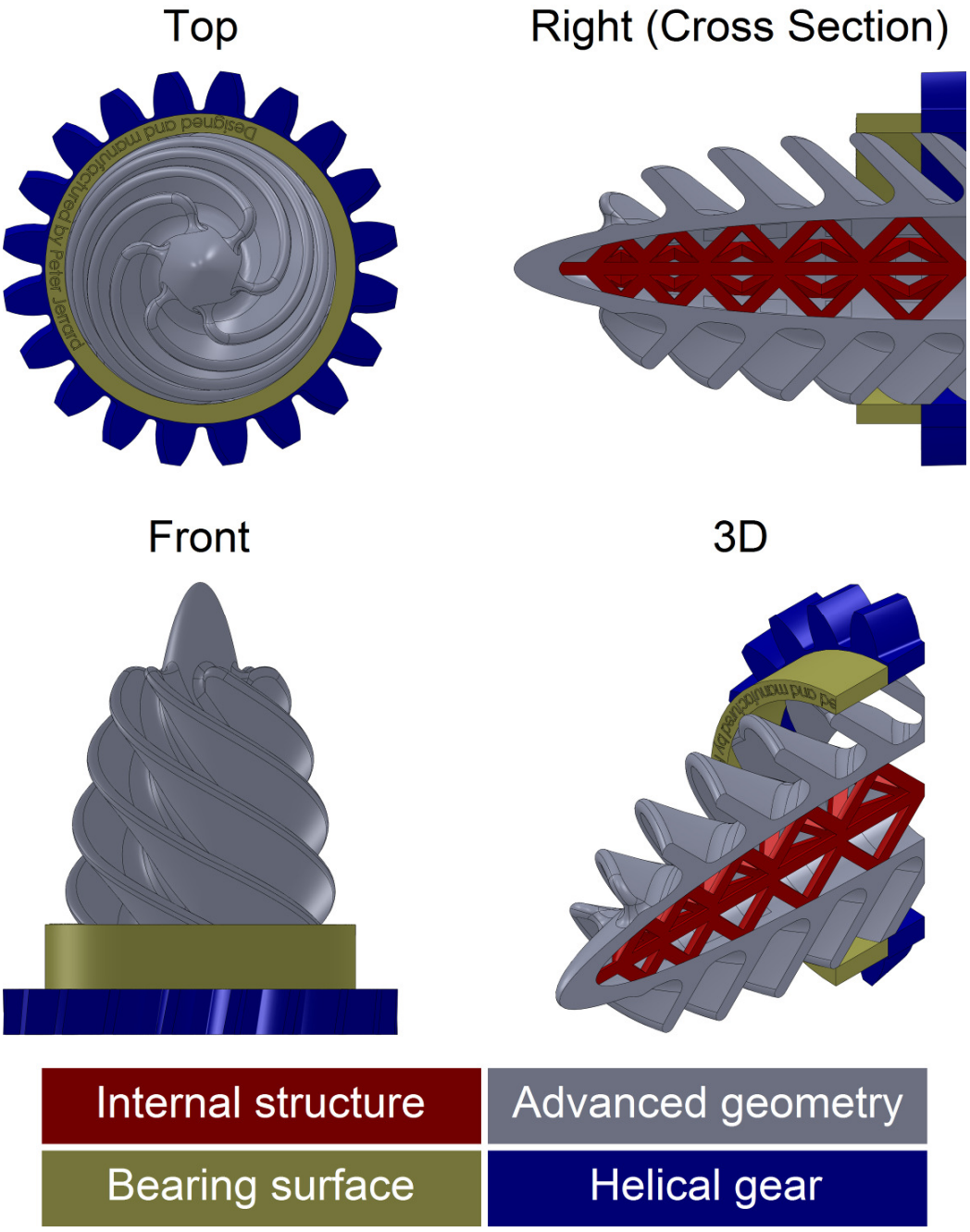

Fig. 9.1: Original demonstration part design: note that that the top, right and front views are third angle projection. Height of the part is 72.5 mm.

Turbine like geometries are arguably a common occurrence within aerospace designs, and so a turbine 'theme' was followed to produce an advanced geometric shape. The design features 'blades' that would be (at the very least) difficult to manufacture conventionally: in regards to SLM limitations, the blades are self supporting and have a

2 mm thickness, which results in a 2.8 mm thick cross section in the build plane. It was not known at the time if the thickness of the blades would be sufficient but considering the lack of literature available at the time of designing and manufacturing of the part estimates based on intuition were implemented.

9.2.3 Internal structure

Although internal structures investigated to date can consist of relatively thin support structures (an example being the structures built by Yadroitsev *et al* [89] having a material thickness of 120 µm and 150 µm), it was decided to use thicker support structures as it was feared that too small an area in cross section would result in excessive balling. As in the design of the advanced geometry blade thickness, this was based on intuition rather than any solid engineering reason.

A simple truss structure was inserted into the centre of the advanced geometry along with a column that would support the top of the internal hollow where the angle of construction became greater than 45 °. Beam thickness was originally set at 2 mm, though later had to be thickened to 3 mm for reasons discussed in the next section.

9.2.4 Bearing surface

With a turbine 'theme' being the design directive, it was decided to represent the ability of compatibility with other components in an assembly by adding a surface that a theoretical bearing could be fitted on to. After manufacture, this section of the model could then be machined to a suitable size and finish if necessary.

9.2.5 Functional grading

Functional grading is not so much a part of the design (though a part intended for true use would have to take into account changes in properties) but rather a variable in the manufacturing process. As demonstrated in Chapter 7, hardness of the consolidated material could be influenced by the number of scans per layer. It was decided to alter

the aforementioned parameter during manufacture as a crude method of demonstrating functional grading through variation of process parameters.

9.2.6 Thickness of geometry

There was a limited amount of literature concerning the design of Al alloy SLM parts available during the design and manufacture of the demonstration part, namely parts manufactured by Wong [6] and Zhang [105]. Parts produced by Zhang had an apparent minimum thickness of 1 mm and appeared to be more sturdy compared to the relatively thin geometries produced by Wong, so it was deemed that doubling this thickness would ensure a higher chance of successfully completing a build.

9.3 Fabrication

9.3.1 Pre/during manufacture

Before starting manufacture, an additional 4 mm of material was added to the bottom of the part by way of a simple extrude feature; this would allow removal from the base plate without removing material that was integral to the final part (a standard practise in SLM). A cutaway was also added to the model to allow a view of the internal structure. Material choice was a 20 wt% Cu alloy (see Chapter 7) since it demonstrated high strength without brittleness

Building parameters were originally set to be identical to those used to produce what was considered to be the best settings for the 20 wt% Cu powder mixture (90W laser power, 125 mm s^{-1} scan speed, 50 µm hatching, 50 µm layer thickness, four scans per layer and a heated base plate) but back reflection became prevalent. This was solved for the most part by reducing the number of scans per layer to one. When the build was nearing completion the number of scans per layer was increased back to four for the 'nose' of the part, of which the visual effects can be seen in Fig. 9.2.

Immediately from the start of the build, an area of material showed signs of poor bonding (see Fig. 9.5). The process was paused while a new CAD model was prepared

with the troublesome section removed. This allowed the manufacturing process to continue.

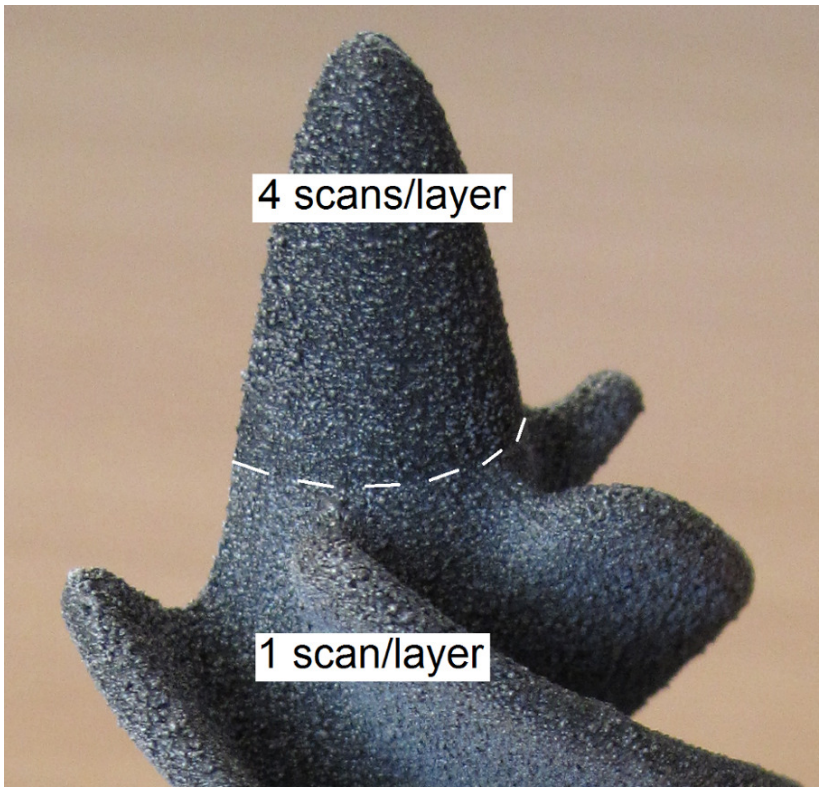

Fig. 9.2: Photograph of example of attempted functional grading of the processed demonstration part. There is a difference in surface colour between sections built with one and four scans per layer.

As the build started to progress beyond the initial 4 mm of material added to the part, the introduction of the internal support structure started to suffer from balling as had smaller cross-sections when subjected to multiple scans per layer (see Fig. 9.3), which threatened to disrupt the build due to excess wear on the wiper blade. This balling is presumed to arise from the fact that the heat energy supplied by the laser beam could not diffuse fast enough through the comparatively small volume of solid material beneath and allowed the alloy to stay in a liquid form for longer, hence allowing more time for Rayleigh instabilities to occur. As before, the manufacturing process was temporarily paused as a new CAD model was prepared with thicker supports (see Fig. 9.4). The new CAD part showed no issues for the reminder of the build.

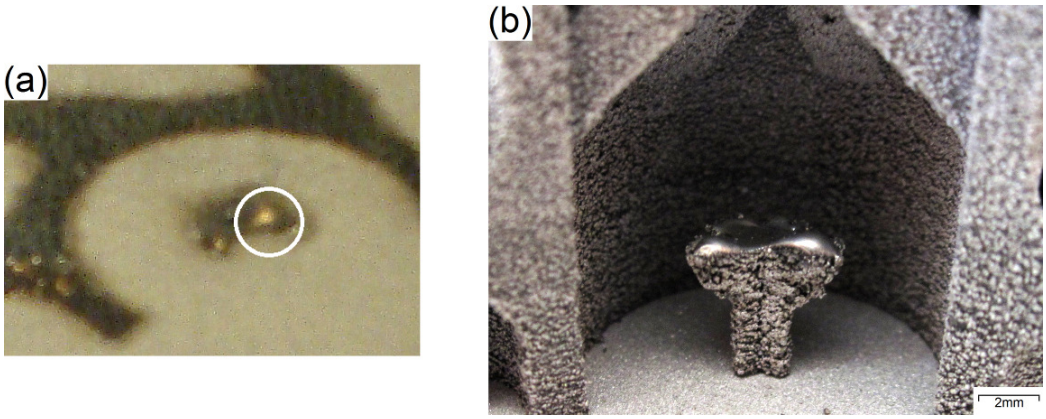

Fig. 9.3: Photographs of balling phenomena observed on original internal supports with 2 mm thickness (a) during processing and (b) afterwards. The supports were partially removed and thickened to 3 mm for the rest of the build (see Fig. 9.4).

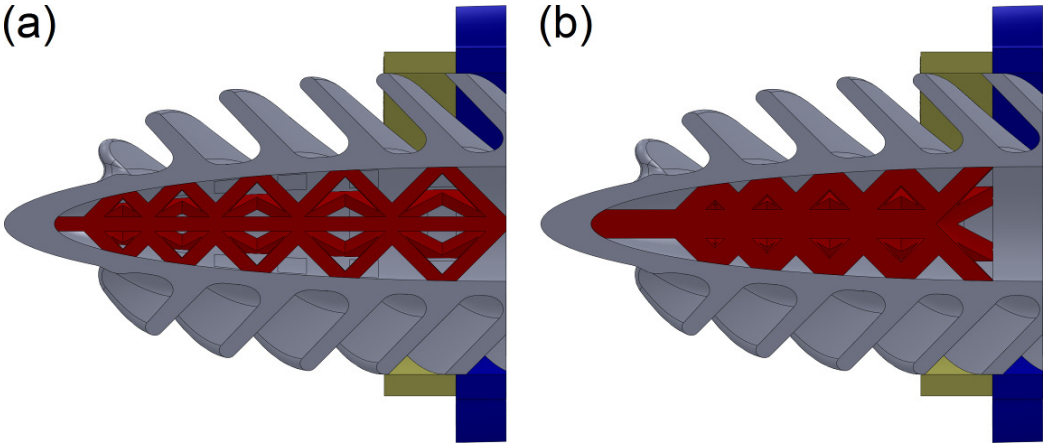

Fig. 9.4: Change in thickness of supports during the demonstration part build from (a) 2 mm to (b) 3 mm.

9.3.2 Post manufacture

After completion of the build, the part (and base plate) were removed from the Realizer and blown with air to remove excess powder. The part can be seen in Fig. 9.5. Of particular interest is the darker appearance of the 'nose' which has been subject to four

scans per layer as opposed to the single scan per layer for the rest of the part. A closer view has already been shown in Fig. 9.2.

The part was then bead blasted to remove loosely consolidated material that had remained attached throughout the air blasting. Originally planned as an *exemplia gratia*, it was ascertained that the part could be used to study incongruities due to geometrical layout. To this end most planar surfaces were ground and polished to allow consolidation and hardness analysis. The processed part can be seen in Fig. 9.6, which shows various resulting surface finishes on the part.

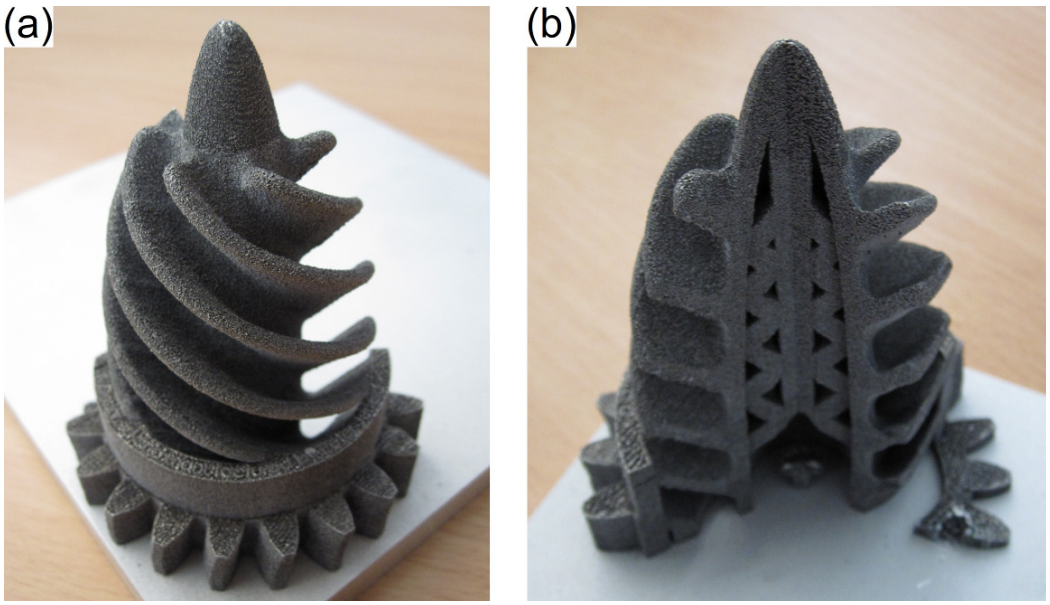

Fig. 9.5: Photographs of the finished demonstration part before post processing: (a) advanced geometry, gear and bearing surface; (b) internal structure.

Bead blasting visually improved the surface finish, making it comparable to a coarsely cast part. In particular, it appears that the 'nose' of the part has responded better to the blasting treatment compared to the rest of the part, which shows small globules of material attached to part surfaces. Surfaces that were parallel to the base plate display signs of balling and have a worse finish than surfaces produced at an angle to the base plate, showing elongated, consolidated globules of material.

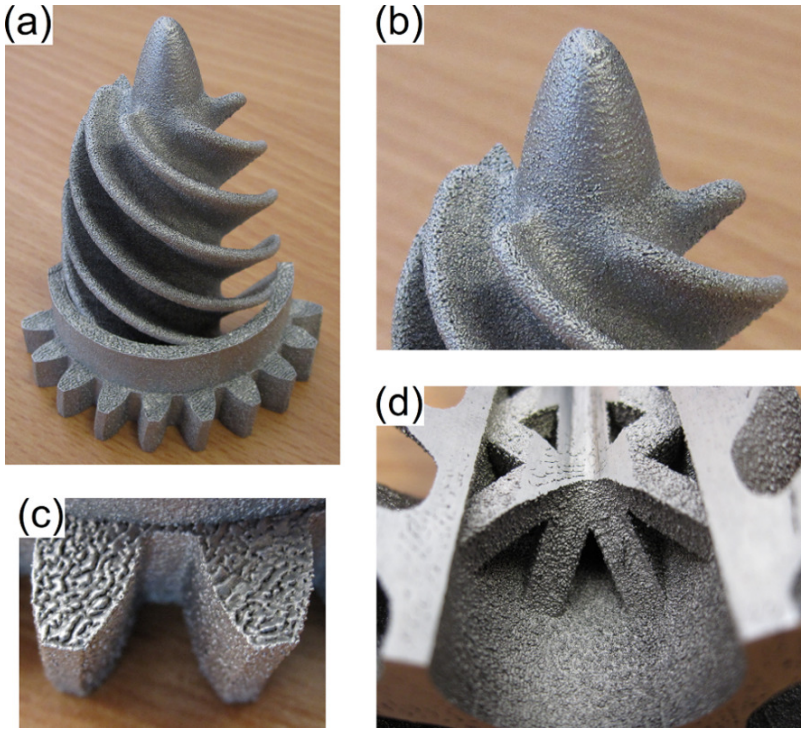

Fig. 9.6: Photographs of demonstration part after removal from base plate and bead blasting: (a) advanced geometry, gear and bearing surface; (b) close up of top; (c) surfaces parallel to the base plate; (c) internal surfaces, with polished surfaces visible.

9.4 Characterisation

To allow measurement of variance of density and strength throughout the component, flat surfaces were ground and polished post manufacture in order to allow analysis. Locations of relevant analyses and corresponding values are shown in Fig. 9.7.

9.4.1 Hardness

Studying the geometry of the part, it would appear that areas with more material directly below (in the build direction) are harder than sections with less material below. For example, position 1 in Fig. 9.7 has the highest recorded hardness value and was measured from a section that had more underlying material and thicker geometry compared to others. Position 4 on the other hand has less surrounding material.

Owing to the geometry of the part and the hardness indenting mechanism, areas close to the central axis of the part could not be analysed.

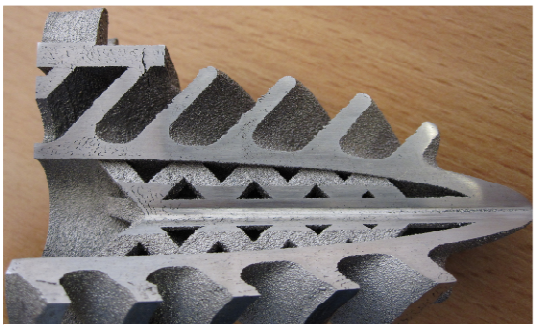

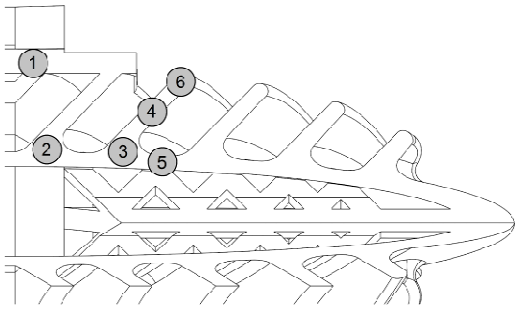

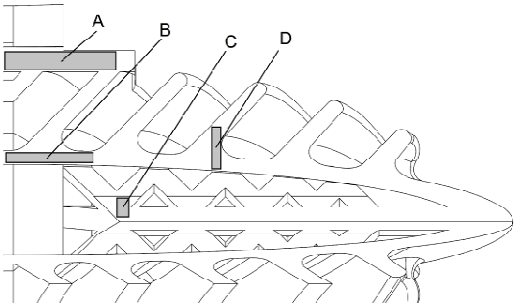

Position	Hardness, HV500	Standard Deviation
1	168.8	4.7
2	140.8	6.6
3	141.6	8.3
4	116.5	8.5
5	143.8	12.9
6	129.7	3.2

Position	Density, %
A	94.2
B	94.3
C	93.3
D	92

Fig. 9.7: Hardness and density analysis of the demonstration part.

9.4.2 Density

Some sections of the part shows the consolidation phenomena described in Chapter 8, but there are also sections which appear effectively fully consolidated. In particular, the 'nose' of the component appears fully dense, though this may be explained by the multiple scans per layer received for that section. Suffice to say, the lowest apparent density recorded was 92 %, which is in accordance with 20 wt% Cu samples in Chapter 8.

9.5 Discussion

The first (and most obvious) observation is that production of a complex part is possible albeit with a porous nature. Manufacturing had to be closely monitored, with back

reflection being a constant issue. Compared to manufacturing steel parts, the operator of the machine had to be more attentive and be especially aware of balling.

9.5.1 Hardness

The hardness values are a case for concern in that there are significant differences related to the difference in location.

From Chapter 8, it is concluded that higher strength results from higher cooling rates, which implies that sections with lower hardness values are cooling at a slower rate. It is therefore possible to theorise that thinner, less supported geometries do not allow heat to be conducted away as quickly as thicker, more supported sections, bearing in mind that unconsolidated powder would act more as an insulator than a conductor of heat [175]. This may have implications for designing parts when using an amorphous or nanocrystalline alloy. Alternatively, a variable scan strategy and/or laser power may be necessary to maintain a similar heating and cooling profile for all areas of the part. Craeghs *et al* [176] have demonstrated an optical method of controlling the weld bead forming during the SLM of steel samples; this may be even more beneficial for Al alloy parts.

9.5.2 Consolidation

As remarked upon when describing issues with manufacturing the part, it was found that multiple scans per layer would exacerbate balling on small cross-sections. This was likely due to allowing the material to re-melt more than usual of the material below the layer, allowing a larger globule of liquid to be formed.

The optimisation of surface roughness for AM parts has been considered by Strano *et al* [38]: it is also known that all AM parts suffer from anisotropic material properties, a notable example being that all AM parts are weaker in the build direction [177]. However, it has been found that there is no published research on the effect that geometry has upon material properties and consolidation, specifically involving varying the thickness of consolidated parts. This may be due to the fact that the steels used within AM have a large parameter 'window' [71], which are somewhat forgiving when applied to a range of geometries.

In the case of Al alloys, geometry seems to have far more influence on consolidation, which must be due to disruption of the weld pool formed during processing. Once again, the work demonstrated by Craeghs *et al* concerning feedback control during the SLM process may be of considerable benefit to allow a more diverse range of geometries to be processed by SLM of Al alloys.

9.6 Conclusion

Customised Al alloy component production has been shown to be possible in the SLM process albeit with porosity and variation in material strength as well as additional limitations in geometry thickness. However, it is thought that a denser, more uniform part could be manufactured with a more suitable machine and with a more advanced scanning strategy that allows for changes in geometry. This may be especially relvant in the case of the potential manufacture of amorphous Al alloys.

The ability to make rapid design updates to AM parts was also demonstrated, adjusting dimensions of internal structure almost 'on the fly'. This level of adaptiveness is extremely hard to implement in more conventional manufacturing.

PART IV: POSTLUDE

Discussion

The scope of the research undertaken was to investigate the feasibility of using Selective Laser Melting (SLM) to produce parts with advanced material properties for aerospace use. In truth, while aerospace influenced the material choice (Al alloys), the work presented is just as applicable to other engineering fields that require the properties of the materials for the SLM process.

The primary aim of the research presented was to demonstrate the ability of AM to manufacture parts with advanced and customised alloys, with a secondary aim of demonstrating the potential of AM to produce complex parts suited to aerospace use using materials developed during the course of the PhD. As such, the following steps were taken:

1. Al alloys were identified amongst a range of materials as being particularly important to the aerospace industry.
2. SLM was identified as an AM process with the ability to manufacture parts with sophisticated geometry, as well as being able to process the higher strength materials available in AM.
3. Initial investigations into consolidating steels and steel mixtures were undertaken to allow comparison to literature, which resulted in the demonstration of the control of magnetic properties and the ability to significantly improve consolidation through the addition of one type of steel to another. Additionally, hybrid steel/CoCr parts were shown to reduce strain incompatibility between two materials.
4. Comparison of single layer SLM processing of pure Al and 6061 resulting in the demonstration of superior consolidation by using an Al alloy suited for welding.
5. Investigation of the use of powder mixtures to manufacture single layer samples of customised Al-Cu alloys, showing changes in the resulting microstructure and increases in hardness.

6. Multilayer production of customised Al-Cu alloys and subsequent analysis, revealing what is thought to be the formation of nanocrystalline Al matrix phases with dispersed Al-Cu quasicrystals.
7. SLM fabrication of a complex part using a new Al alloy material.

There is however two main issues that comes to the forefront when focusing on the Al alloy results for this study. Firstly, by not having an inbuilt optical isolator, back reflection may have prevented the use of parameters that would have produced better samples in terms of decreased porosity through better consolidation. Secondly, the Realizer machine used during experimentation was ultimately not well suited to producing Al alloy parts due to its limited laser power and large spot size.

SLM of steels, steel mixtures and hybrid steels

The first round of experiments on stainless steels showed that in the case of single layer samples, increasing the energy delivered per unit area resulted in better consolidation and thicker samples. Laser power was found to be the dominant parameter as below a certain power, the samples only showed signs of Liquid Phase Sintering (LPS) rather than full melting. Different steels were also found to have changes in consolidation mechanisms for single layer samples: 17-4PH showed full melting throughout the majority of samples whereas 316L resulted in samples with a top half showing full melting and a bottom half believed to be showing LPS and Solid State Sintering (SSS). By mixing a 25 wt% fraction of 17-4PH with 316L, dramatic improvements in consolidation were shown with comparatively small increases in magnetic behaviour and hardness. On the other hand, adding a small fraction of 316L to 17-4PH allowed dramatic changes in hardness and magnetic properties which was attributed to the certain amount of martensite that formed. Ultimately, a part could be tailored to have desired magnetic variation throughout, or the part could have the more ductile 316L deposited in regions that are required to be tough.

The multilayer experiments using 316L and CoCr showed the advantages of blending materials, specifically removing strain incompatibility between materials and increasing the elongation at failure.

Single layer pure Al and Al alloy production

The attempted SLM processing of single layer pure Al was not deemed successful. Pure Al was prone to balling and showed considerable microporosity, a result thought to be caused by poor wetting, hydrogen content and cavitation (caused by Marongoni convection).

6061 Al alloy, a material known for its good welding properties, was then investigated and found to show superior consolidation compared to pure Al, forming single, large globules when enough energy was applied (much the same as steels, it was found that increasing energy resulted in a more consolidated sample). Microporosity was also found to be dramatically reduced.

Adding Cu powder to the 6061 powder was found to affect the microstructure of the resultant samples, and therefore the hardness as well. Adding Cu refined the grain structure, which would explain the increase in hardness (and theoretically the strength as well) as well as introducing Al_2Cu intermetallics, which would act similar to a ceramic filler. Cu also forced oxygen to the grain boundaries, which may act as an additional strengthening mechanism. In the case of a eutectic alloy (33 wt% Cu) the resultant alloy was found to contain effectively no oxygen. While the formation of recognised microstructures was an encouraging sign, a more homogenous microstructure would be beneficial.

Multilayer Al alloy production

The SLM of 6061 Al alloy and Al-Cu custom alloys represents very different phenomena from stainless steels. The SLM of single layer samples of stainless steels allowed an insight into the correct parameters to use for multilayer part production. For steels, the more energy imparted to the material in the SLM process the denser the consolidated part becomes, whereas Al alloys required a high laser power and faster scan speeds for successful consolidation. This was attributed to the balling effect, since the longer the material is molten, the more time it has to achieve a geometry that minimises surface energy.

Pure 6061 SLM samples were found to have a high hardness (effectively double that of the single layer 6061 samples) and to be extremely resistant to corrosion: this corrosion resistance was apparently undiminished by adding Cu, though a eutectic

mixture displayed faint signs of etching. It was found that adding Cu to 6061 improved hardness and consolidation, though there were different trends for these properties. Hardness increased linearly with increasing Cu content, displaying signs of a composite-like material. Consolidation was found to improve with the addition of Cu on two levels of porosity: a 2 wt% Cu powder mixture (the lowest Cu content mixture processed) showing dramatically reduced signs of microporosity, as did higher content Cu mixtures; macroporosity however only seemed to improve when at least 15 wt% Cu was used, which was attributed to reaching a critical value for improving wetting.

Larger samples were made using a 20 wt% Cu powder mixture in order to manufacture compression testing samples. It was found that samples with a comparatively good level of consolidation displayed impressive mechanical strength despite the hindrance of having a poor structure. XRD analysis was undertaken, which revealed that the Al_2Cu that formed during processing had achieved a quasicrystal formation, which is associated with possible amorphous or nanocrystalline materials.

Nanocrystalline Al alloy production

Given the reported superior properties of nanocrystalline alloys [178], one must be careful when claiming to be able to manufacture such materials. Hence, the evidence in favour of the theoretical production of nanocrystalline materials is summed up here:

- Multilayer Al alloy samples produced demonstrate superb corrosion resistance - a feature of amorphous and/or nanocrystalline materials.
- Attempted etching showed no signs of a microstructure - nanocrystalline microstructures are very small in scale and the SEM available during research was not up to the task of investigating at the level of magnification required.
- Hardness of pure 6061 Al alloy samples was almost double that of the single layer samples, which can be attributed to a finer microstructure.
- Extremely high cooling rates on the order of approximately 10^6 K s^{-1}, which allow the formation of amorphous/nanocrystalline structures in conventional materials, are predicted to occur.
- Quasicrystals, which were detected by XRD in the 20 wt% Cu samples, are associated with amorphous and/or nanocrystalline phases and high cooling rates.

The XRD also reported the Al matrix as an FCC crystal formation, which lends weight to the argument that the Al has formed a nanocrystalline phase.

- Increasing Cu content resulted in a linear increase in hardness, which implied a composite-like behaviour rather than the behaviour seen by alloying. This is assumed to be due to dispersion of quasicrystals.

The possibility of having manufactured nanocrystaline Al alloys can be considered a breakthrough and thus must quite frankly be treated with trepidation. The analyses available all agree with the possibility. As to why it has not been previously reported, there are two reasons for this:

- The base alloy used (6061 Al alloy) has a comparatively high thermal conductivity compared to the more typical AlSi10Mg used by others. This would have lowered cooling rates to 10^5 K s^{-1} or less, which are not fast enough for the formation of amorphous/nanocrystalline Al alloys.
- In the case of 6061 Al alloy use, the base plate/bed temperature was higher than the precipitation temperature of the alloy and so there would have been no 'snap' freezing of the material, as well as ageing during the build.

SLM may open the door to producing Al based amorphous/nanocrystalline metals from conventional alloys. So, while SLM may only be able to currently process a limited range of conventional materials, it may be able to counter this disadvantage by being able to process these materials with a superior microstructure.

Demonstration part analysis

The demonstration part produced establishes the capability of the SLM process to manufacture complex parts from a customised alloy. The manufacturing process also revealed that Al alloy part geometry may have to be considered more carefully than comparatively easy to process materials such as steels. Part geometry was also found to influence hardness throughout the part, indicating that geometry plays a role on cooling rates. Hence, if a part consisting of an amorphous Al alloy is desired, it may be that careful consideration has to go into geometry and processing parameters. It may even be

necessary to computationally model the heat flow of the complete manufacturing process to predict suitable parameters for different sections of a part.

Conclusions

Research began with evaluating materials and current Additive Manufacturing (AM) processes for their suitability to aerospace applications: it was found that investigating SLM of Al alloys fulfilled criteria for manufacturing parts with advanced geometries out of metals. Since Al alloy usage was extremely limited at that point in time, the first work phase focused on stainless steel based materials to allow observation and study of a material previously used in SLM. Investigations then moved on to the single layer SLM of Al and Al alloys to find suitable materials for use in SLM that would be able to show strengths comparable to high performance aerospace grade Al alloys. Multilayer samples of 6061 Al alloy and customised 6061/Cu alloys were then manufactured and analysed. Finally, a demonstration part was designed and manufactured to show that a part with aerospace style geometry could be made out of a customised Al alloy.

The primary contributions of this PhD are:

- A demonstration of manipulating the magnetic nature of a material by the selective mixing and SLM of two stainless steels, one austenitic and with a relatively low degree of magnetic susceptibility, the other martensitic with a high degree of magnetic susceptibility. This could be used to further develop Functionally Graded Materials (FGMs) with regions of varying magnetic susceptibility.
- A detailed investigation of material and process mechanisms governing the characteristics and mechanical performance of single layer and multi-layer samples prepared by the SLM of Al alloy and its powder mixtures for various material compositions (including pure Al, pure Al/Cu, 6061 alloy and 6061 and Cu alloy).
- A discovery of the theoretical capability of the SLM process to fabricate nanocrystalline multi-layer Al sample parts through rapid cooling and consolidation which is attributed to the rapid melting of SLM process and the rapid heat dissipation of suitable Al alloys (i.e. alloys with a sufficiently high thermal diffusivity).

- A discussion and interpretation of material microstructure evolution and laser consolidation mechanisms governing the SLM of advanced and customized stainless and Al alloy through experimental findings.

The experimental results show that mixing different material powders prior to SLM processing should not be thought of just in terms of improving mechanical strength as a conventional composite. Mixing in additional powders can also help consolidation either in improving density or refining microstructure which will further improve mechanical properties. For example in the case of adding 17-4PH to 316L stainless steel, it was found that a small amount of 17-4PH could dramatically improve density whilst only slightly affecting hardness.

The rapid solidification of Al alloys in SLM is of considerable interest as it is far higher than any conventional process. This affects traditional phase diagrams, altering the temperatures and material compositions at which certain phases occur, as well as the formation of a nanocrystalline single phase that is not believed to be seen in any other method of manufacture. This may open a new field of metallurgy that is based on metallic additive manufacturing processes as the rapid solidification gives rise to new microstructure possibilities. SLM, rather than limiting material choice as initially thought, may actually open up the manufacture of new materials: the process may prove itself to be of more use than 'just' being able to produce parts with complex geometries or being material efficient.

The final work stage utilised SLM to manufacture a part with advanced geometry from a customised alloy, demonstrating the potential to manufacture advanced, high performance components for aerospace applications.

Ultimately, the work presented has been limited by both the maximum laser power of the SLM machine utilised and the lack of an optical isolator. Despite this, the results show interesting potential for the production of nanocrytalline (or even amorphous) Al alloys and would benefit from further research using a more capable SLM machine.

Further work

As with any engineering project, there are avenues of research that the author would have liked to investigate but had neither the time nor the funding to do so. In this final chapter, further areas of research are suggested that lead on from the work presented in this thesis

Manufacturing with an updated system

Discussed in Chapter 8, the laser power of the SLM Realizer was found to be insufficient, as well as being limited by instances of back reflection. An obvious next step would be to process the experimental alloys developed in this research on a more capable machine, which would allow the production of denser parts, which in turn would allow further mechanical properties analysis. Ideally, the machine would have: an optical isolator with polarising filters fitted to stop back reflection occurring; a laser of at least 300 W that can operate in pulsed and continuous modes, with a focusing system that can reduce the laser spot size to 50 µm and less; and a scanning system that can scan at speeds of up to 1 km s^{-1}. The option of being able to process parts under a vacuum as well as inert gases other than argon may also be desirable.

Transmission electron microscopy analysis

Transmission Electron Microscopy (TEM) would allow more advanced analysis of samples, specifically the determination of whether the phases observed in Chapter 7 are amorphous or crystalline through analysis of diffraction patterns.

Alternative alloys and materials

The work demonstrated in this thesis could also be applied to mixtures of 6061 Al alloy, replacing Cu with typical alloying elements such as Zn, Si, Mg and Li. The work

doesn't have to be limited to a binary powder mixture either; three or more powders could be mixed at the same time.

Amorphous/nanocrystalline metals

The nanocrystalline alloy research in this thesis has focused on Al alloys, but could be applied to other suitable materials too. As well as investigating the processing of more conventional amorphous alloys, other materials with suitably high thermal conductivities such as Cu alloys could be processed using SLM to produce parts with amorphous and/or nanocrystalline microstructures. Even steels may be possible to form in an amorphous state if the surrounding environment is cooled prior to processing.

Functionally graded materials

In regards to FGMs, the SLM process could be adapted to selectively deposit mixtures of Al-Cu powders. The idea of an FGM can be extended to selectively processing amorphous regions within a part. Consider that an amorphous metal is reported to have superior wear, fatigue and corrosion characteristics compared to its conventional alloy counterpart: a plain bearing surface may be directly formed within the part, or a corrosion resistant outer layer may be implemented. Microstructure control could be implemented by fast raster scanning of selected areas, controlling the cooling rate to leave a microstructure with desired grain size.

FGMs may also allow the bonding of Al and steel parts since the joining region may be gradually graded as to allow a smooth transition from one material to the other. Steel/Al joining is a common occurrence in aerospace assemblies.

Control of process atmosphere

All experiments run in this work used argon as an inert shielding gas to deliberately reduce oxidation. However, it may be possible to form *in-situ* MMCs by two methods. First, the deliberate introduction of oxygen into the atmosphere may allow the formation of Al-Al_2O_3 MMCs, which are of benefit to aerospace applications due to their desirable mechanical properties. Secondly, alternate gases could result in the formation of other

MMCs. For example, by using nitrogen as a shielding gas, Al-AlN MMCs could be manufactured; Al-AlN MMCs show promising thermal characteristics .

Metal matrix composites

Al-Cu alloys show potential for the wetting of ceramics. Since ceramics are a typical component in MMCs, it would be logical to pursue the SLM production of MMCs using Al-Cu as the matrix material and a suitable ceramic as the reinforcement.

Magnetic materials

An offshoot of amorphous metals, amorphous and nanocrystalline microstructures result in improved magnetic properties for relevant materials. The rapid cooling rates occurring in the SLM process may lend themselves to producing parts with superior magnetic properties.

Al alloy geometry limitations and design procedure

SLM is subject to new design limitations when compared to conventional manufacturing. The demonstration part produced as part of this thesis was seen to be more difficult to produce out of Al alloy than it would have been to produce out of steel. Therefore, a testing regime would be equally applicable to Al alloys.

REFERENCES

1. Bradbury, J., AM engineer at Airbus Filton, personal consultation, March 2009.
2. Johns, D., AM manager at Airbus Filton, personal consultation, March 2009.
3. Salmoria, G.V., Paggi, R.A., Lago, A. and Beal, V.E., Microstructural and mechanical characterization of pa12/mwcnts nanocomposite manufactured by selective laser sintering, Polymer Testing, In Press, Accepted Manuscript, Available online 27 April 2011.
4. Victrex PEEK Materials Property Guide, available online at http://www.victrex.com/docs/literature-docs/VICTREX%20Materials%20Properties%20Guide%20ENG_FINAL.pdf (last accessed 1st April 2011).
5. Schmidtke, K., Palm, F., Hawkins, A. and Emmelmann, C., Process and Mechanical Properties: Applicability of a Scandium modified Al-alloy for Laser Additive Manufacturing, Physics Procedia, Volume 12, Part 1, 2011, pp.369-374.
6. Wong, M., Tsopanos, S., Owen, I. and Sutcliffe, C.J., Selective laser melting of heat transfer devices, Rapid Prototyping Journal 13 (5), 2007, pp.291–297.
7. Louvis, E., Fox, P., Sutcliffe, C.J., Selective laser melting of aluminium components, Journal of Materials Processing Technology, Volume 211, Issue 2, 1 February 2011, pp.275-284.
8. House of Commons Trade and Industry Committee, The UK Aerospace Industry, Fifteenth Report of Session 2004-2005, available online at http://www.publications.parliament.uk/pa/cm200405/cmselect/cmtrdind/151/151.pdf (last accessed 1st April 2011).
9. Campbell, F.C., Manufacturing Technology for Aerospace Structural Materials, Elsevier, UK, 2006.
10. Boothroyd, G., Dewhurst, P. and Knight, W. Product Design for Manufacture and Assembly, Marcel Dekker Inc., New York, 1994.
11. Callister, W.D.Jr., Materials Science and Engineering—An Introduction, sixth ed., John Wiley, New York (NY), 2003.
12. Aidex Precision LLC website, http://www.aidexprecision.com/ (last accessed 1st April 2011).

13. Leech Industries Inc. website, http://www.leechind.com/ (last accessed 1st April 2011).
14. Multi-Strike Ltd website, http://www.multi-stroke.co.uk (last accessed 1st April 2011).
15. Forging of Carbon and Alloy Steels, in ASM Handbook Vol. 14: Forming and Forging, ASM International, 1996.
16. MCC website, University of Northern Iowa Metal Casting Centre, available at http://www.mcc.uni.edu/ (last accessed 1st April 2011).
17. Peel, C.J., Gregson, P.J., "Design Requirements for Aerospace Structural Materials", in High Performance Materials in Aerospace, Chapman & Hall, 1995, pp. 1–48.
18. Caron, R.N., Staley, J.T., Beryllium: Effects of Composition, Processing, and Structure on Properties of Nonferrous Alloys, ASM metal handbook, Vol. 20, 1997 (ASM International, Metals park, Ohio).
19. Stonehouse, A.J., Marder, J.M., 'Beryllium: Health and Safety Considerations', in ASM Handbook Vol. 2, Properties and Selection: Nonferrous Alloys and Special-Purpose Materials, ASM International, 1990.
20. Boyer, R.R., 'An Overview of the Use of Titanium in the Aerospace Industry', Materials Science and Engineering, A213, 1996, pp. 103–114.
21. Davis, J.R., 'Superalloys', in Alloying: Understanding The Basics, ASM International, 2001, pp. 290–307.
22. Choudhury, I.A., El-Baradie, M.A., 'Machinability of Nickel-Base Super Alloys: A General Review', Journal of Materials Processing Technology, Vol. 77, 1998, pp. 278–284.
23. Campbell, F.C., Manufacturing Processes for Advanced Composites, Elsevier Ltd, 2004.
24. Kainer, K.U., Metal Matrix Composites: Custom-made Materials for Automotive and Aerospace Engineering, Wiley, 2006.
25. Carre C., Barbaux V., Tschofen J., Proc. Int. Conf. on PM-Aerospace Materials, MPR Publishing Services Ltd, London (1991), pp. 36-1–36-12.
26. Buckley, J.D., "Carbon-Carbon Composites", in Handbook of Composites, Chapman & Hall, 1998, pp. 333–351.
27. Hopkinson, N., Additive Manufacturing: Technology and applications, British Educational Communications and Technology Agency (BECTA), corp creator, 2010.

28. ASTM F42 website, http://www.astm.org/COMMIT/COMMITTEE/F42.htm (last accessed 1st April 2011).
29. Wohlers Associates, History of System Manufacturers, 2002, available online at http://www.wohlersassociates.com (last accessed 1st April 2011).
30. Gebhardt, A, Schmidt, F.-M., Hötter, J.-S., Sokalla, W. and Sokalla, P., Additive Manufacturing by selective laser melting the realizer desktop machine and its application for the dental industry,Physics Procedia, Volume 5, Part 2, 2010, pp.543-549.
31. Hague, R., Campbell, I. and Dickens, P., Implications on design of rapid manufacturing, Proceedings of the Institution of Mechanical Engineers, Part C: Journal of Mechanical Engineering Science January 1, 2003 vol. 217 no. 1 25-30.
32. Yan, X. and Gu, P., A review of rapid prototyping technologies and systems, Computer-Aided Design, Volume 28, Issue 4, April 1996, pp.307-318.
33. Hopkinson, N., Hague, R. and Dickens, P., Rapid Manufacturing: An Industrial Revolution for the Digital Age, Wiley, Chichester, 2005.
34. Make Parts Fast website, http://beta.makepartsfast.com/ (last accessed 1st April 2011).
35. Caulfield, B., McHugh, P.E. and Lohfeld, S., Dependence of mechanical properties of polyamide components on build parameters in the SLS process, Journal of Materials Processing Technology, Volume 182, Issues 1-3, 2 February 2007, pp.477-488.
36. Chockalingam, K., Jawahar, N., Chandrasekar, U. and Ramanathan, K.N., Establishment of process model for part strength in stereolithography, Journal of Materials Processing Technology, Volume 208, Issues 1-3, 21 November 2008, pp.348-365.
37. Tolosa, I., Garciandía, F., Zubiri, F., Zapirain, F. and Esnaola, A., Study of mechanical properties of AISI 316 stainless steel processed by selective laser melting following different manufacturing strategies, The International Journal of Advanced Manufacturing Technology, Volume: 51, Issue: 5-8, 2010, pp. 639-647.
38. Strano, G., Hao, L., Evans, K.E., Everson, R.M., Smith, C.W., Meyer, J., Johns, D., Vanard, G. and Scarpa, F., Multi-Objective Optimisation for Additive Layer Manufacturing, Proceeding of Tenth National Conference on Rapid Design,

Prototyping and Manufacturing, Buckinghamshire New University, 12 June 2009.

39. Concept Laser website, http://www.concept-laser.de/ (last accessed 1st April 2011).
40. Becker, D., Additive manufacturing of components out of copper and copper alloys by Selective Laser Melting, Proceeding of the International Conference on Additive Manufacturing, Loughborough University, 12-13th July 2011.
41. Zarringhalam, H., Hopkinson, N., Kamperman, N.F. and de Vlieger, J.J., Effects of processing on microstructure and properties of SLS Nylon 12, Materials Science and Engineering: A, Volumes 435-436, 5 November 2006, pp.172-180.
42. Kruth, J.-P., Leu, M.C. and Nakagawa, T., Progress in Additive Manufacturing and Rapid Prototyping, CIRP Annals - Manufacturing Technology, Volume 47, Issue 2, 1998, pp.525-540.
43. 3D Systems DuraForm GF datasheet, available online at http://www.3dsystems.com/products/datafiles/lasersintering/datasheets/DS-DuraForm_GF_plastic-A4_UK.pdf (last accessed 1st April 2011).
44. TCT magazine, First EOSINT P 800 High Temperature PEEK Processing System Sold by EOS, May/June 2009.
45. Kumar, S. and Kruth, J.-P., Composites by rapid prototyping technology, Materials & Design, Volume 31, Issue 2, February 2010, pp.850-856.
46. Chung, H. and Das, S., Processing and properties of glass bead particulate-filled functionally graded Nylon-11 composites produced by selective laser sintering, Materials Science and Engineering: A, Volume 437, Issue 2, 15 November 2006, pp.226-234.
47. Zhou, M.Y., Xi, J.T. and Yan, J.Q., Modeling and processing of functionally graded materials for rapid prototyping, Journal of Materials Processing Technology, Volume 146, Issue 3, 10 March 2004, pp.396-402.
48. Parthasarathy, J., Starly, B. and Raman, S., A design for the additive manufacture of functionally graded porous structures with tailored mechanical properties for biomedical applications, Journal of Manufacturing Processes, In Press, Corrected Proof, Available online 1 March 2011.
49. 3D Systems Accura Xtreme Plastic datasheet, available online at http://www.3dsystems.com/products/datafiles/datasheets/SLA/DS_Accura_Xtreme_UK.pdf (last accessed 1st April 2011).

50. 3D Systems Accura Bluestone Material datasheet, available online at http://www.3dsystems.com/products/datafiles/datasheets/SLA/DS_Accura_Bluestone_UK.pdf (last accessed 1st April 2011).
51. Karalekas, D.E., Study of the mechanical properties of nonwoven fibre mat reinforced photopolymers used in rapid prototyping. Mater Design 2003;24:665–70.
52. Gupta, A. and Ogale, A.A., Dual curing of carbon reinforced photoresins for rapid prototyping. Polym Compos 2004;23(6):1162–70.
53. Choi, J.-W., Kim, H.-C. and Wicker, R., Multi-material stereolithography, Journal of Materials Processing Technology, Volume 211, Issue 3, 1 March 2011, pp.318-328.
54. Arik Levy website, http://www.ariklevy.fr/ (last accessed 1st April 2007).
55. Melchels, F.P.W., Feijen, J. and Grijpma, D.W., A review on stereolithography and its applications in biomedical engineering, Biomaterials, Volume 31, Issue 24, August 2010, pp.6121-6130.
56. Mansour, S., Gilbert, M. and Hague, R., A study of the impact of short-term ageing on the mechanical properties of a stereolithography resin, Materials Science and Engineering: A, Volume 447, Issues 1-2, 25 February 2007, pp.277-284.
57. Kruth, J.-P., Wang, X., Laoui, T. and Froyen, L., Lasers and materials in selective laser sintering, Assembly Automation, Vol. 23 Issue 4, 2003, pp.357 - 371.
58. Kruth, J.-P., Levy, G., Klocke, F. and Childs, T.H.C., Consolidation phenomena in laser and powder-bed based layered manufacturing, CIRP Annals - Manufacturing Technology, Volume 56, Issue 2, 2007, pp.730-759.
59. 3D Systems DuraForm PA datasheet, available online at http://www.3dsystems.com/products/datafiles/lasersintering/datasheets/DS-DuraForm_PA_plastic-A4_UK.pdf (last accessed 1st April 2011).
60. Jar, P.-Y.B., Mulone, R., Davies, P. and Kausch, H.-H., A study of the effect of forming temperature on the mechanical behaviour of carbon-fibre/peek composites, Composites Science and Technology, Volume 46, Issue 1, 1993, pp.7-19.
61. Sewell, N.T., Felstead, M. and Sloan, M. A study of the degradation of Duraform PA due to cyclic processing, VRAP 2007 17-22 Oct Leiria Portugal, 2007.

62. MTT Website, MTT Technolgies Group, http://www.mtt-group.com/ (last accessed 1st April 2011).
63. EOS GmbH, http://www.eos.info/en/home.html (last accessed 1st April 2011).
64. Arcam website, http://www.arcam.com/ (last accessed 1st April 2011).
65. Hagedorn, Y.-C., Wilkes, J., Meiners, W., Wissenbach, K. and Reinhart, P., Net shaped high performance oxide ceramic parts by selective laser melting, Physics Procedia, Volume 5, Part 2, 2010, pp.587-594.
66. Gu, D., Hagedorn, Y.-C., Meiners, W., Wissenbach, K. and Reinhart, P., Selective Laser Melting of in-situ TiC/Ti5Si3 composites with novel reinforcement architecture and elevated performance, Surface and Coatings Technology, Volume 205, Issue 10, 15 February 2011, pp.3285-3292.
67. Shiomi, M., Osakada, K., Nakamura, K., Yamashita, T. and Abe, F., Residual Stress within Metallic Model Made by Selective Laser Melting, CIRP Annals - Manufacturing Technology, Volume 53, Issue 1, 2004, pp.195-198.
68. Damascus poster, available online at http://www.x-at.co.uk/downloads/posters/damascus.pdf, (last accessed 1st April 2011).
69. Novichenko, D., Marants, A., Thivillon, L., Bertrand, P.H. and Smurov, I., Metal Matrix Composite Material by Direct Metal Deposition, Physics Procedia, Volume 12, Part 1, 2011, pp.296-302.
70. Mei, Y., Wang, X. and Cheng, G., A feature-based topological optimization for structure design, Advances in Engineering Software, Volume 39, Issue 2, February 2008, pp.71-87.
71. Xie, J.W., Fox, P., O'Neill, W. and Sutcliffe, C.J., Effect of direct laser re-melting processing parameters and scanning strategies on the densification of tool steels, Journal of Materials Processing Technology, Volume 170, Issue 3, 30 December 2005, pp.516-523.
72. Steen, W.M. and Mazumder, J., Laser Material Processing, Fourth Edition, Springer, 2010.
73. Gould, R.G. "The LASER, Light Amplification by Stimulated Emission of Radiation". In Franken, P.A. and Sands, R.H. (Eds.). The Ann Arbor Conference on Optical Pumping, the University of Michigan, June 15 through June 18, 1959. pp. 128.
74. Sharpe M., Henry P., Steen W.M. and Lim G.C. An analysis of the effects of mode structure on laser material processing. Proc Laser '83 Optoelectronic Conf. Munich, June 1983, ed Waidelich, pp. 243-246.

75. Juptner, W., Rohte, W., Sepold, G. and Teske, K., DVS Bericte 63 (1983), 222.
76. Drude, P., Theory of Optics (English edn). Longmans, Green & Co. Inc, New York, 1922.
77. Gusarov, A.V. and Smurov, I., Radiation transfer in metallic powder beds used in laser processing, Journal of Quantitative Spectroscopy and Radiative Transfer, Volume 111, Issues 17-18, November 2010, pp.2517-2527.
78. German, R.M., Sintering Theory and Practice, John Wiley & Sons, Inc, 1996.
79. German, R.M., Suri, P. and Park, S.J., Review: liquid phase sintering, J. Mater. Sci., 44, 2009, pp.1–39.
80. Gusarov, A.V., Mechanisms of selective laser sintering and heat transfert in Ti powder, Rapid Prototyping J., 9/5, 2003, pp.314-326.
81. Levy, G.N., Schindel, R. and Kruth, J.-P., Rapid manufacturing and rapid tooling with layer manufacturing technologies: state of the art and future perspectives, CIRP Annals, 52/2, 2003, pp.589-609.
82. Mercelis, P. and Kruth, J.-P., Residual stresses in selective laser sintering and selective laser melting, Rapid Prototyping J., 12/5, 2006, pp.254-265.
83. Tolochko, N., Arshinov, M., Gusarov, A., Titov, V., Laoui, T. and Froye, L., Mechanisms of selective laser sintering and heat transfer in Ti powder, Rapid Prototyping Journal, Vol. 9 Issue: 5, 2003, pp. 314 - 326.
84. Mills, K.C. and Keene, B.J., Factors affecting variable weld penetration, International Materials Reviews, Volume 35, 1990 , pp.185-216.
85. Mazumder, J., Overview of melt dynamics in laser processing, Opt. Eng. 30 (1991), pp. 1208–1219.
86. Mazumder, J., Fundamentals of Laser Welding, ASM metals handbook. Vol. 6, 1993 (ASM, International, Metals Park, Ohio).
87. Plateau, J., Experimental and Theoretical Statics of Liquids Subject to Molecular Forces Only, 1873.
88. Rayleigh, L., Proc. London Math. Soc. 10, 4 (1878).
89. Yadroitsev, I., Gusarov, A., Yadroitsava, I. and Smurov, I., Single track formation in selective laser melting of metal powders, Journal of Materials Processing Technology, Volume 210, Issue 12, 1 September 2010, pp.1624-1631.
90. Niu, H.J. and Chang, I.T.H., Instability of scan tracks of selective laser sintering of high speed steel powder, Scripta Materialia, Volume 41, Issue 11, 5 November 1999, pp.1229-1234.

91. Das, S., Physical Aspects of Process Control in Selective Laser Sintering of Metals, Adv. Eng. Mater., 5, 10, pp701-711, 2003.
92. Kruth, J.-P., Froyen, L., Van Vaerenbergh, J., Mercelis, P., Rombouts, M. and Lauwers, B., Selective laser melting of iron-based powder, Journal of Materials Processing Technology, Volume 149, Issues 1-3, 10 June 2004, pp.616-622.
93. Kralchevsky, P.A. and Denkov, N.D., Capillary forces and structuring in layers of colloid particles, Current Opinion in Colloid & Interface Science, Volume 6, Issue 4, August 2001, pp.383-401.
94. Thomas, D. and Bibb, R. An Investigation into the Geometric Constraints of Selective Laser Melting for the Development of Design Rules, Ninth National Conference on Rapid Design, Prototyping and Manufacturing, Lancaster, 13th June 2008.
95. Williams, R.J., Bibb, R., Eggbeer, D. and Collis, J., Use of CAD/CAM technology to fabricate a removable partial denture framework, The Journal of Prosthetic Dentistry, Volume 96, Issue 2, August 2006, pp.96-99.
96. TWI website, http://www.twi.co.uk (last accessed 1st April 2011).
97. German, R.M., ASM handbook, volume 7, tenth edition, 1998, pp.355–364 (ASM International, Metals Park, Ohio).
98. O'Neill, W., Sutcliffe, C.J., Morgan, R., Landsborough, A. and Hon, K.K.B., Investigation on Multi-Layer Direct Metal Laser Sintering of 316L Stainless Steel Powder Beds CIRP Annals - Manufacturing Technology, Volume 48, Issue 1, 1999, pp.151-154.
99. Rombouts, M., Kruth, J.P., Froyen, L. and Mercelis, P., CIRP Annals - Manufacturing Technology, 2006, 55 (1), pp. 187-192.
100. Glardon, R., Karapatis, N., Romano, V. and Levy, G.N., Influence of Nd:YAG Parameters on the Selective Laser Sintering of Metallic Powders, CIRP annals – Manufacturing Technology, Volume 50, Issue 1, 2001, pp. 133-136.
101. West, E.G., The Welding of Non-Ferrous Metals, (Chapman & Hall Ltd, London, 1951).
102. CRDM E-Brochure, 2009.
103. Wohlers, T. and Gornet, T., 'History of Additive Fabrication', Time Compression Technologies Magazine, March 2008.
104. Matweb website, http://www.matweb.com/index.aspx (last accessed 1st April 2011).

105. Zhang, D., Entwicklung des Selective Laser Melting (SLM) für Aluminiumwerkstoffe, PhD thesis, 2004.
106. Molina, J.M., Voytovych, R., Louis, E. and Eustathopoulos, N., The surface tension of liquid aluminium in high vacuum: The role of surface condition, International Journal of Adhesion and Adhesives, Volume 27, Issue 5, July 2007, pp394-401.
107. Shen, P., Fujii, H., Matsumoto, T. and Nogi, K., The influence of surface structure on wetting of α-Al2O3 by aluminum in a reduced atmosphere, Acta Materialia, Volume 51, Issue 16, 15 September 2003, pp4897-4906.
108. ZAP-IT website, http://www.zap-it.com/ (last accessed 1st April 2011).
109. Budzyn, G. and Rzepka, J., Back-reflection effects in a frequency-stabilized two-mode He–Ne laser, Optics Communications, Volume 281, Issue 22, 15 November 2008, pp.5592-5595.
110. Materialise website, http://www.materialise.com/ (last accessed 1st April 2011).
111. Badrossamay, M. and Childs, T.H.C., Further studies in selective laser melting of stainless and tool steel powders, International Journal of Machine Tools and Manufacture, Volume 47, Issue 5, April 2007, pp.779-784.
112. Childs, T. H. C. and Hauser, C., Raster scan selective laser melting of the surface layer of a tool steel powder bed. Proc IMechE, Part B: J. Engineering Manufacture, 2005, 219, pp.379–384.
113. Childs, T.H.C., Hauser, C., and Badrossamay, M., Selective laser sintering (melting) of stainless and tool steel powders: experiments and modelling. Proc IMechE, Part B: J. Engineering Manufacture, 2005, 219, pp.339–358.
114. Sandvik Osprey Ltd., Powder Group, 316L material data sheet available from http://www.smtsandvik.com/osprey (last accessed 1st April 2011).
115. EOS GmbH, EOS stainless steel PH1 material data sheet available from http://www.eos.info/en/home.html (accessed 1st April 2011).
116. Lagutkin, S., Achelis, L., Sheikhaliev, S., Uhlenwinkel, V. and Srivastava, V., Atomization process for metal powder, Materials Science and Engineering A, Volume 383, Issue 1, 10 October 2004, pp.1-6.
117. Lochmann, K., Oger, L. and Stoyan, D., Statistical analysis of random sphere packings with variable radius distribution, Solid State Sciences, Volume 8, Issue 12, December 2006, pp1397-1413.
118. Vander Voort, G.F., Embrittlement of ASM metals handbook, Vol. 1, 1993 (ASM, International, Metals Park, Ohio).

119. Tyler, D.E. and Black, W.T., Introduction to Copper and Copper Alloys, ASM metals handbook, Vol. 2, 1992 (ASM International, Metals Park, Ohio).
120. Tan, L.-K., Baumgartner, R. and German, R. Advances in powder metallurgy and particular materials, volume 4, 2001, pp. 191–198 (MPIF, New York).
121. Simchi, A., Rota, A. and Imgrund, P. An investigation on the sintering behavior of 316L and 17-4PH stainless steel powders for graded composites. Mater. Sci.Engng. A. Struct. Mater., Prop. Microstruct. Process., 2006, 424(112), pp. 282–289.
122. Imgrund, P., Rota, A., and Simchi, A. Microinjection moulding of 316L/17-4PH and 316L/Fe powders for fabrication of magnetic–nonmagnetic bimetals. J. Mater. Process. Technol., 2008, 200(1–3), pp.259–264.
123. Skelly, H. M. and McGoey, J. T. Int. J. Powder Metall. Powder Technol., 1978, 2(14), pp. 99–102.
124. Smithells, C. J. Metals reference book, Volume 1, Second edition, 1955 (Interscience, New York).
125. Lloyd EZ20, details available at http://www.lloyd-instruments.co.uk (last accessed 1st April 2011).
126. ASM metals handbook, Vol. 9, 2004 (ASM International, Metals park, Ohio).
127. Wisti, M. and Hingwe, M., Tempering of Steel, ASM metals handbook, Vol. 4, 1991 (ASM International, Metals park, Ohio).
128. ASM metals handbook, Vol. 1, 1993 (ASM International, Metals park, Ohio).
129. Tani, G., Orazi, L., and Fortunato, A. Prediction of hypo eutectoid steel softening due to tempering phenomena in laser surface hardening. CIRP Ann. Mfg Technol., 2008, 57(1), 209–212.
130. Chung, H. and Das, S. Functionally graded Nylon-11/ silica nanocomposites produced by selective laser sintering. Mater. Sci. Engng A, struct. Mater. Prop. Microstruct. Process., 2008, 487(1–2), 251–257.
131. Krishna, B.V., Xue,W., Bose, S., and Bandyopadhyay, A. Functionally graded Co–Cr–Mo coating on Ti–6Al–4V alloy structures. Acta Biomater., 2008, 4(3), 697–706.
132. SLAMFunc website, http://www.slamfunc.org/ (last accessed 1st April 2011).
133. ASTM Volume 3.01, E0008M-04, January 2005.
134. Rooy, E.L., Introduction to Aluminum and Aluminum Alloys, ASM metals handbook, Vol. 2, 1992 (ASM International, Metals park, Ohio).

135. Brooks, C.R., Principles of Heat Treating of Nonferrous Alloys, ASM metals handbook, Vol. 4, 1991 (ASM International, Metals park, Ohio).
136. Alpoco (The Aluminium Powder Company Ltd), http://www.alpoco.co.uk/ (last accessed 1st April 2011).
137. Jallo, L.J., Schoenitz, M., Dreizin, E.L., Dave, R.N. and Johnson, C.E., The effect of surface modification of aluminum powder on its flowability, combustion and reactivity, Powder Technology, Volume 204, Issue 1, 10 December 2010, pp.63-70.
138. Hao, L., Dadbakhsh, S., Seaman, O. and Felstead, M., 'Selective Laser Melting of a Stainless Steel and Hydroxyapatite Composite for Load-Bearing Implant Development', Journal of Materials Processing Technology, submitted for publication, 11 Feb. 2009.
139. Praveen, P. and Yarlagadda, P.K.D.V., Meeting challenges in welding of aluminum alloys through pulse gas metal arc welding, Journal of Materials Processing Technology, Volumes 164-165, 15 May 2005, pp.1106-1112.
140. Asta, M., Beckermann, C., Karma, A., Kurz, W., Napolitano, R., Plapp, M., Purdy, G., Rappaz, M. and Trivedi, R., Acta Materialia, 2009, 57 (4), pp. 941-971.
141. Chan, C.L., Mazumder, J. and Chan, M.M., Metall. Trans. A., 1982, 15, p. 2175.
142. Zaeh, M.F., Branner, G., Krol, T.A., (2009) A three dimensional FE-model for the investigation of transient physical effect in Selective Laser Melting. Proceedings of the 4th International Conference on Advanced Research and Rapid Prototyping pp.415-424.
143. Todd I, The Development of Metallic Materials for Additive Layer Manufacturing: Which Materials Suit Which Platforms and What We Can Do to Improve Properties? Proceeding of TCT Live 2009; 2009 Oct 20-21.
144. Copper powder materials safety data sheet, Sandvik Osprey.
145. ASM metals handbook, Vol. 3, 1990 (ASM International, Metals park, Ohio).
146. Rodriguez, J., Kuhn, M. and Hrbek, J., The interaction of Cu and S2 with aluminum and alumina surfaces: a comparative study, Surface Science, Volume 380, Issues 2-3, 15 May 1997, pp397-407.
147. Moffatt, W.G., Pearsall, G.W. and Wulff, J., The Structure and Properties of Materials, Vol 1, Wiley, New York, 1964.
148. Talyscan 150, Taylor Hobson Ltd, website available at http://taylor-hobson.virtualsite.co.uk/talyscan150.htm (last accessed 1st April 2011).

149. NRL website, http://www.nrl.navy.mil/ (last accessed 1st April 2011).
150. ASTM E9 -89a, Standard Test Methods of Compression Testing of Metallic Materials at Room Temperature (reapproved 2000).
151. Li, C.X., An, X.Z., Yang, R.Y., Zou, R.P. and Yu, A.B., Experimental study on the packing of uniform spheres under three-dimensional vibration, Powder Technology, In Press, Corrected Proof, Available online 15 January 2011.
152. Peyre, P., Sierra, G., Deschaux-Beaume, F., Stuart, D. and Fras, G., Generation of aluminium–steel joints with laser-induced reactive wetting Materials Science and Engineering: A, Volume 444, Issues 1-2, 25 January 2007, pp.327-338.
153. Lienhard IV, J.H. and Lienhard V, J.H., A Heat Transfer Textbook, 3rd edition, Phlogiston Press, Cambridge Massachusetts, 2003.
154. Jiang, G-r., Li, Y-x. and Liu, Y., Influence of solidification mode on pore structure of directionally solidified porous Cu-Mn alloy, Transactions of Nonferrous Metals Society of China, Volume 21, Issue 1, January 2011, pp.88-95.
155. Contreras, A., Wetting of TiC by Al–Cu alloys and interfacial characterization, Journal of Colloid and Interface Science, Volume 311, Issue 1, 1 July 2007, pp.159-170.
156. Childs, T.H.C., Hauser, C. and Badrossamay, M., Mapping and Modelling Single Scan Track Formation in Direct Metal Selective Laser Melting, CIRP Annals - Manufacturing Technology, Volume 53, Issue 1, 2004, pp.191-194.
157. Rosazza Prin, G., Baffie, T., Jeymond, M. and Eustathopoulos, N., Contact angles and spreading kinetics of Al and Al–Cu alloys on sintered AlN, Materials Science and Engineering A, Volume 298, Issues 1-2, 31 January 2001, pp34-43.
158. Chen, S., Ke, F., Zhou, M. and Bai, Y., Atomistic investigation of the effects of temperature and surface roughness on diffusion bonding between Cu and Al, Acta Materialia, Volume 55, Issue 9, May 2007, pp. 3169-3175.
159. Gill, S.C. and Kurz, W., Rapidly solidified Al---Cu alloys—I. experimental determination of the microstructure selection map, Acta Metallurgica et Materialia, Volume 41, Issue 12, December 1993, pp.3563-3573.
160. Zimmermann, M., Carrard, M. and Kurz, W., Rapid solidification of Al-Cu eutectic alloy by laser remelting, Acta Metallurgica, Volume 37, Issue 12, December 1989, pp.3305-3313.
161. Schroeder, V.C., Gilbert, J. and Ritchie, R. O., Comparison of the Corrosion Behavior of a Bulk Amorphous Metal, Zr41.2Ti13.8Cu12.5Ni10Be22.5, with Its

Crystallized Form, Scripta Materialia, Volume 38, Issue 10, 14 April 1998, pp.1481-1485.

162. Gostin, P.F., Gebert, A. and Schultz, L., Comparison of the corrosion of bulk amorphous steel with conventional steel, Corrosion Science, Volume 52, Issue 1, January 2010, pp.273-281.

163. Ruan, S., Torres, K.L., Thompson, G.B. and Schuh, C.A., Gallium-enhanced phase contrast in atom probe tomography of nanocrystalline and amorphous Al–Mn alloys, Ultramicroscopy, In Press, Uncorrected Proof, Available online 28 January 2011.

164. Mu, J., Zhu, Z.W., Zhang, H.F., Hu, Z.Q., Wang, Y.D. and Ren, Y., Thermal behaviors of Al-based amorphous alloys bearing nanocrystalline In particles, Acta Materialia, Volume 58, Issue 19, November 2010, pp.6267-6275.

165. Shechtman, D., Blech, I., Gratias,D. and Cahn, J. W., Metallic Phase with Long-Range Orientational Order and No Translational Symmetry, Phys. Rev. Lett. 53, 1984, pp. 1951-1953.

166. Bancel, P.A., Quasicrystals: The State of the Art, D. DiVincenzo, P. J. Steinhardt, Eds. (World Scientific, Singapore, 1991), pp.17–56.

167. Liu, B., Feng, X. and Zhang, S-M., The effective Young's modulus of composites beyond the Voigt estimation due to the Poisson effect, Composites Science and Technology, Volume 69, Issue 13, October 2009, pp2198-2204.

168. Brooks, I., Lin, P., Palumbo, G., Hibbard, G.D., and Erb, U., Analysis of hardness–tensile strength relationships for electroformed nanocrystalline materials, Materials Science and Engineering: A, Volume 491, Issues 1-2, 15 September 2008, pp.412-419.

169. Callister, W.D.Jr., Materials Science and Engineering—An Introduction, sixth ed., John Wiley, New York (NY), 2003.

170. Struers, Hardness Conversion Table, available online at http://www.struers.com/ (last accessed 1st April 2011).

171. Zhang, D., Ma, C. and Cai, M., Effect of oxide layer thickness over Al and Al alloy powders on quality of their explosive compacts, Acta Metallurgica, Volume 6, Issue 1, February 1991, pp.25-28.

172. Dadbakhsh, S., Hao, L. and Sewell, N., A Test Procedure for Mechanical Qualification of Additive Layer Manufacturing Parts, 10th National Conference on Rapid Design, Prototyping & Manufacturing, Buckinghamshire, United Kingdom, 12th June 2009, pp.53-61.

173. SolidWorks, Dassault Systèmes SolidWorks Corp., http://www.solidworks.com/ (last accessed 1st April 2011).
174. Takeuchi, Y., Idemura, T. and Sata, T., 5-Axis Control Machining and Grinding Based on Solid Model, CIRP Annals - Manufacturing Technology, Volume 40, Issue 1, 1991, pp.455-458.
175. Gusarov, A.V. and Kruth, J.-P., Modelling of radiation transfer in metallic powders at laser treatment, International Journal of Heat and Mass Transfer, Volume 48, Issue 16, July 2005, pp.3423-3434.
176. Craeghs, T., Bechmann, F., Berumen, S. and Kruth, J.-P., Feedback control of Layerwise Laser Melting using optical sensors, Physics Procedia, Volume 5, Part 2, 2010, pp.505-514.
177. Thompson, D.C. and Crawford, R.H., Computational quality measures for evaluation of part orientation in freeform fabrication, Journal of Manufacturing Systems, Volume 16, Issue 4, 1997, pp.273-289.
178. Rizzi, P., Doglione, R. and Battezzati, L.,Mechanical properties of Al-based amorphous/nanocrystalline alloys, Materials Science and Engineering: A, Volumes 375–377, 15 July 2004, pp.969-974.